Klondike Placer Gold

New Tools for Examining Morphology, Composition and Crystallinity

by

Evan Cameron Crawford

B.Sc., The University of Victoria, 2005

A THESIS SUBMITTED IN PARTIAL FULFILMENT OF
THE REQUIREMENTS FOR THE DEGREE OF

Master of Science

in

The Faculty of Graduate Studies

(Geological Sciences)

The University Of British Columbia

August, 2007

Abstract

This work focuses on developing and expanding the utility of several new and previously used methods for examining the morphology, composition and crystallinity of placer gold. Several studies using samples from the Klondike District and surrounding areas in west-central Yukon investigating each of these properties are presented, along with potential future applications for the methods, and implications of the results already obtained.

The new method for examination of the morphology of placer gold is centered around semi-automated digital image analysis. Automating morphological analysis allows more accurate and reproducible measurement of much larger number of grains as compared to manual methods, allowing for improved statistical analyses of placer gold morphology.

Combining results from these new methods of morphological analysis with conventional electron microprobe analysis of composition has produced a detailed model relating placer gold grain morphology to the distance it has been alluvially transported. This model was developed with regard to geology and gold composition and is significantly superior to previous models.

A new method using laser ablation - inductively coupled plasma - mass spectroscopy (LA-ICP-MS) has been developed to examine minor and trace element composition of placer gold. This new method allows for compositional fingerprints to be defined, and spatial variations in trace and minor elements to be measured within individual grains.

Placer gold crystallinity has been observed, however remains poorly examined. We have utilized X-ray diffraction to study the internal crystallographic texture of placer gold, and confirm that several other methods previously used for this purpose do probe internal crystallinity.

These new methods have significantly broadened the range of techniques available to investigate placer gold. Examination of the results from these methods has yielded new insights into the potential genesis of gold deposits in the Klondike, the nature of gold crystallinity, and the changes in morphology that occur during alluvial transport. These early studies also indicate that there is still significant work to be done, and that these new methods

have significant potential in the study of placer gold.

Table of Contents

List of Tables

List of Figures

List of Equations

List of Abbreviations

acu ..... arbitrary concentration unit
Circum. ..... Circumscribing
cps ..... counts per second
EBSD ..... Electron Backscatter Diffraction
EMPA ..... Electron Microprobe Analysis
EOS ..... Earth and Ocean Sciences
GMTD ..... Gradient Modified Transport Distance
HSE ..... Hofmann Shape Entropy
IGMTD ..... Integrated Gradient Modified Transport Distance
Inscr. ..... Inscribed
KDE ..... Kernel Density Estimation
LA-ICP-MS .....
..... Laser Ablation Inductively Coupled Plasma Mass Spectroscopy
LIF ..... Lithium Fluoride
MDRU ..... Mineral Deposits Research Unit
m/z ..... Mass / charge
PET ..... Pentaerythritol
SEM ..... Scanning Electron Microscope or Scanning Electron Microscopy
UBC ..... University of British Columbia
VBA ..... Visual Basic for Applications
YT ..... Yukon Territory

Acknowledgements

I would like to thank JKM for taking me on as a student and allowing me latitude in this project, and my committee for their help and support. I would also like to thank Rob Chapman for all of his help in the field, and his previous work on this project. Bill LeBarge was indispensable in facilitating access to placer mines and miners and was a tremendous help in the field. Simon Lloyd and David Bond also provided much appreciated assistance in the field.

I would like to thank everyone at the UBC EOS X-ray facility, particularly Mati Raudsepp for his help with EMPA, and Elisabetta Pani for helping me with the SEM on so many occasions. Numerous other people at UBC provided me with much appreciated help on this project; Richard Friedman was always available for conversations, for assistance in the lab and was kind enough to help sort out the bugs in the shape analysis macro. Arne Toma was an invaluable resource when dealing with any computer technical problems, and helping me sort through any and all printing difficulties. Luke Beranek was kind enough to help me out in the field, and along with Reza Tafti, was tolerant of listening to me scream at my computer in the office. Kirsten Rasmussen was gracious enough to help me test out the shape analysis plugin, and my overall method for morphological analysis. Amber Henry, Meghan Jackson, Paul Jago and Andrew Shannon provided commiseration, help and good conversation in East 260, and everywhere else. Bert Mueller also provided a great deal of assistance in developing the laser ablation method. All of my fellow grad student in the EOS department provided a great deal of support throughout my degree. Anita Lam was kind enough to help me to understand the X-ray diffraction system, and to collect the diffraction data for me. Mary Mager, Chad Sinclair and Lori Kennedy all generously donated their time to help me test out the possibility of using EBSD for my project.

I would also like to thank all of the parties who supported me financially: the Natural Sciences and Research Council through a Canada graduate scholaship to me and through a discovery grant to JKM, UBC through the Thomas and Marguerite MacKay and Egil H. Lorntzen Scholarships,

the Yukon geological survey for field assistance and helicopter time, the Klondike Star Mineral Corporation for providing field accommodations, logistical support and most of the funds for analytical work, and the MDRU for funding my attendance at a number of conferences and technical support at UBC.

I would also like greatly to thank Michael McNeil Forbes for creating the UBC thesis LaTeX files, and Max Read for distributing them.

Dedication

To my parents, for their endless support through all of my academic wanderings.

Statement of Co-Authorship

The entirety of this thesis was written by, and all of the figures and tables generated by Evan Crawford, with significant editorial input from Dr. James Mortensen. The following people assisted with various parts of the research described:

- Dr. James Mortensen provided the overall focus for the project, and provided constant assistance in analyzing the results obtained and guiding the path the project followed.
- Dr. Mati Raudsepp helped significantly in running the electron microprobe, setting up and running the instrument.
- Anita Lam was responsible for developing the procedure to perform the X-ray diffraction analyses, and performed all of the data collection.

Chapter 1

Introduction

1.1 Project Goals

A detailed investigation of the nature of placer gold in the Klondike District in western Yukon Territory has been undertaken. The goals of this project can be grouped into several categories; these categories will each be discussed separately.

Morphological Analysis

The main aim of the morphological studies undertaken was to develop a new method to record objective, quantitative information on placer gold based on automated or semi-automated image analysis. This allows for the quick collection of large morphological data sets which can be used to perform a detailed, statistically based analysis of the relationship between placer grain morphology and alluvial transport distance.

Compositional Analysis

The compositional aspect of this project had two main focuses; electron microprobe analysis (EMPA) and laser ablation inductively coupled plasma mass spectrometry (LA-ICP-MS) analysis. EMPA analysis was been used widely in placer gold studies by other researchers, however LA-ICP-MS examinations of placer gold are relatively rare. This work aimed to develop a method for performing LA-ICP-MS analysis of placer gold, use that information to examine a large number of placer gold samples, and determine the utility of these studies.

Crystallographic Analysis

The main aim of the crystallographic studies undertaken for this project was to investigate the applicability of a number of methods used to examine crystal structures in the study of placer gold. Limited examinations, suffi-

cient to indicate their potential future use, were performed using each of the methods to evaluate their utility.

Combining Methods

For all of this work, each grain was given a unique identifier code, allowing correlation of results between every analysis type. This allows individual aspects of placer gold to be examined in combination:

- Geological studies and previous investigations have shown that it is extremely likely that there are multiple sources for each placer deposit within the Klondike District. Morphology of placer gold has been used alone in the past to estimate distances to source. By combining shape and EMPA information, it has been to possible to identify individual populations in a given sample and improve the accuracy of distance to source as well as examine the effect of composition on shape change during alluvial transport.

- EMPA results have been used to aid in LA-ICP-MS studies, and together these methods have allowed a detailed examination of the compositional fingerprint of individual lode sources, and placer sample populations. Furthermore, the LA-ICP-MS results have been able to reveal compositional trends not evident from major element compositions alone, which may reveal information on the nature of the gold deposits across the Klondike.

- Compositional information is also required to interpret some crystallographic results, in particular chemical etching features. For example, it must be confirmed that individual etching features are crystallographic and not compositional in nature. The overall crystallographic nature of the grains must be compared with their composition and geological location, as it is unknown how composition and alluvial transport processes may affect internal crystallinity.

- All of these methods have be used to examine the formation of gold rich rims on placer gold. Rims have previously been identified using EDS mapping and EMPA analysis. Examination of crystallographic textures on and near gold rich have been made. These methods provide new evidence indicating how these rims form.

1.2 Anticipated Results

1. A new method for rapidly obtaining quantitative morphological information on placer gold. This method should also be generally applicable to the morphological analysis of any separated particles.

2. A model describing the morphological changes of placer gold during alluvial transport based on the statistical analysis of fully quantitative morphological data sets. This model, although generated for the Klondike District, will hopefully provide a case study for generation of similar models for locations worldwide.

3. A new method for the collection and analysis of trace and minor element concentrations using LA-ICP-MS.

4. Several new methods for extracting crystallographic information from placer gold grains, and a comparison between those methods and the results obtained from them.

5. New insights into the general behavior of placer gold including a better understanding of the morphological changes in placer gold during alluvial transport and the importance and/or meaning of crystallinity.

6. A detailed examination of trace and minor element concentrations for gold from across the Klondike District. This may provide insight into the nature and genesis of gold deposits in this region.

1.3 Background Information

This study was performed in the Klondike gold district for several reasons: the area is still being mined resulting in easy access, there are numerous known deposits, there are significant differences in geology and stream geology over the area, the area is unglaciated, and there has been significant previous work in the area providing a solid background for this study.

Anecdotal evidence has long indicated that placer gold morphology can be documented and used as an exploration tool, and qualitative observations of these changes (e.g., Dilabio, 1991; Loen, 1994; Márquez Zavalía, 2004) have been used to target exploration for bedrock gold sources since the inception of placer gold mining. Some modern attempts at quantifying grain morphology have monitored many aspects of grain morphology simultaneously by using semi-quantitative classification systems based on visual comparison

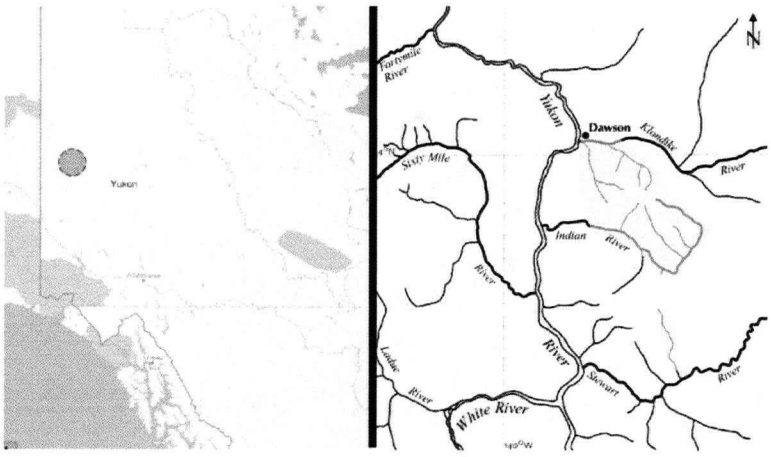

Figure 1.1: Study Location

to standard grain shapes (e.g., Knight, 1999a; Wierchowiec, 2002). Assigning each type grain a numerical value produces quantitative data which can then be treated with conventional statistics. These approaches represent a substantial improvement over strictly qualitative observations since the type grains can be standardized, however, they still suffer from significant user bias, making comparisons between results obtained by different users difficult. A useful review of several studies focusing on placer gold, as well as an overview of several other examples using tracer minerals to locate lode deposits has been written by McClenaghan (2005).

Several studies have examined placer gold morphology in a quantitative manner (Loen, 1995; Youngson and Craw, 1999; Townley et al., 2003); however, their scope has been limited by the amount of labour required to manually record shape data. Since there is no easy way to incorporate qualitative descriptions of sample shape (such as observing that one group is generally flattened) into a rigorously statistical analysis, it is necessary to measure a large number of grains to ensure an accurate representation of the morphological range of a given sample. Unfortunately this is difficult using manual methods. Digital image analysis offers a number of improvements over manual morphological measurement. It still requires that each grain be handled for positioning prior to imaging, but once images are collected, automated analysis offers significantly increased speed, accuracy and reproducibility when compared to manual measurement (Ferson, 1985; Crawford et al., 2007).

There has also been a large amount of work done applying various types of morphological parameters to other problems in the geological sciences (e.g. Barrett, 1980), however these studies have focussed on relatively hard, brittle silicate minerals, and many of these results of these studies are not particularly relevant to the study of a relatively soft mineral such as placer gold. Some of the works examining certain morphological parameters such as roughness (Bergey, 2006) and the relative utility of different morphological parameters are however useful (Le Roux, 1997; Le Roux, 2004). The use of fourier shape analysis is also well described, and has been applied to numerous problems in a variety of fields (Kuhl et al., 1982; Bowman et al., 2000; Ferson, 2005). Fourier shape analysis can be used to examine morphology in a purely quantitative manner. By decomposing the shape of objects into a set of purely numerical parameters, it becomes possible to compare numerous aspects of object morphology (overall form, surface roughness, specific shape axes) in a quantitative, statistically based manner.

Numerous localities exist around the world where extensive placer gold deposits have been recognized and mined but for which no lode sources

have been conclusively identified; the Klondike Gold District in the Yukon, Canada is a prime example. This region makes a good study area; it has numerous identified lode gold sources, and likely many unidentified ones. Furthermore, the region has not undergone glaciation, and the current drainage pattern is believed to have been the same since formation and exposure of the gold deposits present (Duk-Rodkin et al., 2001; Westgate et al., 2002; Lowey, 2004). This eliminated many possible complications associated with studying transport relationships, but still present a situation that should allow for a model to be developed from known deposits, and tested on unknown deposits in the same area.

Previous studies in the Klondike (Knight et al., 1999b; Mortensen et al., 2005) have shown that there are multiple lode sources located over several spatial ranges, and that different source areas display distinct compositions (Outridge et al., 1998). Previous work on placer gold in this areas has been carried out with the goal of identifying the nature and approximating the location of the undiscovered lode sources. Together with the morphological analyses already mentioned, most of these studies have incorporated geochemical fingerprinting of the placer gold using electron microprobe, or in rare cases, laser ablation inductively coupled plasma mass spectrometry (LA-ICP-MS) methods (Outridge, P.M. et al., 1998; Knight, J.B. et al, 1999b; Knight, J.B. et al., 1994; Mortensen, J.K. et al., 2004; Márquez Zavalía, M.F., 2004; Mortensen, J.K. et al., 2006; Palacios, C. et al., 2001; Dumala, M.R., 2002; Youngson, J.H. et al., 2002). The composition of mineral microinclusions has been examined in some samples from the Klondike, and has shown significant promise in relating placer gold grains to specific lode sources (Leake et al., 1998; Chapman et al., 2000; Chapman et al., 2006). An examination of this type is underway in the Klondike as a part a the larger project that includes this thesis, but did not fall under the purview of this study.

There have also been several studies using LA-ICP-MS to study gold composition, mainly focussing on tracing the provenance of bullion samples for forensic purposes (Watling et al., 1994; Boshoff, 1995; Grigorova et al., 1998). There have been studied examining the composition of placer gold using LA-ICP-MS (McCandless et al., 1997; Outridge et al., 1998); these studies have been focused mostly on aspects of experimental methodology. There has yet to be a study examining a large number of samples from a large region with the goal of understanding the lode : source relationship, the variability observed or the implications of gold composition with respect to geology or metal source. There have also been some limited studies investigating aspects of the methodology for performing LA-ICP-MS examination

of gold, specifically looking at aspects of standardization (e.g. Kogan et al., 1994).

Placer grain shape : transport distance relationships are of particular interest in situations where lode sources remain unidentified, especially where the number and style of specific lode sources are poorly understood. Most previous studies of areas where the location of lode source(s) are unknown have taken the oversimplified approach of assuming that all of the gold grains in a given sample are derived from a single lode source (a monodisperse population) and have based transport distance : shape relationships on an average of some shape parameter for identified grain populations as opposed to individual grain measurements. Although this assumption may be valid in some simple cases, in many localities, multiple sources are more likely. These incorrect assumptions can lead to determining poorly fit population values that in some cases do not actually represent any of the true population values if the sample being considered is polydisperse. This can lead to the identification of fictitious relationships (or the observation of no relationships at all), and erroneous predictions. Kernel density estimation (Parzen, 1962) will be used in this study; it should allow for the determination of the underlying morphological and compositional population parameters in placer gold samples in a rigorously statistical manner, allowing many of these problems to be avoided.

Several potentially important parameters must be considered when attempting to identify shape : transport distance relationships . Shapes of gold grains are expected to be modified during alluvial transport by physical interaction with the stream (rock type, co-transported sediments etc.), so it is reasonable to expect that changes in these variables may affect the rate of shape change. The effect of stream gradient has been evaluated previously in a general way (Youngson et al., 1999), and will be examined further here. Furthermore, the composition of the gold may dictate the rate at which shape change occurs since pure gold is softer than alloys (Sterner-Rainer, 1926), and a range of compositions exists in the Klondike study area (Knight et al., 1999b). Neither of these potential complications has previously been examined in a detailed or quantitative manner.

Gold crystallinity is also being examined in this project. While this aspect of placer gold has drawn considerable interest from mineral collectors (Francis, 2004; Mauthner, 2004), the academic examination of gold crystallinity has been limited to qualitative descriptions of gross external morphology (Taber, 1942; Kulp III, 2004). Internal gold crystallinity has been almost completely ignored by the academic community, except for limited examinations related to gold precipitated by biological action (e.g. Klaus,

1999).

The formation of gold rich rims on placer gold grains is a matter of considerable debate. Numerous possible mechanisms have been proposed, including chemical leaching of all elements other than gold (Knight et al., 1999a), bacterial precipitation of new gold (Southam et al., 1994; Southam et al., 1996; Southam, 1998; Reith, 2006), surface self-electrorefining (McCready, 2003), transport and precipitation of gold by environmental organic acids (McCready, A.J., 2003), leaching by hydrothermal fluids, and growth of new gold in situ by inorganic methods (Groen, J.C., 1990; Benedetti, 1991; Craw, D., 1992). It has also been proposed by some workers that these compositional zones are formed in primary lode deposit (Loen, 1994). Much of the debate is between groups studying gold deposits in different parts of the world, which may indicate that each proposed mechanism is valid, with each process occurring in a different geological or surface weathering environment. Some of the debate has arisen from experimental methods (Watterson, 1991; Knight, 1993; Watterson, 1994), which indicates it is especially necessary with placer gold to confirm results seen from any one analytical method.

1.4 References

Barrett, P.J. The shape of rock particles, a critical review. Sedimentology, 1980, Vol. 27, pp. 291-303.

Benedetti, M., Boulgue, J. Mechanism of gold transfer and deposition in a supergene environment. Geochimica et Cosmochimica Acta, 1991, Vol. 55, pp. 1539-1547.

Bergey, E.A. Measuring the surface roughness of stream stones. Hydrobiologia, 2006, Vol. 563, pp. 247-252.

Boshoff, F., Barzev, A.I., Theron, S.J., de Wit, M.C.J. AARL Project No. R/94/208 gold characterization study. 2005. Anglo American Research Laboratories (Pty) Limited, Johannesburg, the Republic of South Africa.

Bowman, E.T., Soga, K., Drummons, T.W. Particle shape characterisation using fourier analysis. Cambridge University Engineering Department D-Soils TR315, Cambridge, United Kingdom, 2000, 20 pp.

Chapman, R.J., Leake R.C., Moles, N.R. The use of microchemical analysis of alluvial gold grains in mineral exploration: experiences in Britain and Ireland. Journal of Geochemical Exploration, 2000, Vol. 71, pp. 241-268.

Chapman, R.J., Mortensen, J.K. Application of microchemical characterization of placer gold grains to exploration for epithermal gold mineralization in regions of poor exposure. Journal of Geochemical Exploration, 2006, Vol. 91, pp. 1-26.

Craw, D. Growth of Alluvial Gold Particles by Chemical Accretion and Reprecipitation, Waimumu, New Zealand. New Zealand Journal of Geology and Geophysics, 1992, Vol. 35, pp. 157-164.

Crawford, E.C., Chapman, R.J., LeBarge, W.P., Mortensen, J.K. Developing a new method to identify previously unrecognized geochemical and morphological complexity in placer gold deposits in western Yukon. In: Yukon Exploration and Geology 2006, D.S. Emond, L.L. Lewis and L.H. Weston (eds.), 2007, Yukon Geological Survey, pp. 139-148.

Dilabio, R.N.W. Classification and interpretation of the shapes and surface textures of gold grains from till. In: Gisements alluviaux dor, La Paz, Bolivia, 1991, 297-313.

Duk-Rodkin, A., Barendregt, R.W., White, J.M., Singhroy, V.H. Geological evolution of the Yukon river: implications for placer gold. Quaternary International, 2001, Vol. 82, pp. 5-31.

Dumala, M.R., Mortensen, J.K. Composition of placer and lode gold as an exploration tool in the Stewart River map area, western Yukon. In: Yukon Exploration and Geology 2001, D.S. Emond, L.H. Weston and L.L. Lewis (eds.), Exploration and Geological Sciences Division, Yukon Region, Indian and northern affairs Canada, 2002, pp. 1-16.

Ferson, S., Rohlf, J., Koehn, R.K. Measuring chape variation of two-dimensional outlines. Systematic Zoology, 1985, Vol. 34, No. 1, March, pp. 59-68.

Francis, C.A. Gold Crystals: A Primer. Rocks and Minerals, 2004, Vol. 79, January/February, pp.24-29.

Grigorova, B., Anderson, S., de Bruyn, J., Smith, K., Stúlpner, K., Barzev, A. The AARL gold fingerprinting technology. Gold Bulletin, 1998, Vol. 31, No. 1, pp. 26-29.

Groen, J.C., Craig, J.R., Rimstidt, J.D. Gold-rich rim formation on electrum grains in placers. Canadian Miineralogist, 1990, Vol. 28, pp. 207-228.

Klaus, T., Joerger, R., Olsson, E., Granqvist, C. Silver-Based Crystalline Nanoparticles, Microbially Fabricated. Proceeding of the National Academy of Sciences, 1999, Vol. 96, No. 24, pp. 13611-13614.

Knight, J. Preliminary Evidence for the Involvement of Budding Bacteria in the Origin of Alaskan Placer Gold : Comment and Reply. Geology, 1993, Vol. 21, No. 3, pp. 279-280.

Knight, J.B., Morison, S.R., Mortensen, J.K. The relationship between placer gold particle shape, rimming, and distance of fluvial transport as exemplified by gold from the Klondike District, Yukon Territory, Canada. Economic Geology, 1999a, Vol. 94, 635-648.

Knight, J.B., Mortensen, J.K., Morison, S.R. Lode and placer gold composition in the Klondike District, Yukon Territory, Canada: Implications for the nature and genesis of Klondike placer and lode gold deposits. Economic Geology, 1999b, Vol. 94, pp. 649-664.

Kogan, V.V., Hinds, M.W., Ramendik, G.I. The direct determination of trace metals in gold and silver materials by laser ablation inductively coupled plasma mass spectrometry without matrix matched standards. Spectrochimica Acta, Vol. 49B, No. 4, pp. 333-343.

Kuhl, F.P., Giardina, C.R. Elliptical Fourier Features of a Closed Contour. Computer graphics and image processing, 1982, Vol. 18, 236-258.
Kulp III, J. L., Sarikaya, M., Evans, J.S. Molecular Characterization of a Prokaryotic Polypeptide Sequence that Catalyzes Au Crystal Formation. Journal of Materials Chemistry, 2004, Vol. 14, pp. 2325-2332.

Le Roux, J.P. A hydrodynamic classification of grain shapes. Journal of Sedimentary Research, 2004, Vol. 74, No. 1, pp. 135-143.

Le Roux, J.P. Comparison of sphericity indices as related to the hydraulic equivalence off settling grains. Journal of Sedimentary Research, Vol. 67, No. 3, pp 527-530.

Leake, R.C., Chapman, R.J., Bland, D.J., Stone, P., Cameron, D.G., Styles, M.T. The origin of alluvial gold in the Leadhills area of Scotland: evidencee from interpretation of internal chemical characteristics. Journal of Geochemical Exploration, 1998, Vol. 63, pp. 7-36.

Loen, J.S. Origin of placer gold nuggest and history of formation of glacial gold placers, Gold Creek, Granite country, Montant. Economic Geology, 1994, Vol. 89, pp. 91-104.

Loen, J.S. Use of placer gold characteristics to locate bedrock gold mineralization. Exploration and Mining Geology, 1995, Vol. 4, No. 4, 335-339.

Lowey, G.W. Placer Geology of the Stewart River (115N&O) and part of the Dawson (116B&C) map areas, west-central Yukon, Canada. Yukon Geological Survey, 2004, 275p.

Márquez-Zavalía, M. F., Southam, G., Craig, J.R., Galliski, M.A. Mor-

phological and chemical study of placer gold from the San Luis Range, Argentina. The Canadian Mineralogist, 2004, Vol. 42, pp 169-182.

Mauthner, M. Morphology of Gold Crystals from the Yukon Territory, Canada. Rocks and Minerals, 2004, Vol. 79, March/April, pp.100-109.

McCandless, T.E., Baker, M.E., Ruiz, J. Trace element analysis of natural gold by laser ablation ICP-MS: a combined external/internal standardisation approach. Geostandards Newsletter, 1997, Vol. 21, No. 3, pp. 271-278.

McClenaghan, M.B. Indicator mineral methods in mineral exploration. Geochemistry: Exploration, Environment, Analysis, 2005, Vol. 5, pp. 233-245.

McCready, A. J., Parnell, J., Castro, L. Crystalline Placer Gold from the Rio Neuquén, Argentina: Implications for the Gold Budget in Placer Gold Formation. Economic Geology, 2003, Vol. 98, pp. 623-633.

Mortensen, J.K., Chapman, R., LeBarge, W., Crawford, E. Compositional studies of placer and lode gold from western Yukon: implications for lode sources. In: Yukon Exploration and Geology 2005, D.S. Emond, G.D. Bradshaw, L.L. Lewis and L.H. Weston (eds.), Yukon Geological Survey, 2006, pp. 247-255.

Mortensen, J.K., Chapman, R., LeBarge, W., Jackson, L. Application of placer and lode gold geochemistry to gold exploration in western Yukon. In: Yukon Exploration and Geology 2004, D.S. Emond, L.L. Lewis and G.D. Bradshaw (eds.), Yukon Geological Survey, 2005, pp. 205-212.

Outridge, P.M., Doherty, W., Gregoire, D.C. Determination of trace elemental signatures by laser ablation inductively coupled plasma mass spectrometry as a potential aid for gold exploation. Journal of Geochemical Exploration, 1998, Vol. 60, pp. 229-240.

Palacious, C., Hérail, G., Townley, B., Maksaev, V., Sepùlveda, F., de Parseval, P., Rivas, P., Lahsen, A., Parada, M.A. The composition of gold in the Cerro Casale gold-rich porphyry deposit, Maricunga, belt, northern Chile. The Canadian Mineralogist, 2001, Vol. 39, pp. 907-915.

Parzen, E. On Estimation of a probability density function and mode. The Annals of Mathematical Statistics, 1962, Vol. 33, No. 3, pp. 1065-1076.

Reith, F., Rogers, S. L., McPhail, D. C., Webb, D. Biomineralization of Gold: Biofilms on Bacterioform Gold. Science, 2006, Vol. 313, 14 July, pp. 233-236.

Southam, G. Quantification of Sulfur and Phosphorous Within Secondary Gold Rims on Yukon Placer Gold. Geology, 1998, Vol. 26, No. 4, April, pp. 339-342.

Southam, G., Beveridge, T. J. The Occurrence of Sulfur and Phosphorous Within Bacterially Derived Crystalline and Pseudocrystalline Octahedral Gold Formed in vitro. Geochimica et Cosmochimica Acta, 1996, Vol. 60, No. 22, pp. 4369-4376.

Southam, G., Beveridge, T. J. The in vitro Formation of Placer Gold by Bacteria. Geochimica et Cosmochimica Acta, 1994, Vol. 58, No. 20, pp 4527-4530.

Sterner-Rainer, I.L. Properties of gold-silver-copper alloys. Zeitschrift fur metallkunde. Vol. 18, No. 5, May 1926, pp. 143-148.

Taber, S. Gold Crystals from the Southern Appalachians. American Mineralogist, 1942, Vol. 27, pp. 219-229.

Townley, B.K., Hérail, G., Maksaev, V., Palacios, C., de Parseval, P., Sepulveda, F., Orellana, R., Rivas, P., Ulloa, C. Gold grain morphology and composition as an exploration tool: application to gold exploration in covered areas. Geochemistry: Exploration, Environment, Analysis, 2003,Vol. 3, 29-38.

Watling, R.J., Herbert, H.K., Delev, D., Abell, I.D. Gold fingerprinting by laser ablation inductively coupled plasma mass spectrometry. Spectrochimica Acta, 1994, Vol. 49B, No. 2, pp. 205-219.

Watterson, J. R. Artifacts Resembling Budding Bacteria Produced in Placer-Gold Amalgams by Nitric Acid Leaching. Geology, 1994, Vol. 22, December, pp. 1144-1146.

Watterson, J. R. Preliminary Evidence for the Involvement of Budding Bacteria in the Origin of Alaskan Placer Gold. Geology, 1991, Vol. 20, April,

pp 315-318.

Westgate, J.A., Sandhu, A.S., Preece, S.J., Froese, D.G. Age of the gold-bearing White Channel Gravel, Klondike District, Yukon. In: Yukon Exploration and Geology 2002, D.S. Emond and L.L. Lewis (eds.), 2003, Yukon Geological Survey, pp. 241-250.

Wierchowiec, J. Morphology and chemistry of placer gold grains indicators of the origin of the placers: an example from the East Sudetic Foreland, Poland. Acta Geologica Polonica, 2002, Vol. 52, No. 4, 563-576.

Youngson, J.H., Craw, D. Variation in placer style, gold morphology, and gold particle behaviour down gravel bed-load rivers: an example from the Shotover/Arrow-Kawarau-Clutha river system, Otago, New Zealand. Economic Geology, 1999, Vol. 94, 615-634.

Youngson, J.H., Wopereis, P., Kerr, L.C., Craw, D. Au-Ag-Hg and Au-Ag alloys in Nokomai and Nevis valley placers, northern Southland and Central Otago, New Zealand, and their implications for placer-source relationships. New Zealand Journal of Geology and Geophysics, 2002, Vol. 45, pp. 53-69.

Chapter 2

An ImageJ[1] plugin for the rapid morphological characterization of separated particles and an initial application to placer gold analysis.[2]

2.1 Preface

Anecdotal evidence has long indicated that placer gold morphology could be monitored and used as an exploration tool, and qualitative observations of these changes (e.g., Dilabio, 1991) have likely been used to target exploration for bedrock gold sources since the inception of placer gold mining. Some modern attempts at quantifying grain morphology have monitored many aspects of grain morphology simultaneously by using semi-quantitative classification systems based on visual comparison to standard grain shapes (e.g., Knight et al., 1999; Wierchowiec, 2002). Assigning each type grain a numerical value produces quantitative data which can then be dealt treated with conventional statistics. These approaches are an improvement over strictly qualitative observations since the type grains can be standardized, however they still suffer from significant user bias, making comparisons between results obtained by different users difficult.

A number of purely quantitative studies have examined placer gold morphology (Loen, 1995; Youngson and Craw, 1999; Townley et al., 2003); however, their scope has been limited by the amount of labour required to

[1] ImageJ. http://rsb.info.nih.gov/ij

[2] A version of this chapter has been submitted for publication in the Journal "Computers and Geosciences"

manually record shape data. Since there is no easy way to incorporate an impression of sample shape (such as observing that one group is generally flattened) into a rigorously statistical analysis, it is necessary to measure a large number of grains to ensure an accurate representation of the morphological range of a given sample. Furthermore, manual measurement of morphological parameters is generally limited to identifying and measuring the three major axis lengths. These are the main problems that have limited studies to adequately characterizing a few samples, or superficially examining a larger number of samples.

Digital image analysis offers a number of improvements over these methods. It still requires that each grain be handled for positioning prior to imaging, but once images are collected, automated analysis offers significantly increased speed, accuracy and reproducibility when compared to manual measurement. Furthermore, image analysis allows measurement of morphological parameters which are either extremely time consuming or essentially impossible to obtain manually. Lastly, these improvements are easy to implement; most geoscience laboratories already contain all of the equipment necessary to collect the required data, and perform digital image analysis.

Here, we present a new technique based on an ImageJ plugin for gathering morphological information on samples of separated grains. By automating the collection of physical measurements, it is now relatively easy to obtain the quantity of data necessary for proper statistical analysis of grain morphology. This approach is currently being employed to re-examine the evolution of placer gold morphology during alluvial transport in a quantitative, statistically rigorous manner.

2.2 Method Development

In developing this new method, we identified several specific criteria as desirable, including; i) the ability to generate quantitative data, ii) the ability to measure a number of additional parameters not easily available by manual means, iii) part or full automation of the analysis, iv) ease of use, v) cost efficacy, and vi) software platform independence.

The parameters selected for measurement include:

- minor and major axis lengths
- major axis orientation
- feret

- feret orientation
- breadth
- area
- perimeter
- convex area
- convex perimeter
- radii of the smallest inscribed and largest circumscribing circles
- x,y location of the centre of mass of the grain on the image
- coefficients from a fourier analysis of the perimeter shape
- the number of steps taken to perform that analysis

Most of these measurements are shown in Figure 2.1

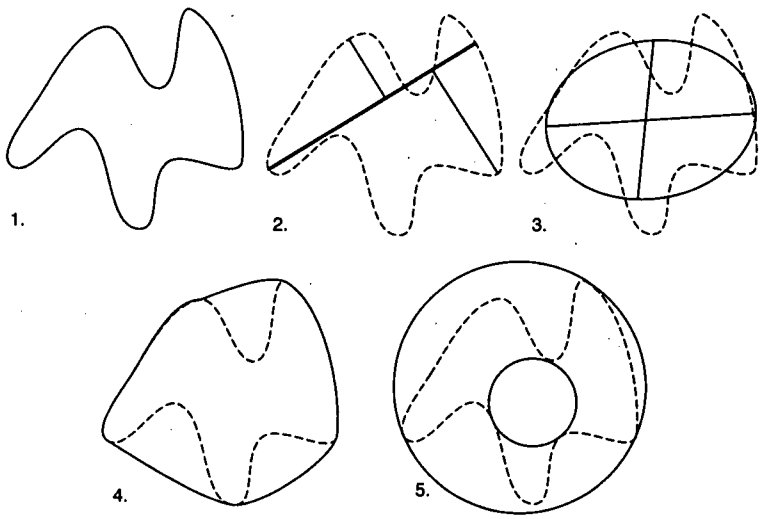

Figure 2.1: Measured Parameters. 1 : original shape perimeter and area, 2 : feret (thick unbroken line) and breadth (thin broken line), 3 : best fit spheroid and minor and major axes, 4 : convex hull which yields convex perimeter and area, 5 : largest inscribed and smallest circumscribing circles.

There are a wide variety of morphological descriptors which are commonly used in sedimentary research (e.g., flatness, roundness, aspect ratio, sphericity, concavity), which each have applications to different problems. In order to keep the utility as broad as possible, it was decided to have the plugin output consist of physical measurements, which are invariant, rather than calculated parameters, since different investigators may choose to examine different parameters. A comparison of some of these shape parameters, as well as a good discussion of the quantification of morphological information is provided by Barrett (1980).

Two dimensional fourier shape analysis mathematically traverses the edge of the shape, then deconstructs that path into two infinite series which describe completely the x and y coordinates of that path, i.e., the shape of the grain (Kuhl and Giardina, 1982). This produces a set of solely numerical parameters which can completely and exactly describe the shape. The two infinite series which describe the trace path are:

$$x(t) = A_0 + \sum_{n=1}^{\infty} ax_n cos(2n\pi\frac{t}{T}) + bx_n sin(2n\pi\frac{t}{T})$$

Equation 2.1: Fourier x Coordinate Series

$$y(t) = C_0 + \sum_{n=1}^{\infty} ay_n cos(2n\pi\frac{t}{T}) + by_n sin(2n\pi\frac{t}{T})$$

Equation 2.2: Fourier y Coordinate Series

where n is the harmonic level and is the major control on the frequency of the trigonometric functions and ay_n, by_n ax_n and bx_n are the variant fourier parameters calculated for each shape. The transform is performed by traversing the edge of the grain in a set period of time T, and t is some time $0 \leq t \leq T$. Fourier analysis is traditionally performed in the time domain and the equations for the analysis are defined in that domain, however the only real requirement is that the value of t/T spans the entire range from 0 to 1. The plugin uses the ratio of the number of the pixel under evaluation to the total number of pixels in the outline; this method ensures that all of the data available (every recorded pixel) is used to produce the fourier parameters. Kuhl and Giardina (1982), Ferson et al. (1985) and Bowman

et al. (2000) provide more detailed discussions of fourier shape analysis.

These equations also allow a trace to be reconstituted from any given set of parameters, by summing over all desired harmonics (n), and for the entire range $0 \leq t \leq T$. It is possible to take any number of shapes, calculate their fourier parameters, average them, and reconstitute a shape from those averages, essentially generating an average shape in the same way it is possible to generate an average wt.% Au or fineness for a population of grains.

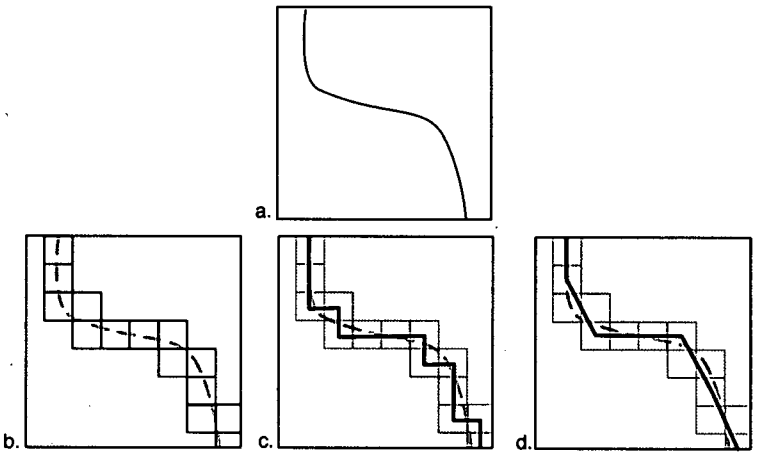

Figure 2.2: Accounting for pixellation errors by skipping pixels during edge traversing. a : original curve, b : pixel representation, c : represented shape with pixels per step = 1, d : represented shape with pixels per step = 3. Original curve shown as grey dashed line in b,c,d.

During fourier analysis, a provision is made to allow for smoothing of the outer border of a grain to account for pixellation; the border of the identified grain is traversed in integer steps of pixels (Figure 2.2).

Generally, the lower frequency fourier parameters (n = 1,2,3 etc.) inform the overall shape of the grain (form) while progressively higher frequency parameters describe finer and finer detail like surface textures. Figure 2.3 demonstrates the effect of fourier parameters at different n levels.

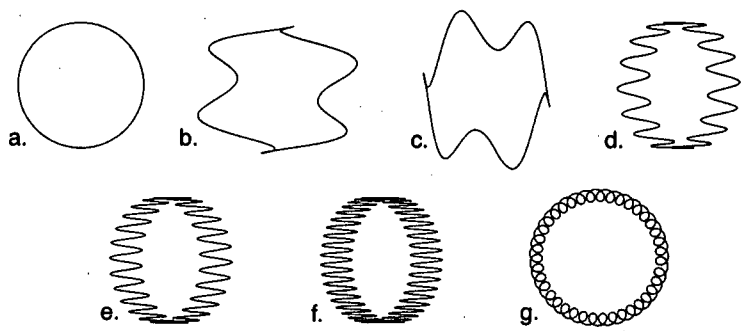

Figure 2.3: Effects of fourier parameters at varying n levels. All shapes drawn with $ax_1 = 1, ay_1 = 1, bx_1 = -1, by_1 = 1$ and all other parameters set at 0. a : no changes, b : $ax_5 = 0.5$, c : $by_5 = 0.5$, d : $ax_{15} = 0.5$, e : $ax_{25} = 0.5$, f : $ax_{40} = 0.5$, g : $(ax_{40}, ay_{40}, bx_{40}, by_{40}) = 0.1$.

2.3 Method Description

2.3.1 Software

The core of the method described in this paper is a plugin designed for ImageJ which satisfies the design criteria previously mentioned. The choice of the Java based ImageJ satisfies the criteria of platform independence, as it can be run on virtually any current major operating system (any Java enabled computer, Mac OS X, Mac OS 9, Linux x86 and Windows). ImageJ is also ideal because it is very easy to add additional functionality by developing macros and plugins to solve any particular problem. It is well suited to image analysis and modification problems as it has the capacity to handle a wide range of formats and has significant built-in image editing functionality. Furthermore, the base program and the vast majority of the macros and plugins that have been developed for it are freeware and open source.

There are several commercial image analysis programs available; however, their use was not pursued for several reasons. First, most are relatively expensive, and are not available for all platforms. Secondly, none of them performed all of the functions desired that are now available using the single macro described in this paper. Most importantly, these commercial packages offer limited customizability. Because of the open source nature of ImageJ, future users will be able to improve the method, or customize it to their own specifications. This is an important consideration, since the quantitative morphological analysis of gold is still a juvenile science, and because it is hoped that the use of this macro will be extended to other applications.

A number of plugins already exist to perform a variety of morphological measurements; however, none are exactly suited to our application. These plugins however did provide a starting point from which to develop our specific solution. Three existing plugins were selected which made many of the measurements previously identified. Particle_8_Plus[1] served as the main base for the image analysis, providing the code for identifying the grain boundaries, measuring feret, breadth, major axis length, minor axis length, area, perimeter, measuring the radii of the largest inscribed and smallest circumscribing circles and producing a labelled image of grain boundaries. The Snake plugin[2] provided some of the code for performing fourier shape

[1] G. Landinis Software.
http://www.dentistry.bham.ac.uk/landinig/software/software.html

[2] Thomas Boudier Softs Snake. http://www.snv.jussieu.fr/ wboudier/softs/snake.html

analyses, and the File Opener plugin [1] provided the base for the batch processing capabilities. These plugins were amalgamated into a single entity; then additional processing capability and numerous other smaller changes were made to streamline the resulting plugin.

There is some user input required for each image (or batch); a dialog box is presented that allows for the appropriate options to be selected. The user must specify the minimum and maximum size of grains to be identified and analyzed; this is a filter to prevent extraneous debris (such as dust) in the image from being identified as grains, or to allow the selective analysis of grains of one size group. The magnification of the image must be selected, which dictates the conversion of measurements in pixels into true units. The number of fourier parameters to be calculated must be input, and as well the step distance in pixels for the fourier analysis. The macro provides the option to generate a labelled or unlabelled image of the grain perimeters reconstructed from the fourier parameters. Also, the option to output the identified grain perimeters (with or without labels), and the option to output the calculated data as a text file or not, are given. These options are provided to increase the utility of the plugin, while allowing users to avoid dealing with the additional files if they are not desired.

2.3.2 Imaging

Grains are prepared for imaging by manually separating them from field panned concentrates under a stereo microscope. The grains are arranged on transparent adhesive sheets with the smallest axis parallel to the sheet. Grains are then imaged using a consumer grade digital camera attached to a petrographic microscope with a blue backlight (transmitted light mode). Grains are imaged individually, or in groups, dictated by the resolution of the camera and the quality of image desired for the analysis. For our study, a full screen image on a 3.34 megapixel camera was sufficient to analyze groups of up to 25 grains. Grains are then rotated 90^o so the minor axis is perpendicular to the transparent sheet, and the grains reimaged in the same groupings as used for the first orientation.

2.3.3 Image Cleanup

Generally, if care is taken during mounting, no clean-up is necessary. If there are large dust particles or extraneous material present in any image, it is easiest to remove them manually at this stage. In some cases, the brightness

[1] File Opener. http://rsb.info.nih.gov/ij/plugins/file-opener.html

and contrast settings must be changed if they were not optimized during the initial image capture.

2.3.4 Software Calibration

The plugin developed has built in conversion values that specify a scaling factor allowing for conversion of pixel measurements to true physical units. The plugin package comes with instructions for properly changing these values in the code, which has been designed to make these changes easy to make for those not familiar with Java coding. This step needs to be completed only once when the package is being set up to run with any specific equipment setup. It is also relatively easy to change the image manipulation routines in the program and the automatic naming system of the output files.

2.3.5 Image Processing

The plugin sequentially opens each image selected for processing and splits them into red, green and blue channels. The blue channel is selected, then thresholded to a 2 bit image. That image is flipped vertically and horizontally (to account for image flipping by the microscope and camera setup during image collection). The plugin then runs the built in image analysis routine of ImageJ to determine the minor and major axis lengths, the area and perimeter of each grain. Next, every pixel of the image is sequentially examined. When a grain is detected, the plugin then proceeds around the edge, identifying the boundary of the grain, and storing the x,y coordinates of these bounding pixels to memory. Mathematical analysis of this coordinate set reveals the remainder of the desired measurements. The plugin can then generate and save to disk a new image consisting of the outlines of the grains analyzed, with or without labels on the outlines. These labels correspond to the numerical measurements which are output along with the labels as a tab delimited text file (if output is desired), and to the labels on the reconstructed fourier images, if those are output. The labelling protocol attempts to identify and number the grains in a normal book reading sense (top left to bottom right), to facilitate correlating the measurements made with any later data requiring further manipulation of the grains. If no grains are identified (usually because of the grain size filter), no files are produced.

2.3.6 Fourier Shape Analysis Calculations

Most of the previously mentioned variables measured correspond to physical properties which are intuitive or easily described. The data produced from the fourier shape analysis, however, is not, so these variables warrant further explanation. The fourier analysis produces a set of variables: $A_0, C_0, ax_n, bx_n, ay_n$ and by_n which collectively describe the shape of each grain. Although the series states a sum over an infinite range, n only needs to go to moderate values (<40) to accurately represent most shapes. Increasing the number of parameters calculated yields a better fit to the trace, and although it is tempting to use a very large value to obtain an extremely accurate fit, the impact on the goodness of fit of the analysis decreases as 1/n (Kuhl and Giardina, 1982), and interpreting the large number of variables generated can become onerous. Finding a reasonable value for n is important, otherwise the amount of data generated becomes overwhelming. A_0 and C_0 can generally be ignored as they simply relate to the location of the object on the image. The analysis of a single shape at the n=40 level then returns 4*40 = 160 variables; if this method was extended to a moderate number of samples (e.g., 100) for several locations (e.g., 10), there are already 160,000 values to be tabulated. If a fourier shape analysis is being considered, the desired outcome should be kept in mind (Bowman et al. (2000), discuss this issue in greater depth). Fourier parameters can describe surface features at a variety of scales; n = 1 $\rightarrow$ 4 values could be used to describe overall particle shape, whereas intermediate terms might describe roundness (e.g., to discriminate between alluvially rounded vs. virgin quartz fragments), and high frequency (large n) terms could describe fine surface roughness or detail. From an analysis at n = 200 one might be able to select 5 or 6 values which could together describe a grain at several diverse size scales.

Since the grains for this analysis have been manually arranged, the orientation of the grains in an image is roughly random, and the grains cover a range of sizes. Thus, if values are to be compared between samples, it is important to use fourier parameter calculations that ignore rotational and translational differences, yielding parameters that describe a shape independent of position, size and rotation. These normalized parameters can then be averaged (for each n) to give an average representation of a group of shapes. The plugin provides rotation normalize parameters by rotating the outlines so that t = 0 for the fourier analysis corresponds to the orientation of the major axis and traversing the perimeter in a counterclockwise direction as shown in Figure 2.4. The fourier variables are also size normalized

by dividing them by the dimension of the minor axis.

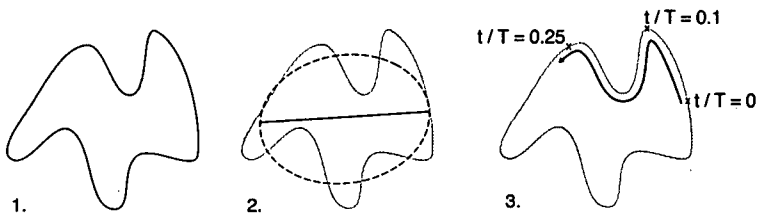

Figure 2.4: Normalizing fourier parameters for shape. 1 : measured grain outline, 2 : best fit ellipse and major axis, 3 : trace is analyzed starting at one intersection of each grains major axis and perimeter proceeding in a counterclockwise direction.

2.4 Results

The method was applied to a large number of samples of placer gold from the Klondike placer gold District in the western Yukon Territory, Canada, and has allowed quantitative morphological measurements to be made for 7977 grains. The most grains previously measured in a single study was ~1500 (Townley et al., 2003). Using the procedure described above, grains can be mounted, photographed and the photos cleaned up at a rate of 500 grains / day. The image processing is now fully automated, and hundreds to thousands of photos can be analyzed overnight (10 hours), depending on the number of grains per photograph, and the speed of the computer. Figure 2.5 shows an example of a set up input and output images from analysing a placer gold sample, and Table 2.1 shows the data that is output into the text file for that analysis. The macro can be instructed to ignore edge grains, so the aperture visible in the photo is not identified as a grain. Also, very thin, translucent or transparent objects do not show up because they appear too light in the image and are interpreted to be part of the background during thresholding, so the reference mark in the lower right corner and most visible dust grains do not need to be deleted before processing.

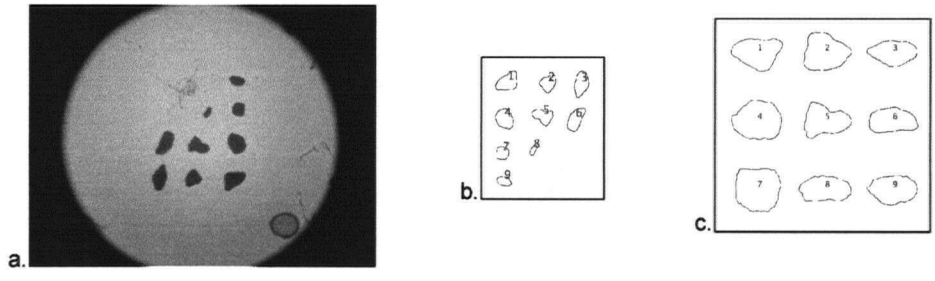

Figure 2.5: Input and output files. a : A raw recorded image suitable as plugin input, b : output labelled image of identified grains and their boundaries, c : output labelled image of a fourier reconstruction at n = 40.

Particle	Area	Perim.	Feret	Breadth	Feret Angle	Min Axis	Maj. Axis	Axis Angle	Convex Perim.
1	4058	262.21	96.426	63.085	40.795	88.94	58.093	33.136	251.44
2	2768	209.04	70.937	57.685	68.499	65.357	53.924	50.128	201.17
3	3763	254.94	99.825	53.394	79.028	95.366	50.24	78.144	244.91
4	3768	239.28	79.259	60.75	119.48	78.325	61.252	122.57	227.81
5	3070	240.94	79.429	59.374	169.11	77.864	50.201	160.62	224.67
6	3709	257.52	96.021	53.905	54.324	97.322	48.524	61.609	245.37
7	1831	166.23	52.431	51.191	34.902	48.924	47.652	91.585	159.71
8	665	107.4	40.497	20.841	57.095	41.782	20.265	61.662	104.62
9	1485	157.44	58.241	34.34	164.05	56.626	33.391	165.36	150.36
Convex Area	Min circum. circ	Max inscr. circ	X pos	Y pos	FP Steps	ax_1	bx_1	ay_1	by_1
4239	49.34	24.33	524.51	316.79	114	1	0.4196	0.27324	-0.70419
2921	38.089	22.358	675.17	321.49	88	1	0.35546	0.30074	-0.84587
3922	53.089	23.51	797.82	322.74	109	1	0.30519	0.18631	-0.58343
3924	41.911	27.792	513.82	450.77	103	1	0.24698	0.21414	-0.8224
3416	43.919	17.405	656.62	441.02	102	1	0.35675	0.24476	-0.70886
3880	52.091	20.228	777.41	451.95	110	1	0.1345	0.087006	-0.5691
1906	27.476	20.332	506.33	575.51	75	1	0.44672	0.44817	-0.97212
716	20.335	7.7841	620.48	565.01	45	1	0.70614	0.38663	-0.56459
1579	30.539	14.795	512.03	679.34	67	1	0.58642	0.37553	-0.6491

Table 2.1: Data output from plugin analysis of grains in Figure 5 analyzed at n=1, magnification = calibrate (all other values default). Table output is formatted into 20 columns x 10 rows, but is split up here for ease of viewing.

Figures 2.6 and 2.7 demonstrate some aspects of the fourier shape analysis. Figure 2.6 qualitatively demonstrates the increase in the goodness of fit with increasing n, and shows that the lower frequency (low n value) terms describe the overall shape; by n = 10 the reconstructed shape generally matches the shape of the grain. Significantly increasing the value of n is required to obtain a reconstructed shape with sharp corners, and an accurate representation of the perimeter roughness. This shows why the purpose of a fourier analysis should be considered before the analysis is performed. A study at n = 3 will be of little use studying fine surface features, whereas a study at n = 200 will be excessive if one is examining only overall grain shape. Figure 2.7 shows how fourier parameters can be used to generate average shapes. The three input shapes (a square, circle and triangle) were measured at n = 40, then the parameters averaged for each pair and for all of the shapes. If fourier parameters are being used to differentiate between groups of shapes, then this allows an average shape to be produced for each group, providing an easy way to visually present the results. These averaged parameters were then used to reconstruct the combined shapes shown in the figure using equations 2.1 and 2.2.

2.5 Discussion

The fourier parameters are essentially independent of size and rotation, however as the size of the images being analyzed decreases, the actual shape of the grains recorded by the digital data changes due to pixellation. The analysis picks up on these changes, and the resulting fourier shape parameter (and other measurements in more severe cases) are affected. This problem has not been fully explored, but initial tests (see Figure 2.8) indicate that ~200 steps or more are required for the parameters calculated to be realistically size independent. Even at this number of steps, there is still scatter in higher frequency terms, attesting to the ability of this analysis to capture detailed shape information, and demonstrating that the images of the grains being analyzed should be of the highest quality (large image size and/or resolution) possible. If this analysis is to be used in the future, a more detailed examination of the effects of image resolution on the values measured should be made.

The development of this new plugin for ImageJ now allows the rapid, easy qualitative morphological analysis of images of separated grains. Work using this plugin has already generated a large amount of data for placer gold morphology in the Klondike gold District, and has formed the basis

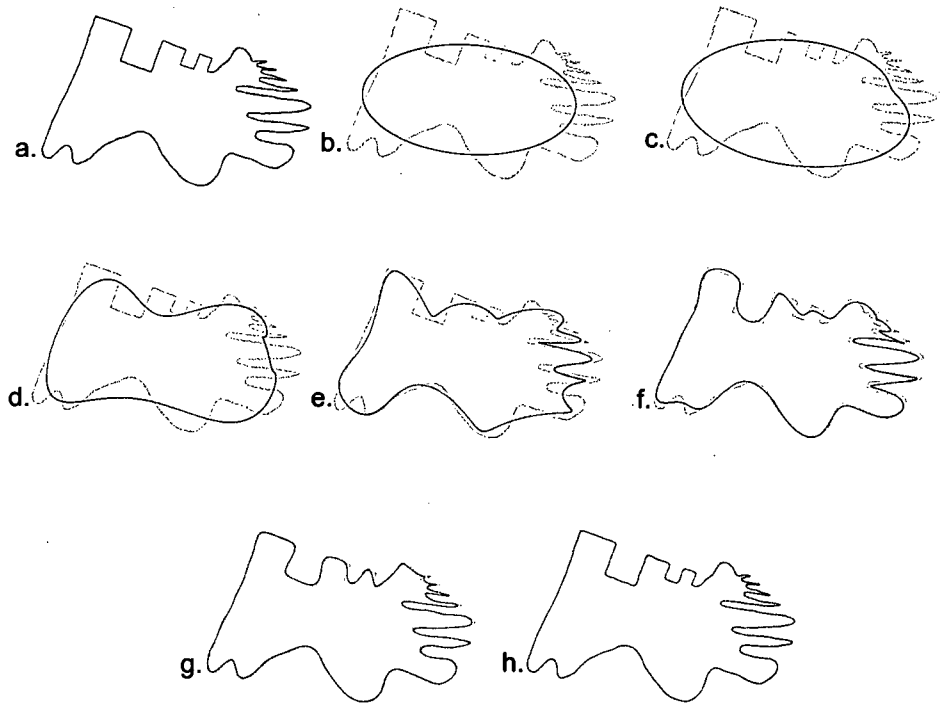

Figure 2.6: Reconstructing grain images from fourier parameters at different n values. a : original grain perimeter, b : n=1, c : n=2, d : n=5, e : n=10, f : n=20, g : n=40, h : n=100. For b,c,d,e,f and g original input shape is also drawn as a grey line.

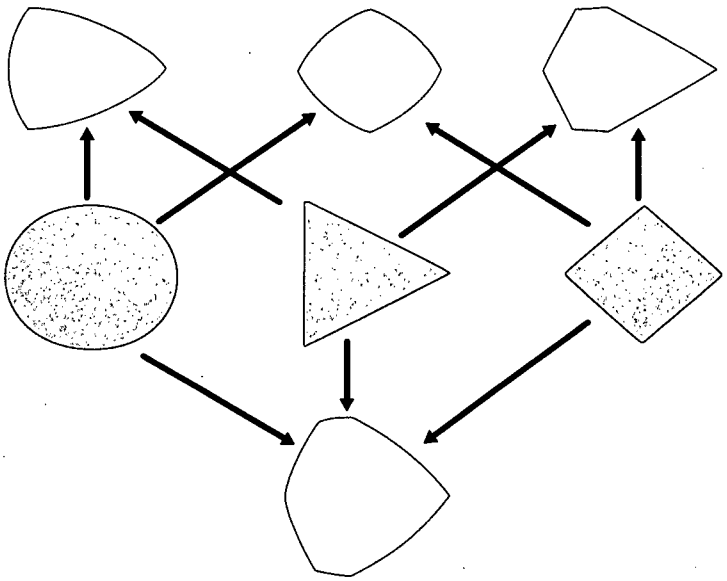

Figure 2.7: Using fourier shape analysis to generate average shapes. Middle row (shaded figures) shows original input shapes; upper row illustrates binary combinations shown by arrows, bottom row shows combination of all three shapes. Shapes were analyzed, parameters averaged and shapes reconstructed at n = 40.

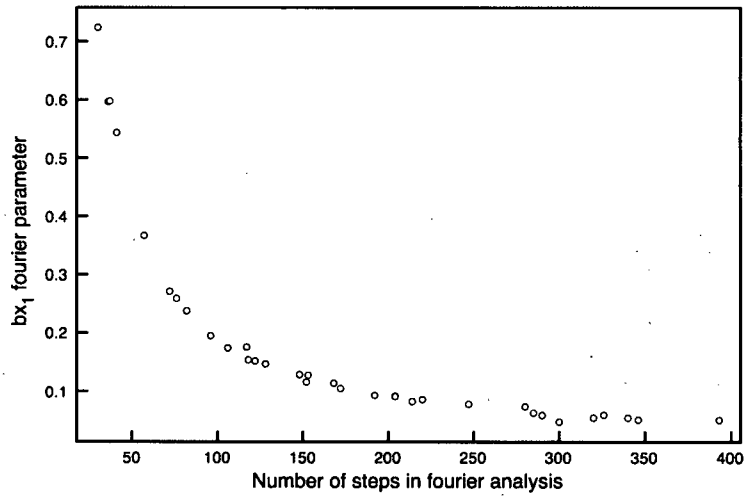

Figure 2.8: Relation between determined fourier parameter bx_1 and number of steps during fourier analysis for circles of various sizes. (2 pixels per step for all analyses).

for a preliminary model describing the evolution of grain shape during alluvial transport. The current morphological study only utilizes the three axis lengths measured for each grain, and an established morphological parameter (the Hofmann Shape Entropy; Hofmann, (1994)). Several shape factors were examined for use in this study, as there has been no best parameter previously identified for examining the alluvial transport of placer gold. Figure 2.9 shows the value of three popular shape factors for the entire range of grain shapes (n.b., the Cailleux shape factor is equivalent to the flatness index). In these plots, the centre of the plot would represent a spheroid shape, with all three axis lengths equal, the edges would represent circular discs, and the vertices would be rods. The major, overriding shape change observed qualitatively for placer gold is an evolution from grains of overall spherical shapes towards flattened discs. To best monitor this change, the chosen shape parameter should thus display the greatest change in value from the centre of the plot towards an edge; the Hofmann shape parameter was chosen because it has the largest change in value between these positions.

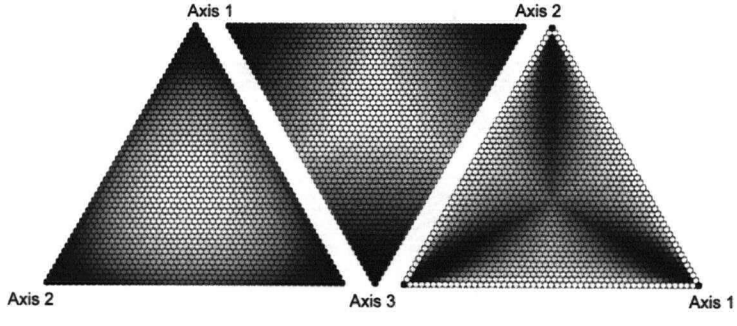

Figure 2.9: Hofmann shape entropy, Cailleux and Corey (from left to right) shape parameter values for all possible combinations of grain axis lengths. White represents a value of 1, black represents a value of 0.

The preliminary model for placer gold grain shape change during transport (measured using the Hofmann Shape entropy) is shown in Figure 2.10. Although this model is a significant improvement over results by previous workers (e.g., Knight et al., 1999), there is still significant scatter, which reduces the accuracy of predictions made using the model. Current work combining morphological and compositional data should allow this model to be better constrained, ultimately producing an accurate method for estimating the travel distance from source for the placer gold in the Klondike

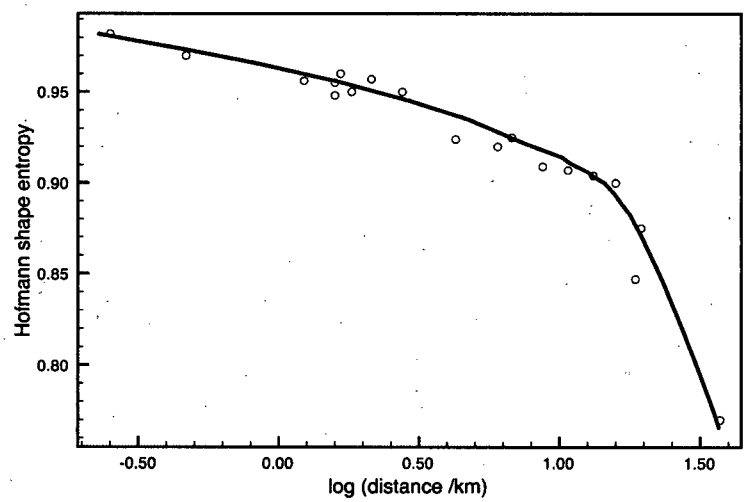

Figure 2.10: Preliminary model showing evolution of Hofmann shape entropy values during alluvial transport for placer gold from the Klondike District, YT, Canada.

District. Initial indications are that monitoring a single well-chosen shape parameter will allow for a model to be generated with an error on the prediction of source location that is small enough to be useful for exploration purposes at the regional scale. It may, however, prove necessary to examine additional shape parameters for locating lode sources over different scales, or to allow even more accurate predictions to be made.

There has also been some previous work attempting to examine grain surfaces, and to correlate surface features with transport distance. This work has been exclusively qualitative, but has generally recorded that grains become smoother with increasing transport. This new plugin allows for several qualitative measures of surface roughness to be made. The ratios of convex perimeter : perimeter (perimeter roughness) and area : convex area (area roughness) will both achieve a maximum value of 1 when a grain presents a rounded, entirely convex cross section such as an oval or circle. A rough grain with indents and promontories will record values less than 1. Additionally, the fourier parameters measured may provide a measurement of surface roughness; higher frequency terms will be significantly non-zero when there is small detail present on a grain surface. Unfortunately, all of these parameters are only calculated in two dimensions; the best approximation this method can do to three dimensions is to take an average (of the absolute values for the fourier parameters) of the parameters for the two cross section images analyzed of each grain. These three roughness measurements are compared against the Hofmann shape parameter for all of the grains imaged for this study in Figures 2.11, 2.12 and 2.13. Figure 2.11 shows that grains with higher Hofmann shape entropy values generally have a wider range of perimeter roughness values, but the overall range in the roughness values and scatter in the data makes it difficult to use predictively. Figures 2.11 and 2.12 both show the opposite relationship expected, at least in the maximum value observed for the roughness; the grains with smaller Hofmann entropy values (observed in far traveled samples) have generally lower roughness values (indicating rougher grains). The bulk of the samples (where the density of data points results in a black wedge) do however indicate that roughness decreases on average with decreasing values of the Hofmann shape entropy. Little or no relationship was observed between the fourier parameter ax_6 and the Hofmann Shape entropy. Similar results were seen for a comparison between the Hofmann shape entropy and the fourier parameter ax_{15}. Area roughness and perimeter roughness values correlate fairly well (Figure 2.14), indicate that these two parameters likely are monitoring similar changes in morphology. These results may indicate that surface roughness is removed extremely quickly during alluvial transport, and

systematic changes will not be observed over the transport distances these samples represent. Future studies examining extremely short transport distances, however, may find use for these measurements. It is also possible that the information recorded in the two cross sections is not representative of the entire grain surface, the parameters chosen may simply not be an accurate measure of surface roughness, or the surface roughness does not experience a well-defined systematic change during alluvial transport.

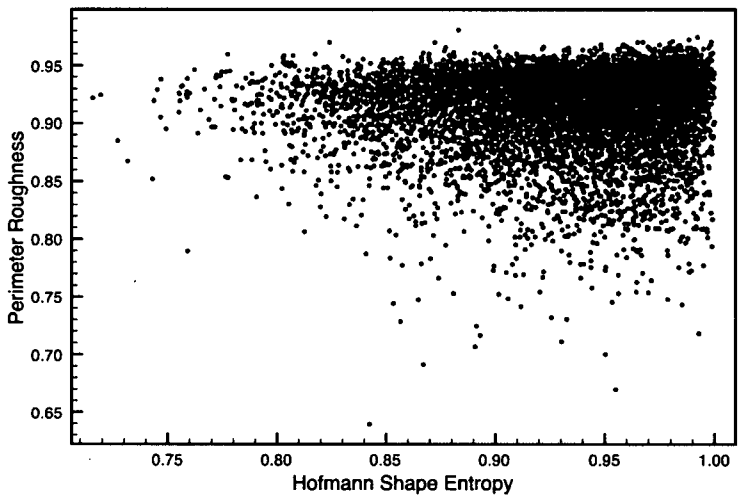

Figure 2.11: Perimeter roughness versus Hofmann shape entropy for Klondike District and surrounding area placer gold grains.

We do not suggest that the qualitative examination of surface texture is without merit; however, such observations are difficult, if not impossible, to analyze statistically or include in a purely quantitative model. Qualitative surface feature observations still play an important role in understanding the processes that occur during alluvial transport, and may provide insight into additional quantitative morphological parameters that should be examined to quantify alluvial transport. There is also a balance to be made between determining the least number of descriptors that can be used to predict transport distance to the accuracy level desired; arguably, by examining an extremely large number of parameters one may be able to make much more precise predictions, however the added time and computational complexity in examining numerous parameters may be unnecessary to make

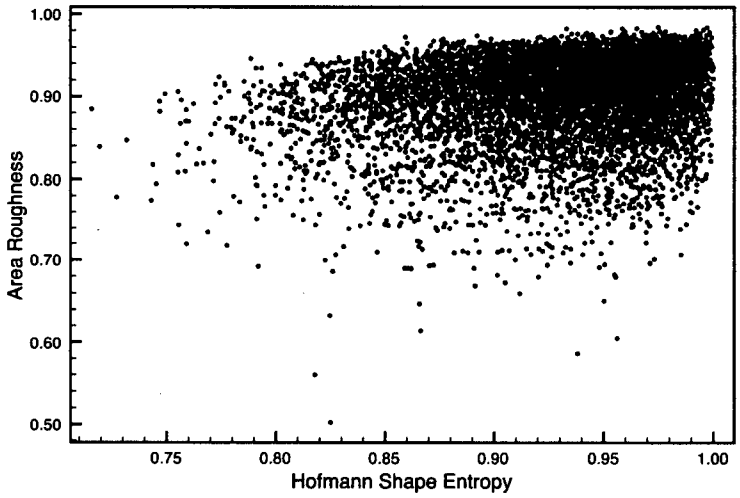

Figure 2.12: Area roughness versus Hofmann shape for Klondike District and surrounding area placer gold grains.

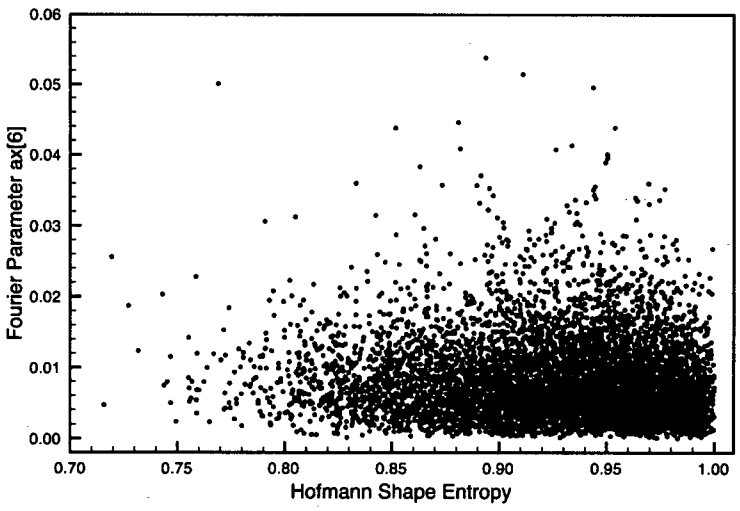

Figure 2.13: Fourier parameter ax_6 versus Hofmann shape entropy for Klondike District and surrounding area placer gold grains.

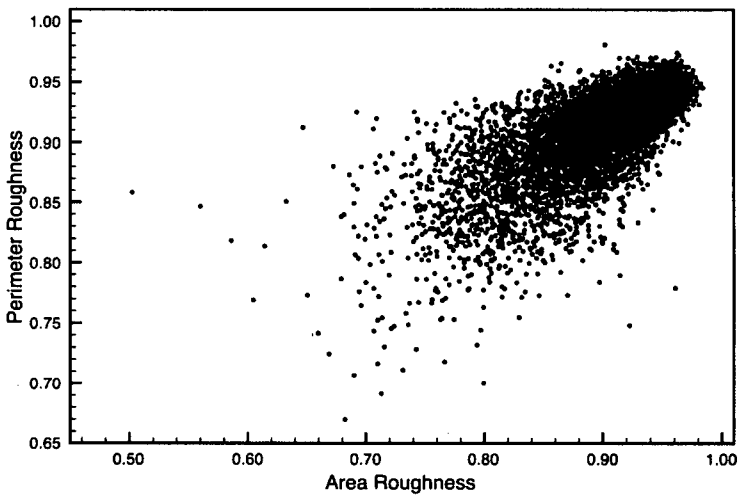

Figure 2.14: Perimeter roughness versus area roughness for Klondike District and surrounding area placer gold grains.

useful predictions.

This new method is a substantial improvement, however there are still some limitations. The manual arrangement of the grains is time consuming and can impose a user bias; the user must identify the minor axis, and accurately rotate each grain 90°. The input images must also be relatively clean of dust and debris. Even taking these factors into account, this method is a significant improvement over the methods employed by previous investigators. Additional automation could eventually be incorporated, such as by using laser grain sizing, or some novel automated grain handling and imaging system. Image processing and physical measurement technology also continue to improve at a rapid pace, and it may soon be possible to automatically digitize grain shape in 3D, allowing for the parameters discussed in this work, as well as many others (e.g., surface area, volume), to be calculated with increased accuracy.

2.6 Other Applications

Although the impetus for the development of this plugin was for the morphological analysis of placer gold, the data produced is not specific to placer gold, and can be applied to any grain morphology analysis. Work is currently underway modifying this plugin for the morphological analysis of zircon and apatite; estimating grain volumes and surface areas for use in calculating of U/Th-He ages. The data produced by the macro could be applied to similar problems of tracking grain morphology evolution such as the study of kimberlite/diamond tracer minerals, or any other placer mineral (platinum, diamond, sapphire). The plugin could even be extended to biological applications; previous studies have quantified differences between phenotypes using fourier shape parameters (Ferson et al. 1985). This new plugin would provide a way to measure these fourier parameters quickly, and at the same time collect additional information such as size. Since the macro can be scaled to process images of any size, it might even play roles in fields such as archeological artifact examination.

2.7 Acknowledgements

The authors wish to thank the numerous placer miners who provided samples for this study, as well as Dr. Rob Chapman and Bill LeBarge for help in sample collection. Dr. Richard Friedman and Kirsten Rasmussen were invaluable in testing the plugin, and helping to work out the final bugs.

2.8 References

Barret, P.J. The shape of rock particles, a critical review. Sedimentology, 1980, Vol. 27, 291-303.

Bowman, E.T., Soga, K., Drummons, T.W. Particle shape characterisation using fourier analysis. Cambridge University Engineering Department D-Soils TR315, Cambridge, United Kingdom, 2000, 20 pp.

Dilabio, R.N.W. Classification and interpretation of the shapes and surface textures of gold grains from till. In: Gisements alluviaux dor, La Paz, Bolivia, 1991, 297-313.

Ferson, S., Rohlf, F.J., Koehn, R.K. Measuring shape variation of two-dimensional outlines. Systematic Zoology, 1985, Vol. 34, No. 1, 59-68.

Hofmann, H.J. Grain shape indices and isometric graphs. Journal of Sedimentary Research, 1994, Vol. 40, 1054-1056.

Knight, J.B., Morison, S.R., Mortensen, J.K. The relationship between placer gold particle shape, rimming, and distance of fluvial transport as exemplified by gold from the Klondike District, Yukon Territory, Canada. Economic Geology, 1999, Vol. 94, 635-648.

Kuhl, F.P., Giardina, C.R. Elliptical Fourier Features of a Closed Contour. Computer graphics and image processing, 1982, Vol. 18, 236-258.

Loen, J.S. Use of placer gold characteristics to locate bedrock gold mineralization. Exploration and Mining Geology, 1995, Vol. 4, No. 4, 335-339.

Townley, B.K., Hérail, G., Maksaev, V., Palacios, C., de Parseval, P., Sepulveda, F., Orellana, R., Rivas, P., Ulloa, C. Gold grain morphology and composition as an exploration tool: application to gold exploration in covered areas. Geochemistry: Exploration, Environment, Analysis, 2003,Vol. 3, 29-38.

Wierchowiec, J. Morphology and chemistry of placer gold grains indicators of the origin of the placers: an example from the East Sudetic Foreland, Poland. Acta Geologica Polonica, 2002, Vol. 52, No. 4, 563-576.

Youngson, J.H., Craw, D. Variation in placer style, gold morphology, and gold particle behaviour down gravel bed-load rivers: an example from the Shotover/Arrow-Kawarau-Clutha river system, Otago, New Zealand. Economic Geology, 1999, Vol. 94, 615-634.

Chapter 3

A Method for Predicting Lode Source Locations Using Morphological and Compositional Information from Placer Gold[1]

3.1 Introduction

Placer Gold deposits of the Klondike district and surrounding areas in western central Yukon represent extremely large deposits for which no lode sources have conclusively been identified. This area was the location for an extended study attempting to develop a method for predicting lode gold source locations using information from placer gold deposits.

Recent developments allowing the fully quantitative morphological analysis of placer gold combined with traditional methods for analyzing placer gold major element compositions and analytical methods not previously applied to placer gold research have allowed for the development of a well constrained model describing placer gold morphology changes during alluvial transport. This model allows for predictions of alluvial transport distance to source for placer grains taken from the study area, and may provide a way to predict lode gold source locations, and inform future hard rock exploration in this covered terrain.

The limitations of this model are discussed, as are the complicating effects of gold composition, stream geometry and other factors. The indications from this study are that the alluvial transport model developed here may be applicable outside of the Klondike area, and may provide a method for the identification of elusive lode gold sources worldwide where there are

[1]The information in this chapter has not yet been submitted for publication

significant placer deports. At the minimum, this work provides a method for probing the transport distance : shape relationship for a field area, and for developing a model to predict transport distances for placers from that area.

3.2 Introduction

Numerous localities exist around the world where extensive placer gold deposits have been recognized and mined but for which no lode sources have been conclusively identified; the Klondike Gold District in the Yukon, Canada, is a prime example. Many studies of placer gold in these areas have been carried out with the goal of identifying the nature and approximating the location of the undiscovered lode sources. Most of this work has involved geochemical fingerprinting of the placer gold using electron microprobe, or in rare cases, laser ablation inductively coupled plasma mass spectrometry (LA-ICP-MS) methods (Outridge et al., 1998; Knight et al, 1999; Knight et al., 1994; Mortensen et al., 2004). Results of some previous studies have also strongly suggested that quantifiable relationships exist between placer gold grain shape and transport distance. Until this point, however, no study has taken a fully quantitative approach to examining this relationship. Most previous studies have also been hindered by working with relatively small data sets or by not using a rigorous statistical approach to the problem, and/or by failing to consider many potentially complicating factors such as stream gradient. In addition, only a limited attempt has been made in previous studies to correlate morphological and compositional data, instead examining each of these data sets in isolation. Establishing a quantitative relationship between grain shape and transport distance, and developing a protocol for integrating shape : transport distance information with compositional data, has the potential to provide a powerful tool for locating potentially significant undiscovered lode gold deposits.

Placer grain shape : transport distance relationships are of particular interest in situations where lode sources remain unidentified, especially where the number and style of potential lode sources is poorly understood. Most previous studies of areas where the location of lode source(s) are unknown have taken the oversimplified approach of assuming that all of the gold grains in a given sample are derived from a single lode source (a monodisperse population) and have based transport distance : shape relationships on an average of some shape parameter for identified grain populations as opposed to individual grain measurements. Although this assumption may

be valid in some cases, in many localities, multiple sources are more likely. These potentially incorrect assumptions can lead to determining poorly fit population values that in some cases do not actually represent any of the true population values if the sample being considered is polydisperse. This can lead to the identification of fictitious relationships (or the observation of no relationships at all), and erroneous predictions.

A new approach to dealing with these complications forms a keystone of the current study. The study area for testing this approach is the Klondike Gold District in Yukon, Canada. Previous studies in the Klondike (Knight et al., 1999; Mortensen et al., 2004) have shown that there are multiple lode sources located over several spatial ranges, and that different source areas display distinct compositions (Outridge et al., 1998). For this study, grain populations will be identified based on composition and morphology simultaneously. Our analysis also begins with the initial assumption that most samples are polydisperse, with geological information being applied to inform the possible number of component populations in any given sample. For example, a sample located within a few hundred meters of a stream, and close to the head of that stream is likely only to have a single source, whereas a sample collected from a major stream that is fed from several individual tributaries is likely sourced from more than one lode.

Several potentially important parameters must be considered when attempting to identify shape : transport distance relationships . Shapes of gold grains are expected to be modified during alluvial transport by physical interaction with the stream (rock type, co-transported sediments, etc.), so it is reasonable to expect that changes in these variables may affect the rate of shape change. The effect of stream gradient has been evaluated previously in a general way (Youngson et al., 1999), and will be examined further here. Furthermore, the composition of the gold may dictate the rate at which shape change occurs, since pure gold is softer than alloys (Sterner-Rainer, 1926), and a range of compositions exists in the Klondike study area (Knight et al., 1999a,b). In this study we investigate the importance of these parameters with respect to shape change to determine whether their inclusion in a predictive model is warranted.

3.3 Method

3.3.1 Sample Collection

Most samples were collected from active placer mining areas in the Klondike Gold District, generally from gravels lying directly on fresh or partially de-

composed bedrock (Lowey, 2004). Some samples, especially some of the Indian River area samples in the southern Klondike and samples from White Channel Gravel deposits, were obtained from gravel units deposited on higher level benches. Gold grains were separated from gravel by hand panning, or using a small, portable, gravity fed sluice (bed area $1m^2$), with subsequent cleanup done using a hand pan. Generous thanks is due to the numerous placer miners who permitted the collection of samples from their placer claims or provided gold samples directly. The samples provided directly by placer miners were usually from the smaller size fractions (<2 mm^2 in largest cross section) of their bulk recovered material. We examined samples collected from 55 separate locations distributed over the entire Klondike District. A higher density of samples was collected from the Eldorado Creek and Bonanza Creek drainages. Most samples were collected specifically for this study, ensuring that several samples were collected in each drainage. In some locations a single sample in a drainage was collected to obtain more information on the composition range of gold in the region. Sample locations were dictated mostly by available access, and were therefore not always ideal for the desired purposes. Sample locations were determined precisely in the field using a hand held GPSR unit. Alluvial transport distances were measured using watercourse locations on current topographical maps (1:50000 scale), following the current watercourse path. Stream gradients were determined manually from topographical maps.

3.3.2 Sample Processing

In the lab, placer gold samples were dried by rinsing with ethanol several times and allowing to air dry at ambient temperature overnight. Gold was then manually separated from other heavy minerals under a binocular microscope. Gold grains were then roughly sorted by size and mounted on transparent adhesive sheet with their smallest axes parallel to the sheet. Grains were mounted in groups of from one to twenty-five within marked grid squared $25mm^2$. Each of these grid squares was then photographed against a blue backlight using a transmitted light microscope (Nikon Optiphot2-pol) attached to a digital camera (Nikon Coolpix 995, 3.34 megapixel). The image collection and analysis method was calibrated by imaging objects of known size. The grains were then reoriented so the short axis was perpendicular to the adhesive sheet, maintaining the same groupings, and re-photographed. These photographs were then processed using a image analysis routine developed in house (Crawford et al., 2006, Crawford and Mortensen, 2007), which assigned unique identifier numbers to each grain.

The long, intermediate and short axis length measured for each grain were then used to calculate the Hofmann shape entropy (HSE) (Hofmann, 1994) for each grain.

The grains were then transferred to a piece of conductive double sided adhesive tape affixed to a glass slide, arranged in numerical order by their unique identifying number. The grains were then examined using scanning electron microscopy (SEM; Philips XL-30), and images of their external morphology recorded in backscattered and secondary electron modes.

The grains were then cast into one inch diameter epoxy pucks using Buehler^{TM}epoxide resin (5:1 resin:hardener), allowed to cure overnight at ambient temperature and finally baked at 60°C for >5 hours. After cooling, the pucks were ground using Buehler carbimet SiC paper (grits 600, 400, 320, 240) on a Buehler Handimet 2 roll grinder so as to expose a section roughly bisecting the grains. Polishing was continued individually using a Buehler Minimet 100 automated polished with texmet 1000 cloths and 6, 3 and 1 μm diamond paste with Buehler Metadi extender cutting fluid. Polishing times and pressures were 6 minutes at 4 lbs; 8 minutes at 2 lbs and 10 minutes at 1 lb for the 6, 3 and 1 μm pastes respectively, with the soft stop option on in all cases. The pucks were then polished for five minutes at 0.75 kg pressure on a Buehler petro-thin polisher using Buehler micropolish 0.3 μm alumina powder and water as coolant and lubricant. Final polish was obtained using a Chemomet pad and Buehler Masterprep 0.05 μm alumina suspension at 0.5 kgs pressure with water as lubricant and coolant. Mounts were washed with soap and rinsed with hot tap water between each polishing step.

Samples were then carbon coated before a second examination on the SEM, where backscattered electron images were recorded to identify grain cores and rims, as well as any inclusions that might be present. A single spot not on an inclusion and in the core of each grain was then analyzed for Au, Ag, Hg and Cu using a CAMECA SX-50 electron microprobe operating in wavelength dispersion mode under the following conditions: excitation voltage, 20 kV; beam current, 20 nA; peak count time, 40s; background count time, 20s; spot diameter 5μm. Au, Ag and Cu element samples were used to standardize the location of their characteristic X-ray lines, and HgTe was used for Hg. Ag and Au calibrations were monitored over the course of each run by multiple measurements of an Au80:Ag20 standard material. PET crystals were used for Au, Au and Hg, an LIF crystal was used to measure Cu. The following lines were observed: Au, Mα; Ag Lα; Cu, Kα; Hg, Mβ. Data was reduced using the PAP (phi-rho-Z) method of Pouchou and Pinchoir(1985) (Pouchou et al., 1985); peaks were deemed acceptable if the total measured wt% of the four measured elements was between 98 and

102%. Detection limits of 0.20, 0.10, 0.05 and 0.20 wt% were measured for Au, Ag, Cu and Hg.

3.3.3 Data Analysis

Kernel density estimation (KDE) (Parzen, 1962) was used extensively to generate probability density functions for the studied variables. Calculation of these functions was performed in Excel using an in house Visual Basic for Applications (VBA) macro based on first principles. There has been no work done on the underlying distribution of population values; however, the data appears qualitatively to be normally distributed. A normal distribution kernel is thus likely adequate and appropriate, and has the advantage of being computationally simple. During fitting of model populations to the data, normally distributed model populations were also used. The equations used to generate KDEs on one and two variables concurrently were:

$$p_x = \sum_{n=1}^{a} N(o_{x,n}, w_x, x)$$

Equation 3.1: Kernel Density Estimation in One Dimension

$$p_{x,y} = \sum_{n=1}^{a} (N(o_{x,n}, w_x, x) \times N(o_{y,n}, w_y, x))$$

Equation 3.2: Kernel Density Estimation in Two Dimensions

Parameters p_x and $p_{x,y}$ are the probability density at any given point x or x,y; N is a normal distribution with parameters: $o_{x,n}$ or $o_{y,n}$ observation n of the x or y value, w_x or w_y the bandwidth for x or y, and the point x or y; a is the total number of observations in the sample. Bandwidths for the normal distribution kernels were chosen using Silvermans rule of thumb (Silverman, 1986). The equations define the probability density for any point; for this study, probability densities for both samples and models were calculated for a 102 x 102 cell grid (10404 points) in the range from 70-100 wt.% Au and a HSE range of 0.7 to 1.0.

3.4 Results and Discussion

Raw results from the morphological and composition analysis of individual grains are not presented, due to space considerations (this data is available in appendix A). Twelve morphological parameters and 4 composition readings were taken on 4559 grains from 54 locations; 3 morphological and 1 compositional value for each grain was used in the final analysis. The morphology of an additional 3418 grains was analyzed, but not their composition.

3.4.1 Advantages of the 2D KDE approach

KDEs were initially calculated separately from the shape and compositional measurements. From these analyses, component populations were identified, indicating in most cases that the true populations were polydisperse in one or both variables, and that previous studies using an average for whole samples likely did not accurately capture true population values. A shape evolution curve constructed from the results of this first analysis already represents a significant improvement over past attempts. However, the identification of populations separately in shape and composition indicated that examining each variable in isolation was still not sufficient. For example, analysis of a single sample might reveal 2 population by shape present in the proportion 1:3:2, and 3 populations in composition in the proportion 3:5:1. Although 3 populations are identified using each variable, the proportions are not the same, indicating that the 3 populations identified in each variable do not correspond to each other. The confidence with which populations can be identified from a one dimensional analysis is also lower than desired since it is possible to produce several models which accurately fit the data, but indicate different population values.

Linking morphological and compositional data during collection afforded a solution to many of these problems in the form of a bivariate KDE that evaluates both variables simultaneously. This approach confirmed and solved the problem of non-correspondence of shape and composition populations identified by one dimensional analysis. Furthermore, because any modeled population must be matched in two dimensions, the number on non-unique solutions is reduced, increasing the confidence in the determined population values. It is presumed that the core composition of the grains does not change during transport; thus knowing population compositions makes it easier to track populations as they evolve downstream. Populations must match in composition before it can be proposed that their shape values represent a change due to transport. This method is significantly more com-

putationally intensive than the one dimensional method, and requires that individual grains be tracked so that shape and composition measurements can be paired. The increase in utility of the analysis is significant, and our work has shown that the one dimensional analysis is inappropriate for identifying populations in all but the most simple cases. Figure 3.1 shows how individual one dimensional analysis may indicate the incorrect number of populations compared to the two dimensional analysis which clearly shows the true distribution of values. The one dimensional analyses indicated that there were only 2 populations for each variable analyzed separately, whereas the probability surface in two dimensions reveals a more complex situation. Figure 3.2 shows the model result of fitting 6 individual populations to the experimental data shown in Figure 3.1, showing how accurate a fit can be obtained by performing a two dimensional analysis.

3.4.2 Determining Required Population Fitting Accuracy

As with any study, measurements made on a given sample are only an estimation of the true value for the population being sampled. It is particularly important in this study to have an understanding of how good this estimation is so the accuracy of the model developed from the values can be determined. The quality of the estimation has other implications; for example, how similar do population compositions have to be between sample locations to be determined the same in the context of tracking a population between sample locations?

To monitor the quality of the fit, it is first necessary to determine a way to measure it. To generate the models, the difference between the volume under the curve for the model and data-derived probability density surfaces was minimized; the percentage that the volume difference represented of the total volume under the data-derived probability density then gives a measure of the accuracy of the fit. The number of grains that the error represents is then easily calculated by multiplying the error by the number of grains in the sample. Several samples were examined in greater detail in order to more fully understand the values produced from the models.

Small Numbers of Populations

The first sample examined was collected within 50m of a gold bearing quartz vein occurrence near the head of a small tributary in the central Klondike called 7 Pup (Figure 3.18). This sample was reasonably assumed to have a single source. Qualitatively, the probability density surface for the sample

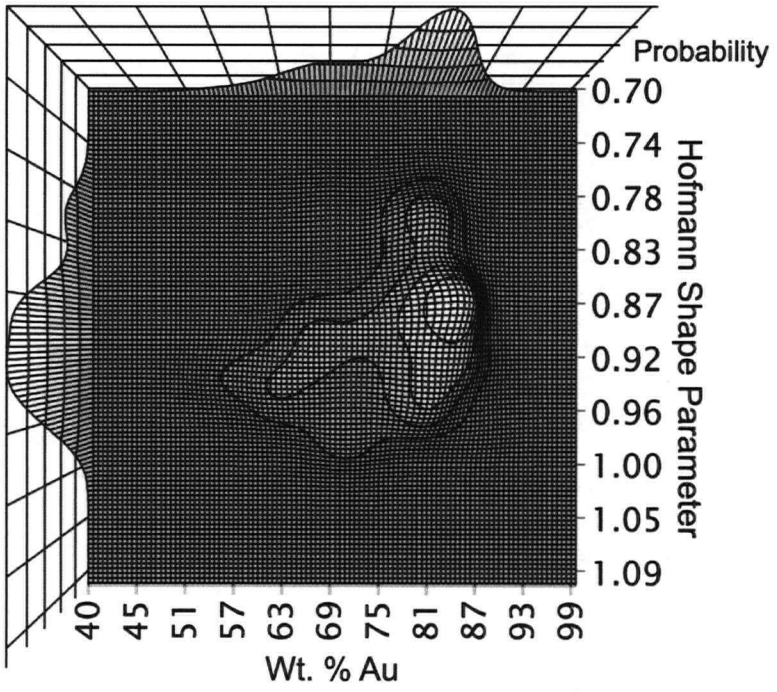

Figure 3.1: Two dimensional KDE for a single sample of 54 grains. The surface color at any represent the probability of observing a grain with the values corresponding to the coordinates of that point. Probability increases dark to light. The two walls show the projection of the probability surface onto each axis, and are equivalent to a one dimensional KDE in the variable for that axis.

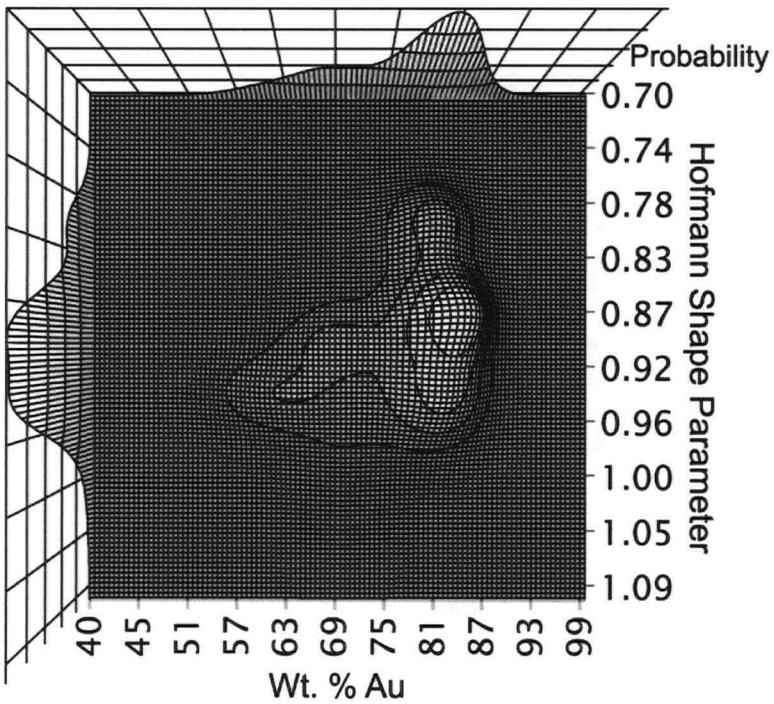

Figure 3.2: Probability density surface for the sample in Figure 3.1 modelled using 6 component populations. Probability increases dark to light. The two walls show the projection of the probability surface onto each axis, and are equivalent to a one dimensional KDE in the variable for that axis.

appears to indicate a unimodal population, although with a non-normal distribution (Figure 3.3). The appearance of the peak with a tail towards lower HSE values is likely due to a physical maximum related to the initial shapes of the gold grains in the source, and may also be due to the nature of the HSE, which reaches a maximum of 1. There are also what appear to be several smaller peaks distinct from the main peak. When fitted, these peaks represent single grain results, and may be due to sampling from the tail of the true distribution or to measurement errors and are likely not significant for this sample. There is also a much higher probability of grain armoring (gold grains contained within quartz, or with quartz or some other mineral attached to the surface) in this relatively immature placer sample, which would affect the HSE measurement. Since the sample location was so close to the presumed source and to the head of the drainage, it is highly unlikely that there is an additional upstream source that is represented in this sample by only a single grain.

The measured data for all of the grains (n = 214) was fitted with a single peak, giving an error of 11.8%. The determined values for this fitted peak were then used as the true values for later comparisons. From all of the measurements, six samples each of 10, 20, 30, 50, 75, 100 and 120 values were randomly chosen, probability density surfaces were calculated for each of these groups, and a single peak was fitted to each. The peak locations are compared separately by HSE (Figure 3.4) and wt.% Au (Figure 3.5).

With 10 grains, the proper location of the peak in wt.% Au is missed 33% of the time, and the HSE peak location is missed in 1 of the 6 samples. This indicates that realistically more than 10 grains are necessary. Even at the n = 30 level, the peak location is not accurately captured 100% of the time. Deciding on a lower limit is subjective, but it appears in this case that at least 50 grains are necessary. Considering that the true population we are sampling is much smaller than the true population in the field, it would be prudent to use a higher lower limit that this. Examining the error in the fits supports this decision: the errors on the fits at n = 50 range from 7.9 to 12.4 %, and at n = 75 from 7.4 to 12.0. Even using n = 120, the error range is 7.1 to 15.4%.

It is interesting to note the errors on the fitted peaks. The standard deviations on the wt.% Au and HSE from the n = 178 analysis were 3.94 and 0.020 respectively. The average standard deviations on the wt.% Au and HSE peaks at the n = 75 level were 4.26 and 0.020 respectively, whereas the standard deviation on the actual determined values was 0.60 and 0.003 for wt.% Au and HSE respectively. There is some natural variability in the composition and shape of the gold grains even directly at source, so

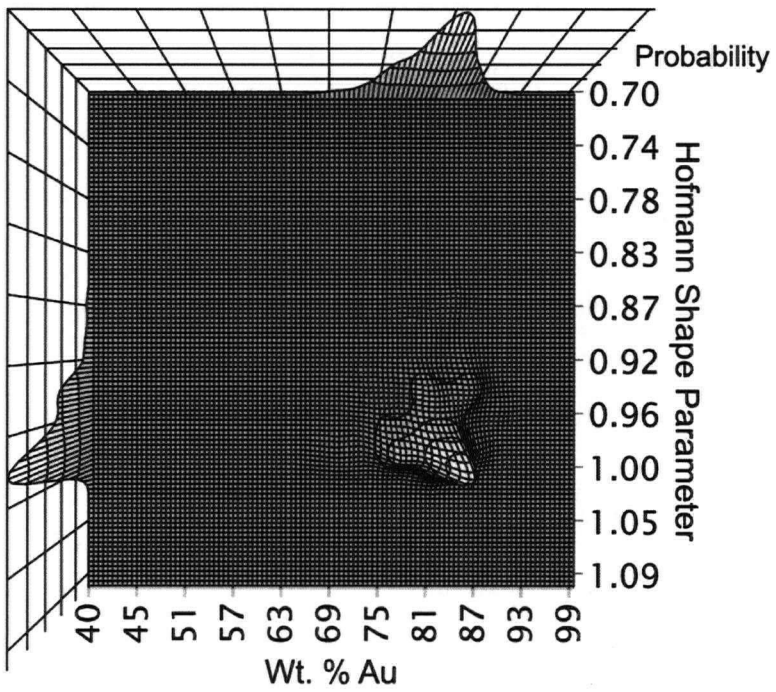

Figure 3.3: Probability density surface for a sample collected from #7 Pup, proximal to a known lode source (n = 214). Probability increases dark to light. The two walls show the projection of the probability surface onto each axis, and are equivalent to a one dimensional KDE in the variable for that axis.

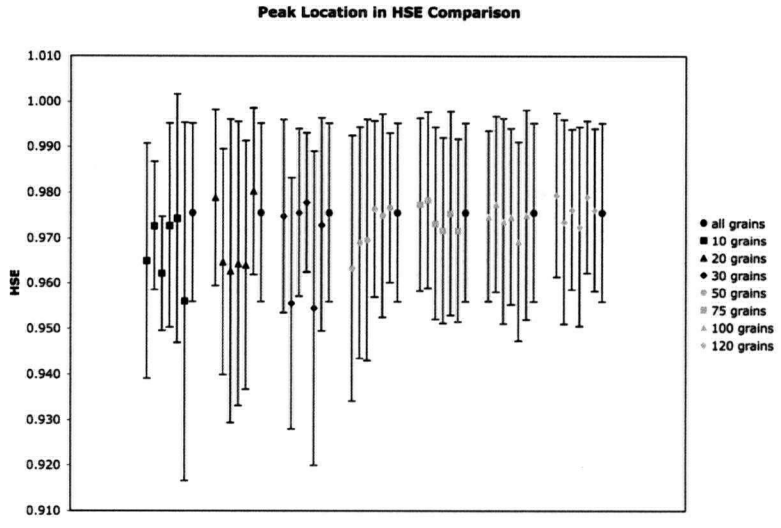

Figure 3.4: Comparison of the Hofmann shape entropy mean values for a single peak fitted to kernel density estimations generated from groups of different numbers of grains sampled from the population used to generate Figure 3.3.

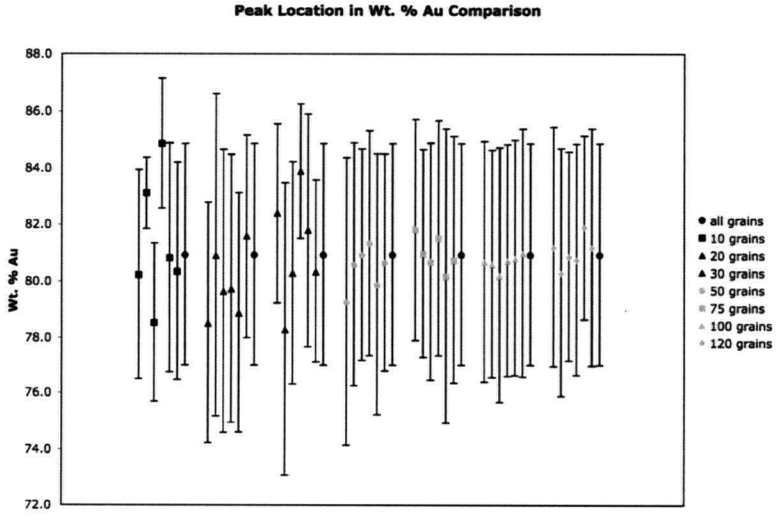

Figure 3.5: Comparison of the weight percent gold mean values for a single peak fitted to kernel density estimations generated from groups of different numbers of grains sampled from the population used to generate Figure 3.3.

the standard deviations on the fitted peaks will include both these natural variations, as well as error due to sampling, and measurement. The fact that the standard deviation on the determined values for this group of samples was much smaller than the standard deviation on any particular fitted peak indicates that much of the standard deviation is due to natural variability, and the determination of the actual peak centre locations is more accurate than the standard deviation determined indicates.

Large Numbers of Populations

A similar analysis was performed on a sample with an unknown number of sources. Qualitatively, the sample is interpreted to contain anywhere from 4 to 7 component populations. For this comparison, we wanted to examine how stringent a fit must be to locate all of the peaks in a sample. From a sample of 178 grains, 6 samples of 80, 100 and 120 were selected. Probability density surfaces were calculated for each of these 18 groups, as well as the entire grain set, and then fitted with 7 peaks.

Fitting 7 peaks to the n = 178 sample produced a fit with an error of only 0.324%. The smallest fitted peak represented 6 grains, which is a sufficient number that this likely represents a true population, and does not simply represent statistical outliers or measurement errors. This indicates that for polymodal samples, the fit must be quite good in order to capture all of the component populations. The percent error in all cases was roughly similar; however, this corresponds to a smaller number of grains in samples of smaller size (Table 3.1). This indicates that with decreasing sample size, the chance that a single observation represents a component population is higher. Even though the % error on the fits is similar, the observations from fewer grains can be ignored if all of the populations are to be identified. Also, compared to the single source example, the fits in for multi-population samples must be of significantly higher quality in order to capture all of the component populations.

	Error As Grains			Error As Percent		
	80 Grains	100 Grains	120 Grains	80 Grains	100 Grains	120 Grains
Group 1	0.225	0.254	0.562	0.281	0.254	0.468
Group 2	0.428	0.328	0.543	0.535	0.328	0.453
Group 3	0.246	0.463	0.777	0.308	0.463	0.648
Group 4	0.595	0.267	0.678	0.744	0.267	0.565
Group 5	0.563	0.868	0.642	0.704	0.868	0.535
Group 6	0.408	0.614	0.508	0.510	0.614	0.423
Average	0.411	0.465	0.618	0.514	0.465	0.515
All Grains	0.580	0.580	0.580	0.324	0.324	0.324

Table 3.1: Comparison of errors between experimental and modeled kernel density estimations generated from groups of different numbers of grains sampled from a polymodal sample.

It is also important to note that the nature of the peaks has a large effect on the accuracy of the fit needed to identify component populations. Comparing the fits at the n = 80, n = 100 and n = 120 (figures 3.6, 3.7, 3.8 respectively) levels, there are some peaks that are located reasonably accurately regardless of the number of grains (the three peaks located at the lowest wt. % Au), as evidenced by the cluster of points with representation from each group. A larger sample size is required for other peaks before all of the groups start to converge on the true population location. Even at n = 120 there are still peaks where the agreement of peak location between groups is poor. These are likely minor contributing populations where the fraction of grains represented is small, and even with n = 120 the peak location is being informed by only a few tens of grains. With samples where the peaks are well separated (by composition or shape) or well represented, it takes relatively fewer measurements to be able to accurately distinguish between populations. Conversely, in samples where there are multiple sources, all of which have similar composition and shape values, a significantly higher number of measurements is required to deconvolute the location of the component populations. As with to the previous comparison, the precision of the peak location values between samples is significantly smaller than the standard deviations for the identified peaks, providing additional evidence that the identified errors are dominated by natural variations in the values.

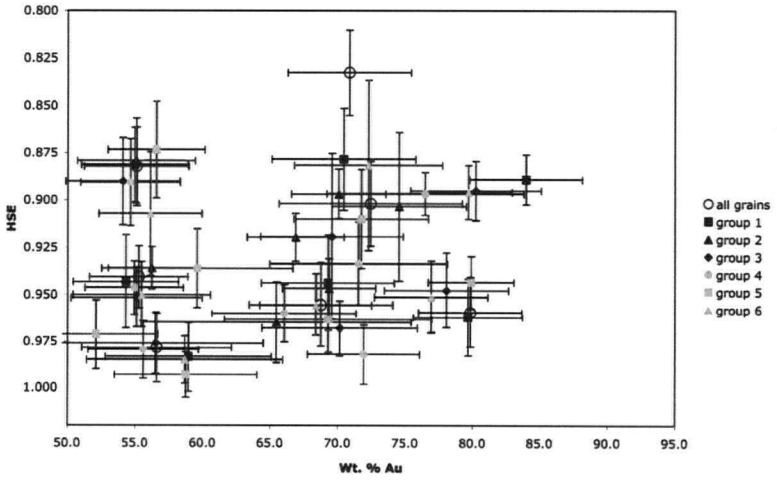

Figure 3.6: Comparison of fitted model KDE peak locations for several groups of 80 grains sampled from a larger population.

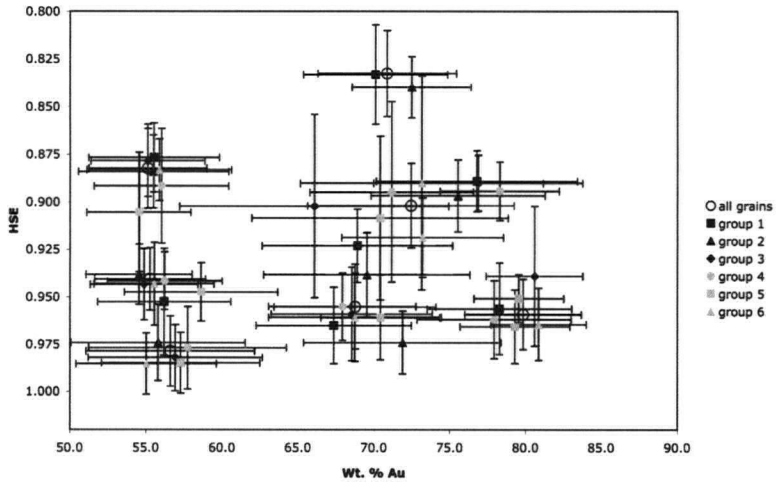

Figure 3.7: Comparison of fitted model KDE peak locations for several groups of 100 grains sampled from a larger population.

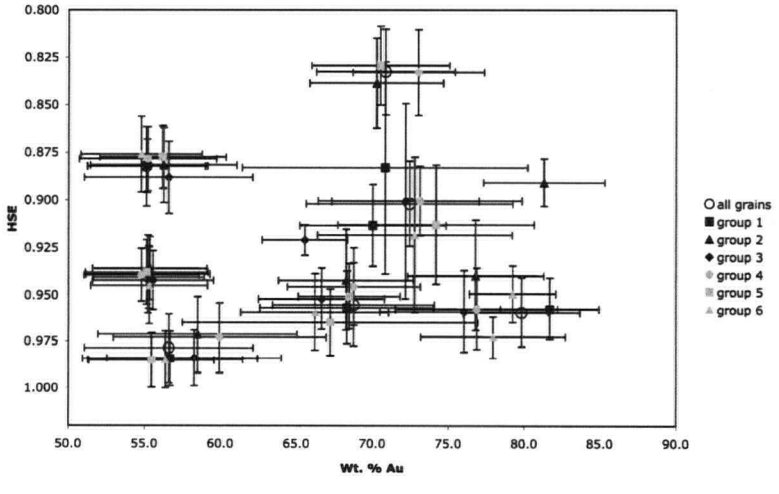

Figure 3.8: Comparison of fitted model KDE peak locations for several groups of 120 grains sampled from a larger population.

3.4.3 Ideal Fitting and Sampling Requirements

Combined with the first single peak comparison, these results show the major consideration for performing a fit. Firstly, it is not reasonable to fit every sample to some arbitrary error level. Reasonable consideration of geological knowledge should be made in determining how accurate a fit is desired. A sample collected very high up a drainage should be fitted with few model peaks, and can have a relatively large error and still accurately identify the component populations. Alternatively, samples collected from major streams with multiple tributaries should be fitted with larger numbers of model peaks, and the fit should be much more accurate in order to ensure that all populations are captured. Secondly, sample size should be considered. With small sample sizes a population may be represented by fewer grains, so the fit must be sensitive to smaller numbers of grains. If the guidelines from the single peak fitting example are applied to each peak individually in a polymodal sample, then ideally at least 50 grains should be measured to accurately provide information of each component populations. Thus, for a sample suspected to have four sources, 200 grains would be the optimum sample size. The fewer the number of grains used than this ideal, the more likely it is that the values identified for the populations have been incorrectly determined. This is also a consideration during sampling; relatively small samples are adequate in locations where there are few suspected sources, whereas much larger samples are required in locations where there are many contributing sources. The intended use for the data from the sample also needs consideration. For constructing a calibration curve between shape, composition and transport distance, high quality fits and accuracy should be targeted, but it may be that a rough single peak fit of a group of similar populations from a complex population will yield sufficient information to generally target subsequent exploration, thus saving the computation and sampling time involved in collecting and processing an unnecessarily large sample.

3.4.4 Practical Fitting Procedures

Several samples from the study area were collected within 1 km of the stream head; these samples were fitted with single peaks unless they displayed significant polymodality. The remainder of the peaks were fit to an arbitrary error representing 1.3 grains. This process is iterative: a model population is added at the point in shape:composition space where the difference between the model and the data is greatest, then all of the model peak locations, stan-

dard deviations and relative weights are optimized to minimize the difference between the data and the model. The fits were then manually examined, and if there appeared to be significant peaks not captured, additional peaks were added, and the fit refined. Also, several samples in locations which drain multiple known gold-bearing streams were fitted with increased numbers of peaks. Additionally, the number of peaks for some samples was reduced, particularly for samples from upstream locations where unreasonably large numbers of peaks were identified due to fitting of peaks which are likely due to measurement of samples located at the extremes of the nature variation. Peak numbers for many samples were also modified based on results of upstream samples. For example, a sample collected downstream from one low fineness (<70 wt.% Au) and two high fineness (>80 wt.% Au) sources would be expected to have at least two populations at high fineness and one at low fineness. The upstream sample provide a lower constraint on the number of populations present which informs the accuracy a fit must have to capture all of the component populations. The upstream samples also provide a guideline for some of the population compositions that should be identified. This method was especially useful in samples from major tributaries in areas with large numbers of sources.

3.4.5 Transport Distance : Shape Evolution Model Generation

Twenty-nine samples representing data from 2515 grains from the entire data set were determined to be suitable for construction of a shape:transport distance relationship. Samples were excluded mainly where there were too few samples from a single stream (two or more samples from a single stream are required to constrain a relationship), where the sampling frequency was too sparse (greater then 15 km between samples), or where the sample size was thought to be too small to accurately portray the actual population (e.g., a sample of 55 grains downstream from greater than 10 known placer bearing streams). The tendency was to be conservative in including samples because of the complexity revealed during the course of the study and the poorly understood nature of these deposits in the context of shape evolution during alluvial transport.

Although numerous lode gold sources have been identified in the Klondike, there are very few places where the specific location where gold from these sources enters a watercourse is known exactly. This presents a problem in that the map distance from a sample to its source cannot be precisely measured, which makes the development of a shape:tranport distance rela-

tionship difficult. In order to solve this problem, samples were collected as close to the head of drainages as possible, leaving only a small area in which the source could possibly be located. During definition of the shape:source distance relationship, the distance from a sample to the source location is then optimized along with model parameters, but is constrained to be a distance of from zero to the distance from the sample location to the actual head of the stream.

Initial Model Development

An attempt at defining a shape:transport distance relationship showed that although a general relationship was apparent, there was significant scatter in the data. As shown in Figure 3.9, there was a negative correlation that appeared better for shorter transport distances; however, the error on any predictions made from the model would be so large to make them of extremely limited use. The errors on the HSE are those determined on the individual fitted populations, and an arbitrary error of 250 m was used for the distance measurements. The stronger correlation at short transport distances was interesting because most of this data came from samples collected in the higher gradient streams. This indicated that there is a possible complication to the relationship involving stream gradient. Intuitively it is likely that relatively high gradient streams will represent higher energy environments in which one might expect more rapid shape modification. It is also possible that streams of different gradient transport gold by different mechanisms which affect shape at different rates, for example, saltation in high energy environments versus rolling and sliding in low energy environments.

In order to improve the transport distance:shape relationship, the effect of the stream gradient was examined in some detail. It is very difficult to identify all of the potential parameters involved in the physical modification of grain shape in an alluvial environment, or to postulate a mathematical function to relate their effects. In trying to develop an arbitrary function the only particular consideration we started with was that a steeper stream will cause grain shape to change more rapidly due to the increased number and energy of collisions between gold grains and other particles in the stream. Through an iterative process we have developed an empirical relationship that best models shape modification in a stream is given in equation 3.3

In this function, parameters A, B and C are empirically determined constants, S is the stream gradient in meters per kilometer and D is the horizontal (map) transport distance in kilometres. The main body of the function, given in equation 3.4, provides a ranged value from 0 to 1 based on

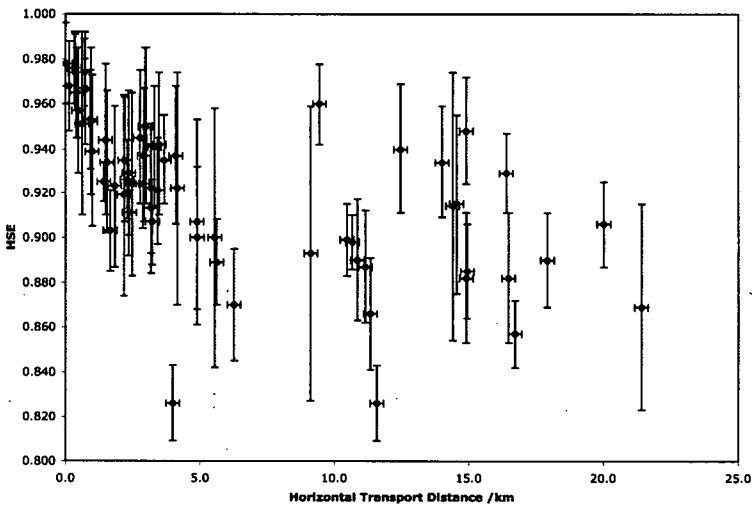

Figure 3.9: First generation grain shape transport distance model.

$$(\frac{1}{1+e^{(-A\times(S-B))}} \times \frac{S}{100})^C \times D$$

Equation 3.3: Gradient Modified Transport Distance Calculation

$$\frac{1}{1+e^{(-A\times(S-B))}}$$

Equation 3.4: Gradient Modified Transport Distance Calculation, Sigmoidal Portion

the gradient. This is a sigmoidal function, with the variable A determining the steepness of the transition, and B locating the transition. Empirically determined values for A and B are 0.94 and 8.96. This produces a gradual transition from value very near 0 to very near 1 over the gradient range from 0.3 to 1.5%, centered at 0.896%. This indicates that very little shape change occurs in steams with a gradient below 0.3%. This scaling term is then multiplied by the stream gradient (/100), which produces a scaled gradient value. The exponent term was added to account for the possibility a non-linear increase in the rate of shape change with increasing gradient. The empirically determined value for C is 1.09. Multiplying by the measured flat transport distance yield the gradient modified transport distance (GMTD). The GMTD for a horizontal transport distance of 1km over a range of gradients is shown in Figures 3.10 and 3.11.

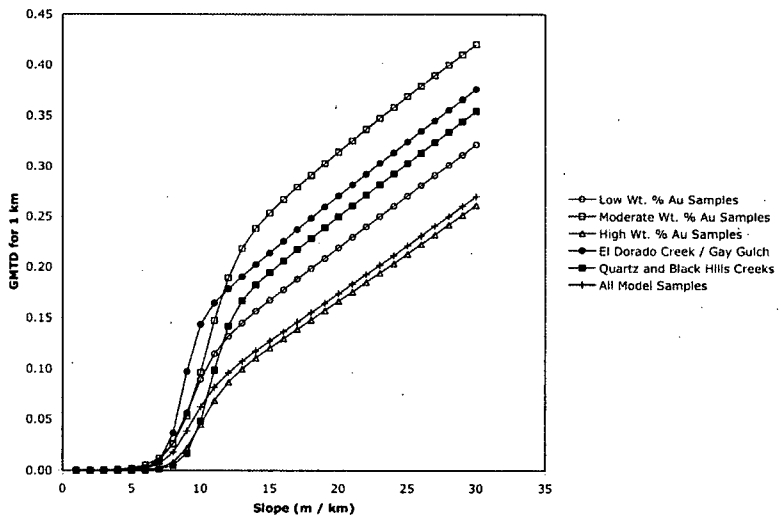

Figure 3.10: GMTD for a horizontal transport distance of 1km at gradients ranging from 0 to 30 m / km.

It was determined that the gradient modified distance must be calculated in an integrated manner; one cannot measure the total elevation difference and divide it by the total linear distance between sample locations, and use that value as the transport distance and the gradient. Instead, it is necessary to calculate the total gradient modified distance between sample locations by calculating it individually for many shorter sections, and summing them. We have termed the sum of these values the integrated gradient

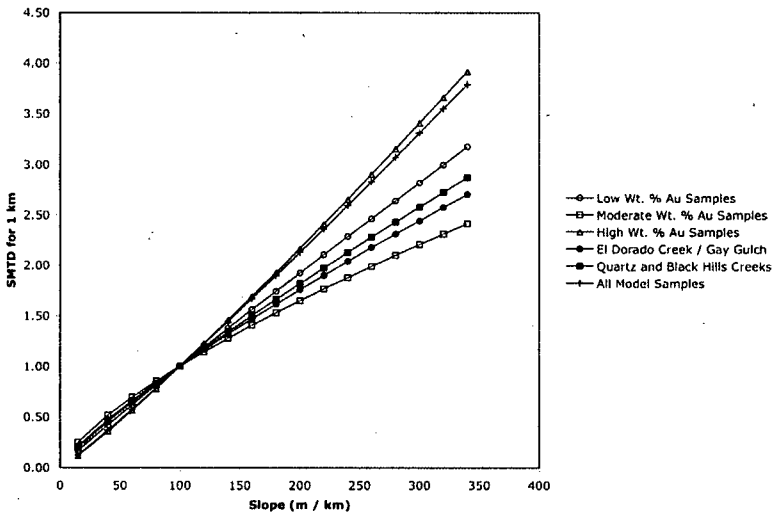

Figure 3.11: GMTD for a horizontal transport distance of 1km at gradients ranging from 30 to 350 m / km.

modified transport distance (IGMTD). This integration is required to account for variations in gradient over the transport distance, and is especially important if the stream gradient changes drastically over the distance being examined. In theory, it would be possible to use GPS or survey techniques to measure the exact stream profile, then do a mathematical integration, however this is likely unnecessary. For this study, at the same time as distances between samples were being measured on the topographical map, the distance between contour intervals was noted, and the gradient modified distance calculated for the distance between each contour (20m contour interval). This provides an easy way to measure gradients that does not require extensive field time. Though not exactly capturing details such as small waterfalls, etc., the averaging interval likely portrays the stream geometry sufficiently accurately compared to the accuracy of the remainder of the measurements and the accuracy of the method in general.

Second Generation Model

Stream gradient appears to have been largely responsible for the spread in the previously defined shape:transport distance relationship. The correlation between gradient modified distance and Hofmann shape entropy is excellent (Figure 3.12), and thus provides much more accurate estimates of distance to source. Translating from this relationship back to true map distance must again take gradient into effect; however, this is a relatively simple task.

The standard deviations on the HSE values plotted for each point in Figure 12 are those determined during peak fitting. As discussed previously, the actual location of the peaks and thus the vertical position of the individual points in this plot is likely more accurate than these error bars indicate. Estimating errors for the IGMTDs is significantly more difficult, because they should include errors from GPSR measurements, measurements of transport distance on maps, assumptions that the current stream geometry is sufficiently similar to stream geometry at the time of transport and deposition, as well as any differences between the true (unknown) and empirically determined values for the constants in the gradient modified distance calculation. It is also possible that the function chosen for the gradient modified distance calculation is not a perfect representation of the physical processes at work, which would introduce additional errors. For this figure, an arbitrary error in the IGMTD of 0.2 was used, which represents a transport distance of $\sim$125 m at a gradient of 15%.

This model represents a significant improvement over past approaches

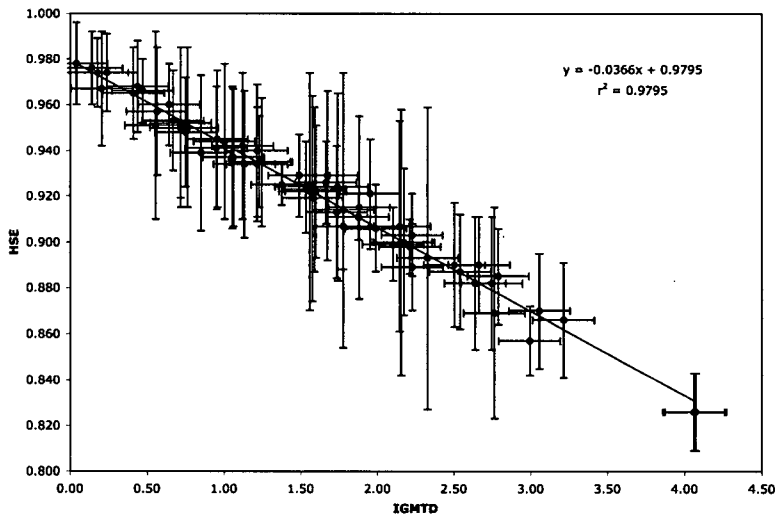

Figure 3.12: Second generation grain shape transport distance model.

to evaluating grain shape:transport distance relationships. Further increasing the accuracy of the model would allow the accuracy of any predictions using it to be increased, and the utility of the model further improved. Unfortunately, as this is the first study of this kind, the quality and quantity of samples which would be required was unknown. In the field, we arbitrarily set a goal of 100 or more grains per sample location. As previously mentioned, this number is likely somewhat smaller than ideal, especially for samples from larger trunk streams with multiple sources. This study utilized the samples at hand, but in several instances the number of grains in a sample was realistically insufficient, so the accuracy of the population identification has likely suffered, resulting in some error in the model. This error is essentially impossible to quantify without performing additional sampling, but should be noted as one likely reason for some spread in the model. The sample size guidelines presented here should help any other workers who attempt to utilize this method minimize this source of error. It is still encouraging that even with non-ideal sample sizes, the resulting model appears to be of good quality, which may indicate that the model is fairly tolerant of poor sampling.

Possible Additional influences - Effect of Composition and Geology

The possible effect of variations in composition of the placer grains was also considered. Pure gold is softer than Au:Ag alloys, hence, it was thought that grains of high fineness might be expected to deform more rapidly under similar transport conditions than grains of moderate to low fineness. To investigate the possible effects of gold composition, we subdivided our gold samples into three groups of varying compositions (wt.% Au less than 72, between 72 and 80, and above 80), and models were generated for each group. First, the model parameters were examined (Figures 3.10 and 3.11). This comparison shows that the modification to account for stream gradient is generally similar in all three cases, and there is no consistent change with increasing or decreasing fineness.

Although Au:Ag alloys comprise the vast majority of placer gold in the Klondike, there are several occurrences with significant Cu (Figure 3.13) and Hg (Figure 3.14); thus examining wt.% gold values alone may be insufficient. In general, the amount of Cu, Hg and other metals is small (only 5% of the grains had Hg or Cu present above 1%, and only 2% of the grain had concentrations above 2%). We consider it likely that the effect on the physical properties of the gold grains at these low concentrations is small enough to

not be observable through the error contributed from other sources. The effect on the hardness of the gold due to added copper at these levels certainly appears to be minimal (Figure 3.15), and the effects of mercury is also likely low. However, it is important to note that if this model is applied to situations where other elements are present consistently in significant amounts, there may be an effect that should be accounted for.

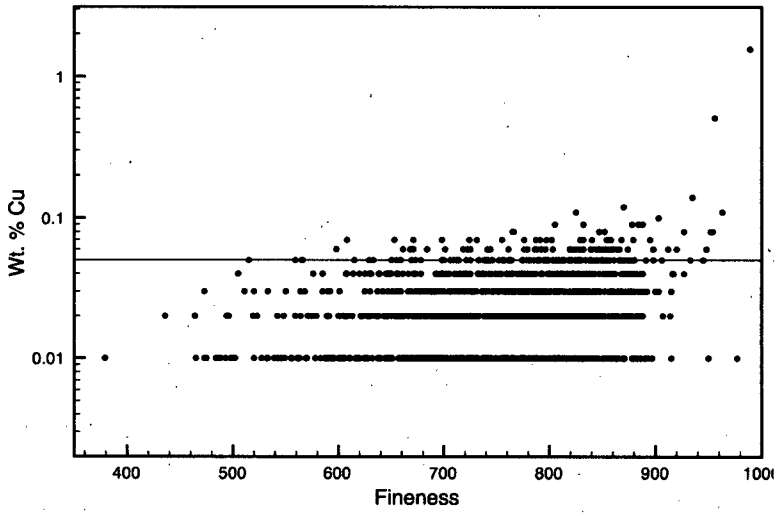

Figure 3.13: Copper content as a function of fineness for all grains used in shape transport distance model. Horizontal line indicates the detection limit for copper during our EMPA.

A second comparison (Table 3.2) used the gradient modification parameters obtained from the entire data set, and examined the parameters of the model for four different compositional groups (wt.% Au of <70, 70-77, 77-82, >82). Again, there is no consistent trend in the slope or intercept of the model curve moving towards higher or lower fineness values. At the 95% confidence level, the slope of the curve for the individual compositional group is identical to that of the slope for the curve generated on the entire data set, and at 99%, this is true for both the slope and intercept of the curve.

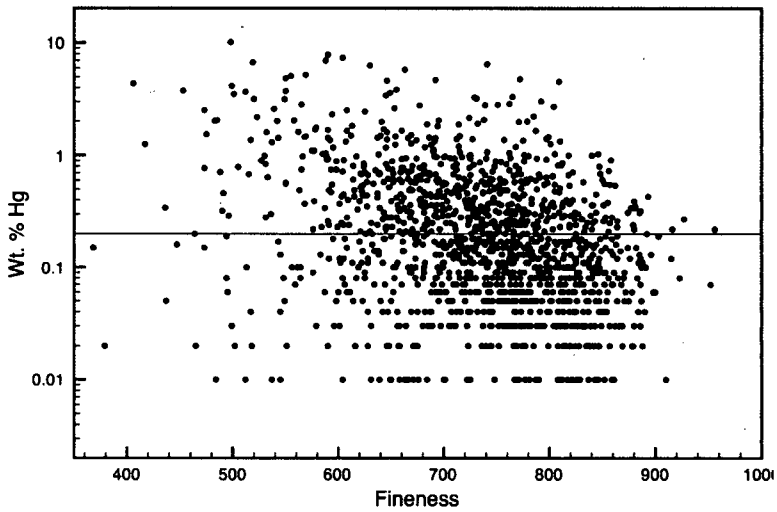

Figure 3.14: Mercury content as a function of fineness for all grains used in shape transport distance model. Horizontal line indicates the detection limit for mercury.

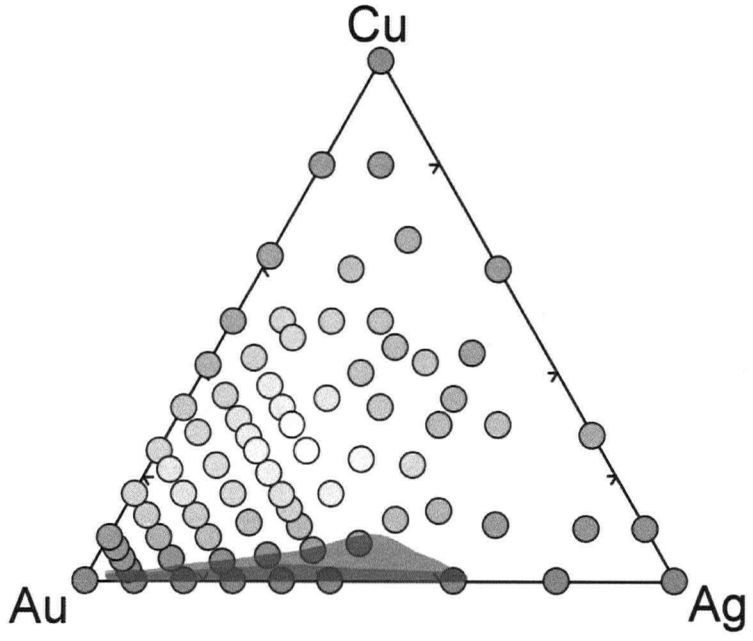

Figure 3.15: Brinell hardness values for the Au-Ag-Cu system. Data from Sterner-Rainer, 1926. Alloy composition is given by location of each point, and the measured hardness for that point dictates the color of the point. Red points are the softest, increasing yellow indicates increasing hardness. The fields locating the samples from this study are plotted in Au-Ag-(Cu+Hg) space, the light blue field covered 100% of the grains, the dark blue encompasses 95% of the samples.

		All Grains	<70 Wt.% Au	70-77 Wt.% Au	77-82 Wt.% Au	>82 Wt.%Au
Slope		-0.03659	-0.03744	-0.03604	-0.03488	-0.03796
Intercept		0.9795	0.9817	0.9784	0.9766	0.9827
95 %	Slope	-0.03526	-0.03309	-0.03397	-0.03054	-0.03574
upper limit	Intercept	0.9819	0.9902	0.9819	0.9827	0.9877
95%	Slope	-0.03792	-0.04179	-0.03811	-0.03923	-0.04019
lower limit	Intercept	0.9771	0.9732	0.9749	0.9705	0.9778
99%	Slope	-0.03481	-0.03140	-0.03321	-0.02879	-0.03482
upper limit	Intercept	0.9827	0.9935	0.9832	0.9852	0.9897
99%	Slope	-0.03836	-0.04347	-0.03887	-0.04097	-0.04110
lower limit	Intercept	0.9763	0.9699	0.9736	0.9680	0.9757

Table 3.2: Comparison of IGMTD : HSE model parameters for groups of different composition.

These observations indicate that the composition of placer gold grains does not significantly affect the rate at which their shape is modified during alluvial transport, or that these effects are sufficiently small that they are not evident in this study. A more detailed study following the sampling suggestions previously discussed may reveal and be able to quantify a compositional effect, but we believe this effect, if present, will be minimal.

Although it is obviously desirable to generate shape modification models such as those described in this paper for every location where this method is to be applied, the observation that the effect of composition is minimal suggests that this shape:transport model may be of applicability even in situations unlike those used to generate the model. We suggest that the model described here should applied with caution in other situations, and with increasing caution the more dissimilar the situation. Samples which contain more significant Cu concentrations, or with uniformly elevated Cu or Hg should be examined particularly closely, because of the possible effect of these metals on alloy hardness.

The effect of bedrock geology was considered next. The rock type over which a stream is flowing will result in a different stream bed (e.g., smooth, rough, angular). Also, factors such as whether the bed is scoured to bedrock, or transport occurs on top of a layer of sediments in the stream bed, and if so, the nature of that sediment (clay, sand or gravel?) may become important. In addition, the co-transported sediments will depend on the host rocks for the entire drainage. The average size and hardness of clasts in the stream, the geometry of the clasts (flat, round, angular, smooth) may have an effect as well: smaller placer grains may be able to fit in the spaces between relatively coarse, smooth, and rounded clasts, but may be compressed more frequently when transported with finer or flatter material. Shape evolution during transport over strongly foliated or stratified rocks may depend on transport direction relative to the foliation or bedding; there may be fewer collisions with bed surfaces while being transported parallel to layering, while perpendicular transport may generate a higher energy bed with eddies and significantly more turbulent flow. Some of these effects may be accounted for inadvertently in the gradient modification; streams with steep gradients are more likely to be scoured with transport occurring directly on bedrock, whereas streams with shallow gradients are more likely to have a bed of soft, fine sediments. Quantifying these effects can be difficult for several reasons, for example, the time requirement to map the foliation of the bed for an entire stream in a complexly deformed environment may be substantial. Deciding on an appropriate model to account for overall hardness of a bed load, or the shape of clasts is far from simple.

Since it is non-trivial to develop a model to account for these factors, it is important to try to identify these effects so the universal applicability of the model can be assessed, and determine if these effects are substantial enough to be monitored and accounted for in future studies. Two groups of samples were identified to probe the effect of geology: first, a group of samples collected from upper Eldorado Creek and Gay Gulch, and second, samples collected from Black Hills and Quartz Creeks (Figure 1.1). The bedrock in the first area is a felsic shist with finely ground metamorphic mica (Mortensen et al., 1990); the stream clasts are generally flat, and there is abundant clay. The second group travels over metamorphic bedrock (mica shist, quartzite, gneiss and foliated granitoids) and some volcanic rocks (Fuller et al., 1992). Sediments in these streams is dominated by sands and gravels, the clasts are generally more rounded, and in general the rocks are harder.

Here, the effect of geology on the model constants appears to be little, as evidenced by the similarity of the gradient modification calculation constants (Figure 3.10 and Figure 3.11). These comparisons use fewer points than the comparisons of composition, so would be expected to have a greater error, and yet the gradient modification models are within the ranges determined for the compositional group, suggesting that the effect of geology is again small. A comparison of the fit parameters for the models demonstrates that the values are not equivalent at the 99% confidence level. This may be due again to the small sample size and increased error, or may be a real effect. In this case, the slope is greater for the model developed using the Black Hills and Quartz Creek data, indicating that shape change occurs more quickly in this environment. If this is a true effect, it could be explained by the harder rocks and lack of cushioning (in the form of clay and silt) causing faster deformation.

The fact that composition and geology have a limited effect on shape change during alluvial transport is surprising; intuitively it would be expected that a softer particle would deform more easily, and thus faster, and that transport in a generally harder bedrock environment would result in stronger and more rapid deformation. Perhaps the rate of transport downstream is identical in all environments, so the number of deformation events is essentially the same in all cases. In this case the hardness of those rocks would be of little importance, provided they are harder than the gold. Gold is relatively soft, so this condition would always apply. This in turn implies that the hardness (witnessed by composition) of the gold plays an effect, but perhaps the timescale of the deformation events negates this (instantaneous collisions versus deformation forces over long times). It may also be that the effect of differences in hardness between grains of different compositions

is too small to be accurately recorded. Lastly, the presence of high fineness (and thus softer) rims on most placer gold grains from the region may play a role, depending on how deformation forces are distributed during any given deformation event. The observation that the major effect observed is the stream geometry supports these postulations; stream geometry dictates the energy of the alluvial environment which will dictate the energy and frequency of the deformations.

Other Possible Effects

It is important to stress that the majority of this study is based on data from relatively steep streams of generally low volume, and that the rate of shape change during transport over extended distances (tens to hundreds of km) at reduced gradients in rivers with significantly higher volumes may be significantly different than observed in this study. Future detailed studies specifically examining these factors are certainly warranted now that the method has been developed.

The presence of micro-inclusions has also been noted in placer gold, and this may have an effect on transport processes. External inclusions (most commonly quartz or pyrite) may armor a grain during transport, and retard the rate of deformation. Qualitative observations indicate that retention of external inclusions is usually limited, especially in the grain sizes typically examined for this study. Internal inclusions may provide a kind of internal skeleton which would also retard deformation. These internal inclusions tend to be retained over longer transport distance; however, for far traveled, flattened grains, any inclusions have usually been pounded out of the gold grains. It is difficult to quantify amounts of internal microinclusions in placer gold samples, and therefore it is difficult to ascertain if this is a significant factor in the model. However, it generally appears that effects other than the stream gradient are of limited importance. In the rare instances that there is a significant effect due to an internal or external inclusion, the averaging effect of the method (calculating a KDA, then fitting that surface) will largely ignore the offending data point as a statistical outlier. These effects are much more likely close to source, and are likely partially responsible for the previously discussed observations that the fits of model to data need not be as stringent close to source.

3.4.6 Utilizing the model

The final pragmatic outcome of this study is a method to predict lode source location using information recorded from placer gold grains. During generation of the model distances to source were optimized for the samples included in the model, providing a number of predicted source locations. Numerous other populations not used to generate the model had also been identified. For all of these samples, the model was used to determine an IGMTD which allowed an estimation of the source location to be made. Unfortunately in many cases, the prediction is not unique because the sample could have traveled down a number of different drainages to reach the location where it was finally collected. In these cases, the estimated source location assuming transport down every possible path was calculated. This results in there being numerous predicted possible source locations, but it is likely that there is a source located only at one or a few of these predicted source locations. Sample locations and all of the predicted source locations are presented in Figures 3.16 to 3.25.

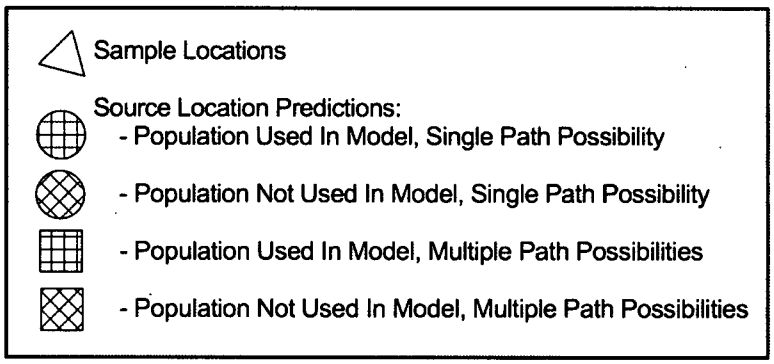

Figure 3.16: Legend for Figures 3.17 to 3.25. Numbers adjacent to predicted source locations indicate the wt.% Au predicted for that source.

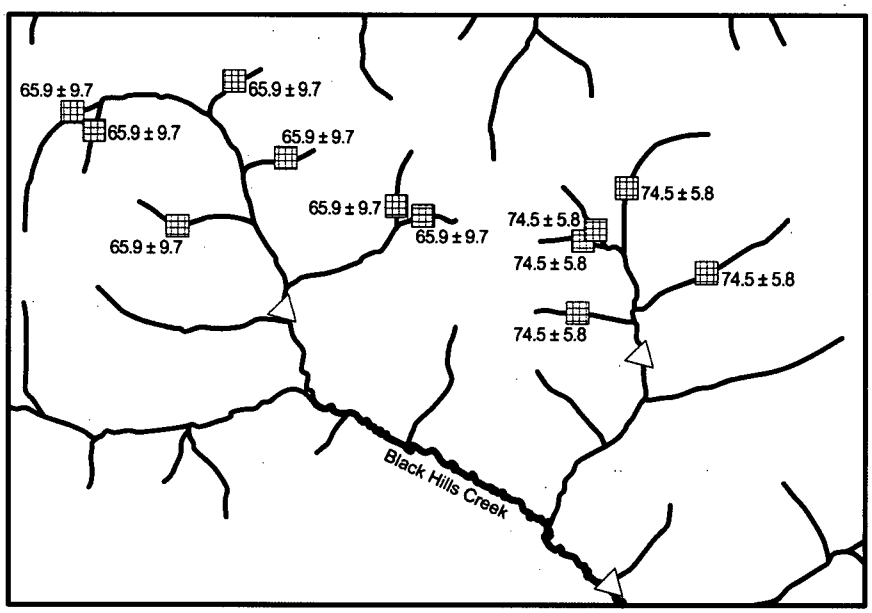

Figure 3.17: Location of samples and predicted source locations for the Black Hills Creek area.

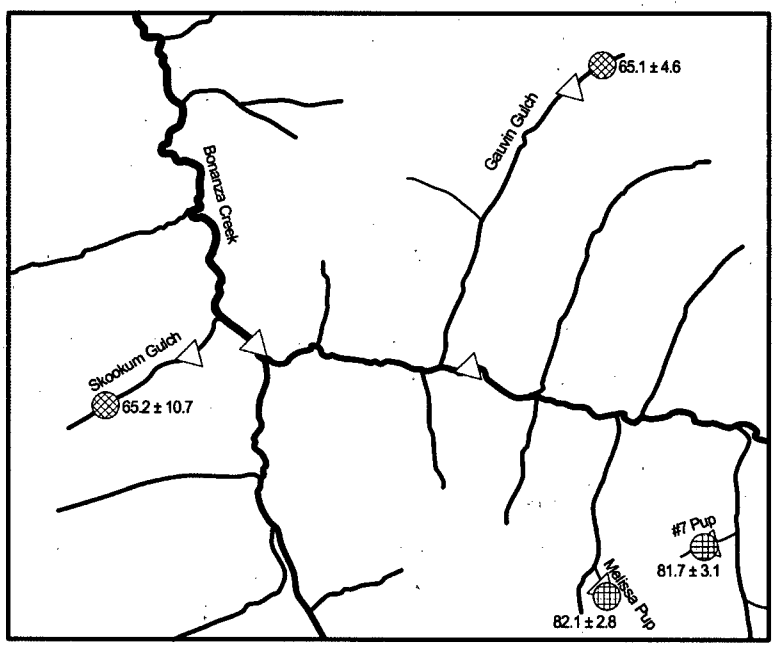

Figure 3.18: Location of samples and predicted source locations for the Bonanza Creek area.

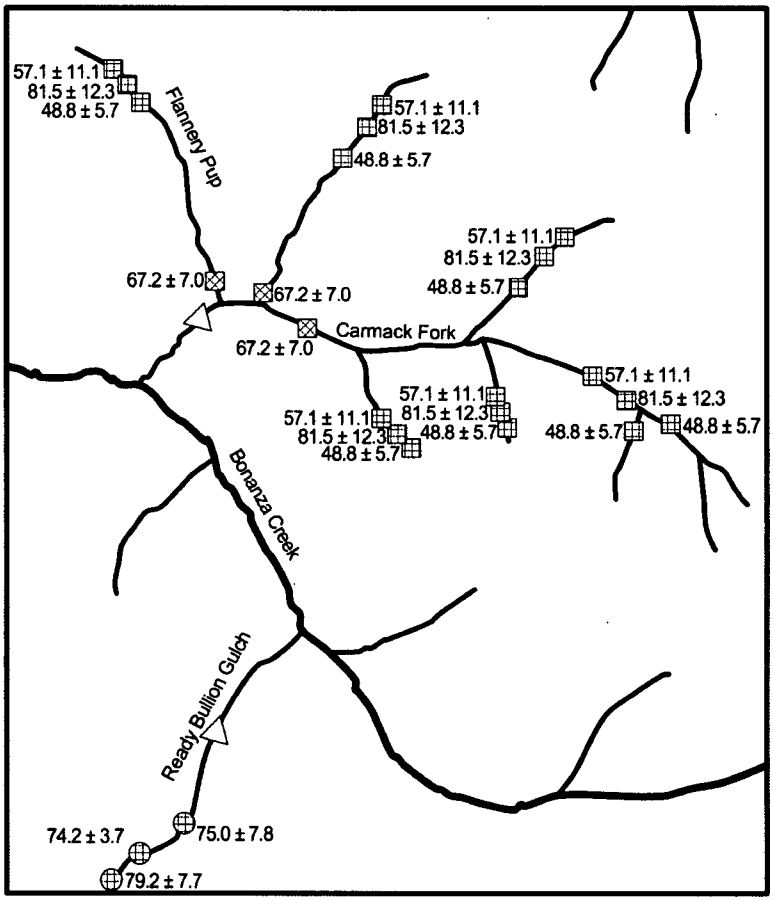

Figure 3.19: Location of samples and predicted source locations for the upper Bonanza Creek area.

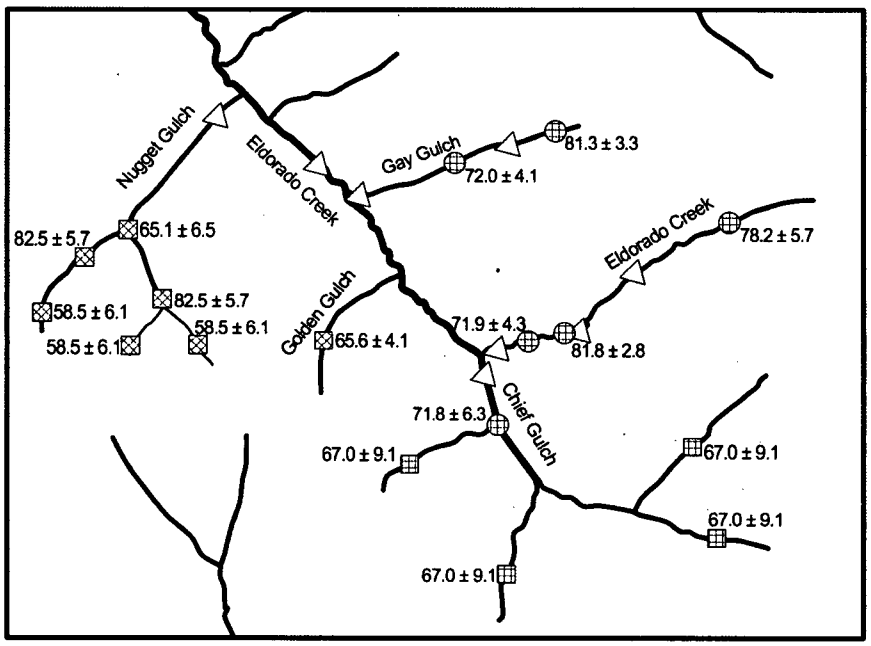

Figure 3.20: Location of samples and predicted source locations for the Eldorado Creek area.

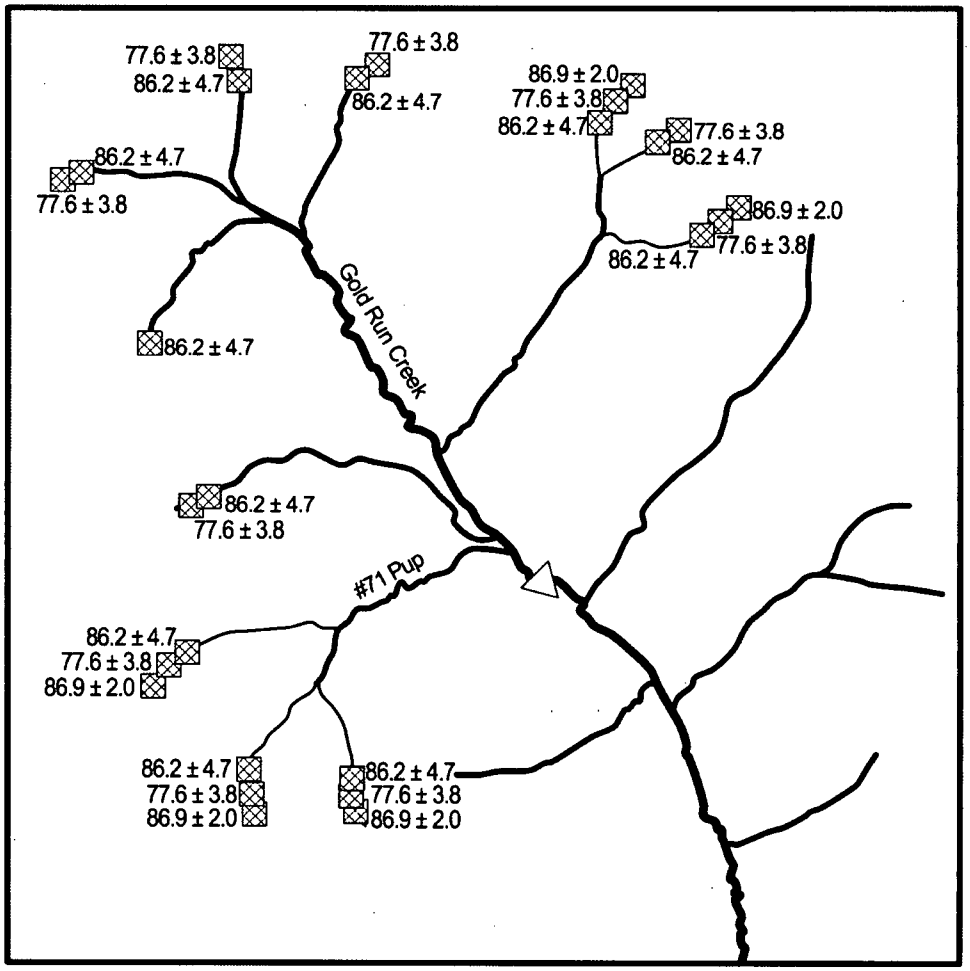

Figure 3.21: Location of samples and predicted source locations for the Gold Run Creek area.

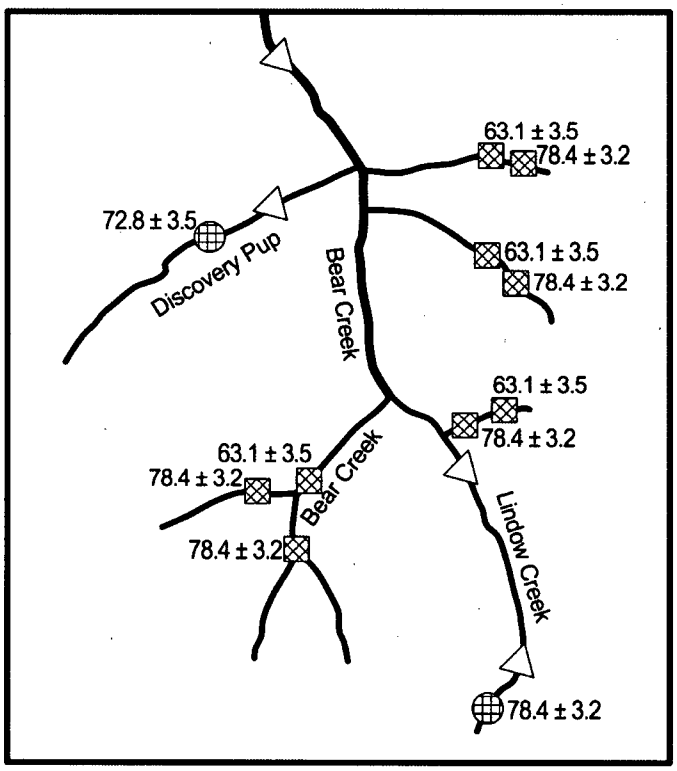

Figure 3.22: Location of samples and predicted source locations for the Bear and Lindow Creek area.

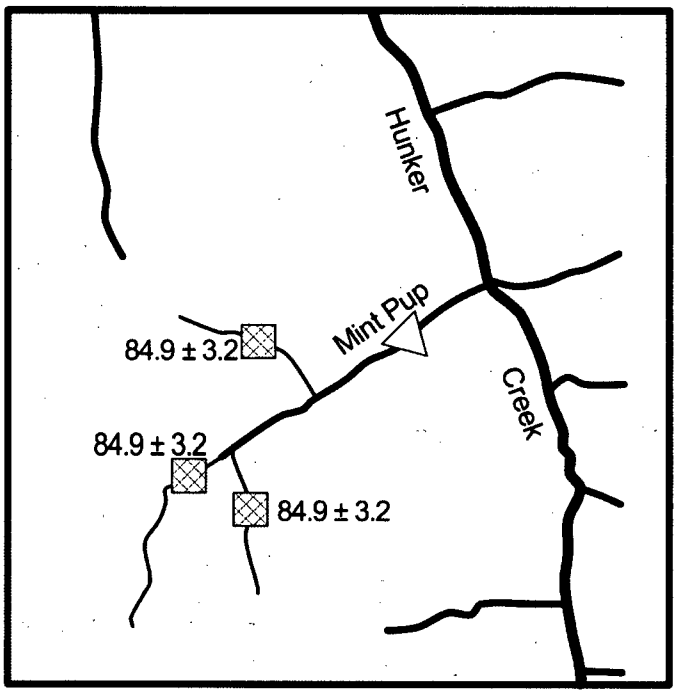

Figure 3.23: Location of samples and predicted sample locations for Mint Gulch.

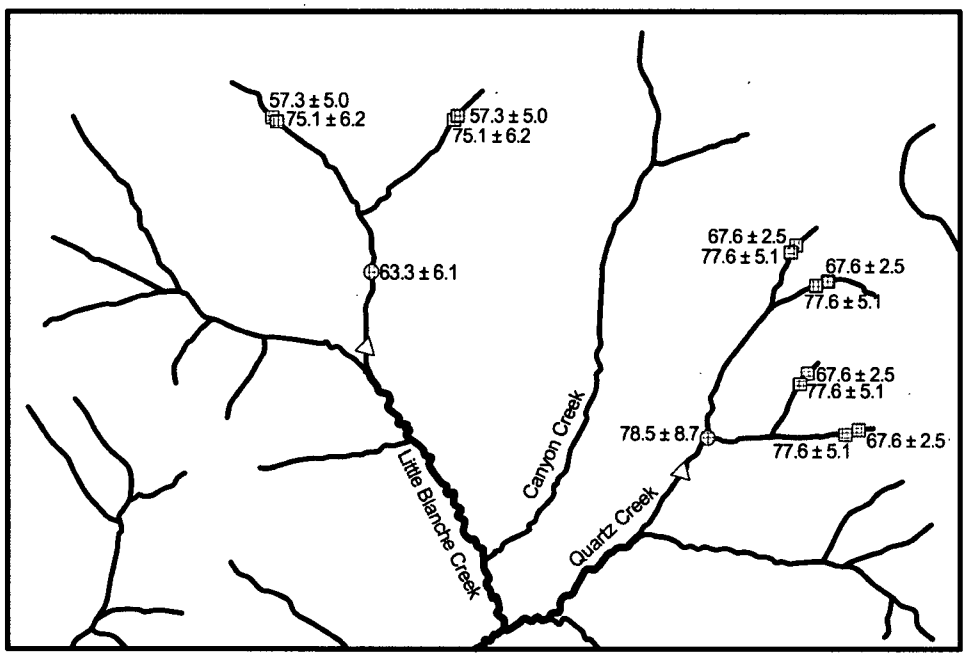

Figure 3.24: Location of samples and predicted sample locations for the upper Quartz and Little Blanche Creek area.

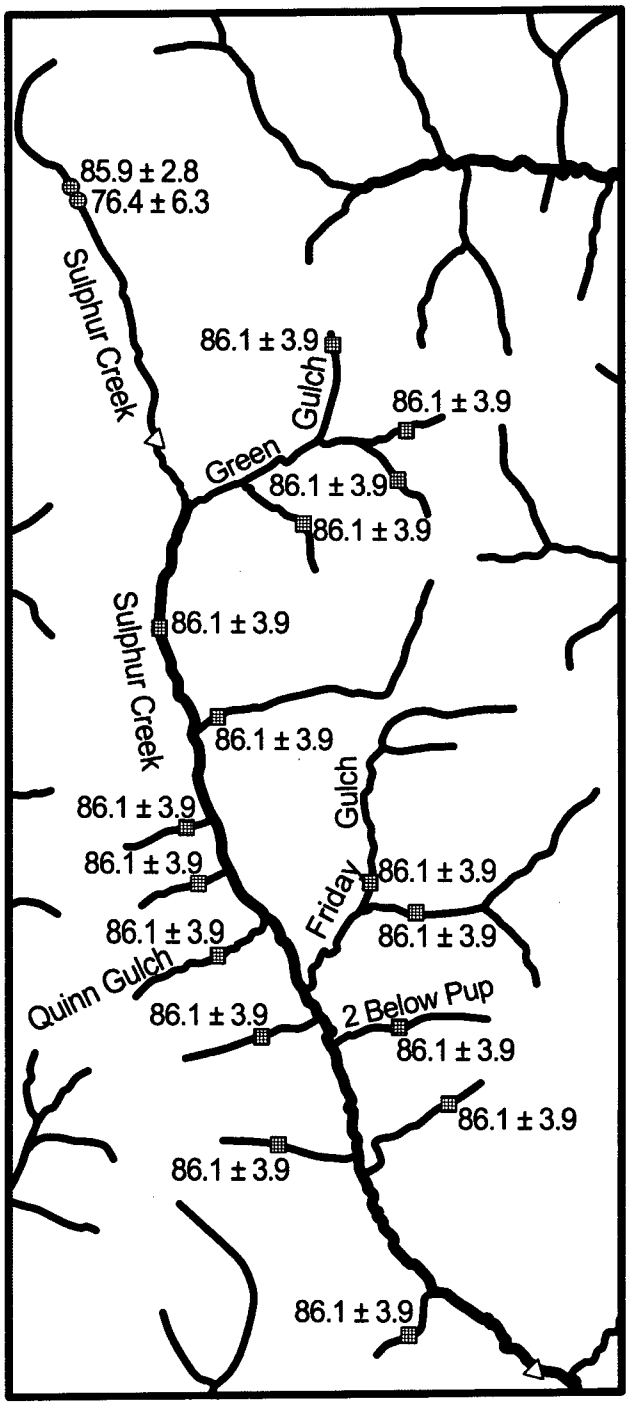

Figure 3.25: Location of samples and predicted sample locations for the Sulphur Creek area.

3.5 Conclusion

A method for the estimation of alluvial transport distance for placer gold grains has been developed through the statistical analysis of grain composition and morphology. This model has been used to predict lode source locations for a number of drainages in the Klondike Gold District; however, the accuracy of these predictions has not been verified. If the accuracy of the model fit is taken as any measure, then the predictions should be reasonably accurate. Although this model has been developed using samples from a single placer district, there are strong indications that the model will be widely applicable as it appears to be largely independent on stream host rock type or composition. It would be worthwhile to conduct a detailed study of this size in several regions of diverse geology, and to expand this study to include transport over greater distances (hundred of kilometers). Additionally, the effect of grain composition may require further scrutiny, as the range of compositions examined in this study is somewhat restricted. Furthermore, the application of this model to glaciated regions needs to be explored, as the effect of glacial transport will likely be significant. It is hoped that a subsequent study will attempt to use the predictions made by this work to locate yet undiscovered lode gold deposits in the Klondike District, and in so doing test the accuracy of this method, model and predictions.

3.6 References

Crawford, E.C., Mortensen, J.K.: An ImageJ plugin for the rapid morphological characterization of separated particles and an initial application to placer gold analysis. Computers and Geosciences, submitted, 2007.

Crawford, E.C., Chapman, R.J., LeBarge, W.P., Mortensen, J.K. Developing a new method to identify previously unrecognized geochemical and morphological complexity in placer gold deposits in western Yukon. In: Yukon Exploration and Geology 2006, D.S. Emond, L.L. Lewis and L.H. Weston (eds.), Yukon Geological Survey, pp. 139-148.

Fuller, E.A., Anderson, F.J. Placer geology of Black Hills Creek (Parts of 115O/7 & 10). In: Yukon Exploration and Geology 1992, Exploration and Geological Services Division, Yukon, Indian and Northern Affairs Canada, pp. 33-38.

Hofmann, H.J. Grain shape indices and isometric graphs. Journal of Sedimentary Research, 1994, Vol. 64, pp. 916-920.

Knight, J.B., Morison, S.R., Mortensen, J.K. The relationship between placer gold particle shape, rimming, and distance of fluvial transport as exemplified by gold from the Klondike District, Yukon Territory, Canada. Economic Geology, 1999, Vol. 94, 635-648.

Knight, J.B., Mortensen, J.K., Morison, S.R. Shape and composition of lode and placer gold from the Klondike District, Yukon, Canada. Bulletin 3, Exploration and Geological Services Division, Indian and Northern Affairs Canada, Yukon Region, 1994, 142 p.

Lowey, G.W. Placer Geology of the Stewart River (115N&O) and part of the Dawson (116B&C) map areas, west-central Yukon, Canada. Yukon Geological Survey, 2004, 275p.

Mortensen, J.K., Chapman, R., LeBarge, W., Jackson, L. Application of placer and lode gold geochemistry to gold exploration in western Yukon. In: Yukon Exploration and Geology 2004, D.S. Emond, L.L. Lewis and G.D. Bradshaw (eds.), Yukon Geological Survey, pp. 205-212.

Mortensen, J.K. Geology and U-Pb geochronology of the Klondike District,

west-central Yukon Territory. Canadian Journal of Earth Science, 1990, Vol. 27, pp. 903-914.

Outridge, P.M., Doherty, W., Gregoire, D.C. Determination of trace elemental signatures by laser ablation inductively coupled plasma mass spectrometry as a potential aid for gold exploation. Journal of Geochemical Exploration, 1998, Vol. 60, pp. 229-240.

Parzen, E. On Estimation of a probability density function and mode. The Annals of Mathematical Statistics, 1962, Vol. 33, No. 3, pp. 1065-1076.

Pouchou, J. L., Pinchoir, F. "PAP" (phi-rho-Z) procedure for improved quantitative microanalysis. In: Microbeam Analysis, J.T. Armstrong (ed.), San Francisco Press, San Francisco, California, USA, 1985, pp. 104-106.

Silverman, B.W. Density estimation for statistics and data analysis. Chapman and Hall, New York, New York, USA, 1986, 175 p.

Sterner-Rainer, I.L. Properties of gold-silver-copper alloys. Zeitschrift fur metallkunde. Vol. 18, No. 5, May 1926, pp. 143-148.

Youngson, J.H., Craw, D. Variation in placer style, gold morphology, and gold particle behavior down gravel bed-load rivers: An example from the Shotover/Arrow-Kawarau-Clutha river system, Otago, New Zealand. Economic Geology, 1999, Vol 94, pp. 615-634.

Chapter 4

A new method for performing LA-ICP-MS analyses of placer gold: development, results and implications.[1]

4.1 Introduction

Inductively coupled plasma mass spectroscopy (ICP-MS) has allowed the rapid analysis of a large number of elements in a broad range of samples. Used in conjunction with the spatially resolved sampling capabilities of LA-ICP-MS, this permits the examination of microscale variations in trace and microtrace element concentrations, and measurement of trace and microtrace element concentrations in very small samples.

Due to the presence of mineral inclusions and compositional variation, the compositional analysis of placer gold requires the ability to spatially resolve the location of the analysis. This has made the use of whole grain dissolution analytical chemistry relatively useless in the analysis of placer gold. EMPA allows for spatially resolved analysis, but is limited to measuring major and some minor element concentrations. This typically means that only gold and silver, and in some cases, mercury, copper and iron can be quantified.

This study aims to develop a method for the analysis of minor and trace element concentrations in placer gold samples using LA-ICP-MS. Ideally, this method should produce data that are comparable between users and instruments, allowing easy comparison between results obtained by other users, facilitating future comparisons between studies. We also intend to

[1]The information in this chapter has not yet been submitted for publication

present several discriminant plots for the evaluation of the results from this method; an initial step towards establishing typical compositional ranges from gold from a wide variety of mineral deposit types. This method may also prove useful in the forensic analysis of placer gold by aiding in the development of a gold composition database which can trace the source of any specific gold sample. This method and these plots are applied in an initial regional scale examination of placer gold from the Klondike District, west-central Yukon, Canada.

The method is useful in examining several unique features of placer gold, the trace element variation across a gold rich rim as well as variations in trace element concentrations between crystallographic domains. It may be possible in the future to use this method to examine the isotope systematics of placer gold. Unfortunately, gold is monoisotopic, but silver and many of the other trace elements that can be quantified by LA-ICP-MS are not and may provide information on deposit formation mechanisms or metal source for example. Energy dispersive spectroscopy (EDS) of mineral microinclusions has been used to approach several of these problems; however, this method is less than ideal because these inclusions are present in a relatively small proportion of the grains analyzed.

4.2 Previous Work

There have been few previous studies using LA-ICP-MS to examine gold, and the majority of the work that has been done has been focused on tracing the provenance of bullion samples for forensic purposes (e.g., Watling et al., 1994; Boshoff, 1995; Grigorova et al., 1998). The majority of previous researchers have also found it sufficient to examine raw plots of observed counts for each element, and perform a visual comparison between samples. Although using "fingerprint"' patterns such as this can be useful, it becomes impractical when large numbers of grains and/or samples are being analyzed. Furthermore, comparing patterns such as this is typically done visually, adding a subjective aspect to any comparison. Most importantly, comparing these "fingerprint" patterns between researchers is essentially impossible due to variations in instrumentation and other factors.

One study specifically examined the use of standards, generating standards of known concentrations of Fe, Ni, Cu, Sn, Pd, Pt, Pb and Bi in a range of gold / silver alloy mixtures (Kogan et al., 1994). This study was performed in collaboration with the Royal Canadian Mint, and required significant amounts of raw materials. No discussion was made of the resulting

homogeneity of the samples, however it was observed that the bulk alloy composition in silver and gold had little effect on the response from the trace elements. Furthermore, silver and gold argide were used successfully as internal standards.

Several studies have investigated the composition of placer gold using LA-ICP-MS (e.g., McCandless et al., 1997; Outridge et al., 1998), however they have been focused mostly on aspects of experimental methodology. There has yet to be a study examining a large number of samples regional sampling with the goal of understanding the lode : source relationship, the variability observed or the implications of gold composition with respect to geology or metal source.

All previous studies have utilized a quadrupole mass spectrometer. While these instruments have the advantage of being able to very quickly examine a large number of isotopes with different m/z values, they are significantly less sensitive than the high resolution double focusing magnetic sector instrument used in this study. Although this instrument takes slightly longer to obtain measurements on a large number of isotopes, it can make these measurements with much higher resolution (avoiding some polyatomic and isotopic interferences), and with much greater sensitivity. This results in the ability to use a much smaller laser spot for ablation, allowing for examination of much finer details.

4.3 Experimental

This study utilized a New Wave 213 nm Nd-YAG laser coupled to a Thermo Finnigan Element2 high resolution ICP-MS. The carrier gas for the ablated materials is He, which is then mixed with a constant Ar steam and fed to the ICP torch.

Placer grains for laser analysis are first hand isolated from field heavy mineral concentrates, then dried by rinsing with ethanol. The grains are arranged on adhesive tape with their major axes perpendicular to the adhesive in groups by sample location, roughly sorted by grain size. The grains then cast into one inch diameter epoxy pucks using Buehler epoxide resin (5:1 resin:hardener), allowed to cure overnight at ambient temperature and finally baked at 60°C for >5 hours. After cooling, the pucks were ground using Buehler carbimet SiC paper (grits 600, 400, 320, 240) on a Buehler Handimet 2 roll grinder so as to expose a section roughly bisecting the grains along the major axis. Polishing was continued individually using a Buehler Minimet 100 automated polisher with texmet 1000 cloths and 6, 3 and 1 μm

diamond paste with Buehler Metadi extender cutting fluid. Polishing times and pressures were 6 minutes at 4 lbs; 8 minutes at 2 lbs and 10 minutes at 1 lb for the 6, 3 and 1 μm pastes respectively, with the soft stop option on in all cases. The pucks were then polished for five minutes at 0.75 kg pressure on a Buehler petro-thin polisher using Buehler micropolish 0.3 μm alumina powder and water as coolant and lubricant. Final polish was obtained using a Chemomet pad and Buehler Masterprep 0.05 μm alumina suspension at 0.5 kgs pressure with water as lubricant and coolant. Mounts were washed with soap and rinsed with hot tap water between each polishing step.

Samples were then carbon coated before an examination on the scanning electron microscope, where backscattered electron imaged were recorded to identify grain cores and rims, as well as any inclusions. A single spot not on an inclusion and in the core of each grain was then analyzed for Au, Ag, Hg and Cu using a CAMECA SX-50 electron microprobe operating in wavelength dispersion mode under the following conditions: excitation voltage, 20 kV; beam current, 20 nA; peak count time, 40s; background count time, 20s; spot diameter 5μm. Au, Ag and Cu element samples were used to standardize the location of their characteristic X-ray lines, and HgTe was used for Hg. Ag and Au calibrations were monitored over the course of each run by multiple measurements of an Au80:Ag20 standard material. PET crystals were used for Au, Au and Hg, an LIF crystal was used to measure Cu. The following lines were observed: Au, Mα; Ag Lα Cu, Kα Hg, Mβ. Data was reduced using the PAP (phi-rho-Z) method of Pouchou and Pinchoir(1985); peaks were deemed acceptable if the total measured wt. % of the four measured elements was between 98 and 102 %. Detection limits of 0.20, 0.10, 0.05 and 0.20 wt. % were measured for Au, Ag, Cu and Hg. The carbon coating necessary for electron microprobe analysis was then removed prior to laser ablation by repeating the final two polishing steps.

4.4 Method Development

4.4.1 Overall Considerations

Ideally, it would be possible to develop a fully quantitative method to measure a variety of trace and microtrace elements in placer gold. Unfortunately, there are few recognized standards for gold and silver in a gold matrix, and none for the wide variety of elements this method seeks to analyze in a gold matrix. With laser ablation, having matrix matched standards is particularly important, due not only to the effects of the matrix on analytes in the plasma that are inherent to all ICP analyses, but the coupling of the laser

to the sample, as well as any effects in the plasma that form transiently at the site of laser ablation. Developing a set of standards would be extremely difficult, especially for placer gold analysis. In addition, the use of external standards would add significantly to the analytical time required, and the cost. Generally, past attempts at alloying metals aside from silver and mercury into gold have yielded inhomogenous materials. Generating a material containing mostly gold with 20 other elements present and completely homogenous would a non trivial exercise. Multiple standards would also be required; ideally with several concentration of each minor / trace element in order to assure a linear response, but also wide range of matrices would also be necessary, as the placer gold samples range from 45-100 wt. % Au, 5-55 wt. % Ag, 0-2 wt. % Cu and 0-15 wt. % Hg. Although there has been some examination of matrix effects in gold / silver alloys (Kogan et al., 1994), the effects of Cu and Hg would need to be considered as well. Considering the difficulty in generating even a single standard, the problems and cost associated with developing a large suite of standards would be prohibitive, and also prevent the widespread application of this method.

4.4.2 Accounting for Instrument Variability

As discussed above, simply examining fingerprints or "bar-code" plots of data in order to compare results from different grains can be useful when there are relatively few samples. It is however impractical when trying to compare and identify trends between hundreds of samples. Furthermore, comparing results between instruments is nearly impossible, since they are complicated by numerous and variable effects from the ablation, the plasma and instrument itself. When measuring elements in solution, an internal standard is usually added to account for these factors, allowing results to be normalized relative to any particular instrument, and allow direct comparisons of results. With placer gold, for the reasons listed previously as well as the nature of the samples, it is essentially impossible to add an internal standard to each sample. Instead, we have chosen to use the silver argide generated in the plasma as an internal standard, following previous workers (McCandless et al., 1997). All grains we have analyzed using LA-ICP-MS have previously had their major elements quantified by electron microprobe analysis. Since the silver content of each grain is known, the silver argide signal can be normalized to that value, providing results which should be free of the random effects of the laser, plasma and instrument, and which should be comparable between instruments. Values representative of the concentration of other trace elements can then be calculated as a ratio of

the recorded count rate for each element to the count rate for the silver argide. These values, although not absolutely quantitative, can be used to examine relative amounts of individual elements between samples, and to generate discriminant plots to identify compositional groups of grains.

4.4.3 Using an Argide as an Internal Standard

The mechanisms of argide production during LA-ICP-MS are poorly understood at best.The use of a silver argide as an internal standard requires that argide production be reproducible or predictable. To test this relationship, we developed a method which monitored ^{109}Ag, $^{107}Ag^{40}Ar$ and $^{109}Ag^{40}Ar$. It was necessary to change some parameters to reduce the ^{109}Ag signal from normal sample runs, in order to not overload the detector. We argue that argide formation occurs exclusively in the torch plasma, and decided to leave the torch setting constant for all analyses, instead changing the laser settings. By significantly reducing the size of the ablated spot, it was possible to have the ^{109}Ag peak on-range in analog mode, while still recording sufficient counts on the argides in ion-counting mode to obtain a good signal : noise ratio. The final ablation parameters for runs monitoring the silver : silver argide ratio were a laser firing frequency of 20 Hz, a laser spot size of 35 μm, and a laser power of 30%. The silver peak was measured in analog mode, and the argide peaks measured in ion counting mode.

For this method, each scan measuring 3 isotopes took 0.8 seconds, and 120 scans were collected for each sample. The first 8 scans were recorded with the laser off, and used as a background measurement; after a rise time during which the ablation and transport of ablated material to the torch stabilized, $\geq$ 78 seconds of sample data was available.

Since the argide is being used to account for instrument variability, it is important to monitor how the Ag : AgAr ratio may vary over an individual run, a day of sampling, and from day to day. Ideally one would examine this parameter between several instruments, however that is impractical for a single study. All of the data for this study was collected over a single 26 hour sample run, and ^{109}Ag : $^{109}Ag^{40}Ar$ (the "argide ratio") measurements were collected at the beginning, near the middle, and at the end of this run. For these runs, no internal standard was utilized; the counts per second for each isotope were averaged for the time over which the laser was not firing, and those value subtracted from the counts for the signal portion of the run. The argide ratio was then calculated for every scan in a run, averaged, and a standard deviation calculated over the signal portion of the run. The variation of this ratio over time is shown in Figure 4.1.

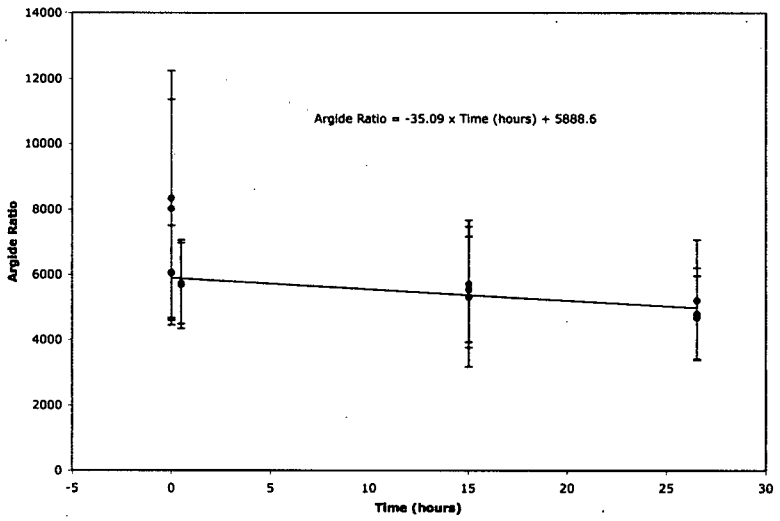

Figure 4.1: Calculated argide ratios and the standard deviation on them over the course of the data collection run. Best fit line shown was used to determine argide ratios for all sample runs.

The measurements of the argide ratio shown in 4.1 show that although argide production is not constant over time, is does appear to change in a reproducible manner. The first several argide measurement runs shown in Figure 4.1 are likely outliers; they were collected at the end of method development, before any sample runs had been performed. The trio of analyses in the group at $\sim$ 0.5 hours was measured after several test samples had been run. These first few point were ignored, then a best fit linear curve fitted to the remaining observations. This curve was used to calculate an argide ratio for all of the remaining samples.

4.4.4 Initial Multi-Element Method

A separate method was developed for the measurement of a large suite of trace elements in placer gold. Initially, an arbitrary number of elements were chosen for analysis based on previous work by other groups, and elements which have been used as discriminants between several types of ore deposits. Individual isotopes for measurement were chosen to achieve maximum signal (by choosing isotopes of high natural abundance), and to avoid potential polyatomic interferences. The initial list of isotopes being measured was ^{53}Cr, ^{57}Fe, ^{59}Cr, ^{63}Cu, ^{65}Cu, ^{66}Zn, ^{75}As, ^{77}Se, ^{95}Mo, ^{111}Cd, ^{118}Sn, ^{125}Te, ^{126}Te, ^{141}Pr, $^{107}Ag^{40}Ar$, ^{175}Lu, ^{178}Hf, ^{182}W, ^{195}Pt, ^{202}Hg, ^{208}Pb, ^{209}Bi, ^{238}U, $^{109}Ag^{40}Ar$. The concentrations of mercury and copper in the samples are measured on the electron microprobe, however those concentrations are only above the detection limit for $\sim$ 20 % and $\sim$ 6.5 % of grains respectively. Since these elements are present in significant amounts, allowing their measurement places an upper limit on the amount of amount that can be ablated (to prevent detector overload). Several grains containing high mercury and copper were selected on which to determine acceptable ablation parameters. The first parameters modified were laser power and firing frequency; at relatively low power and frequency (2 Hz, 10 % power) there was no material ablated, and no signal observed. First, the frequency was increased, then the power was slowly increased until there was good cratering observed with minimal splattering of ablated material. The laser spot size was then increased until the copper and mercury signals obtained from ablation of the grains in the sample suite with the highest measured concentration of mercury and copper was within the observable range on the ICP-MS. The results of the different ablation parameters tried are shown in Figure 4.2.

The final ablation parameters used for the bulk of the analyses were a laser firing frequency of 20 Hz, a laser power of 30%, and a spot diameter of 80 μm. The entire range of isotopes was scanned 80 times per run,

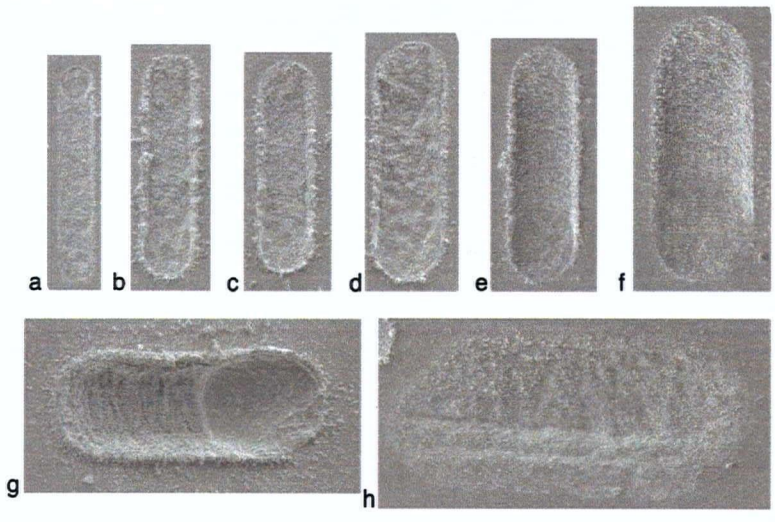

Figure 4.2: Secondary electron SEM images of laser ablation pits made using various ablation parameters. A: 12 μm spot, 20Hz, 30% power; b: 25 μm spot, 20 Hz, 30% power; c: 30 μm spot, 20Hz, 30% power; d: 40 μm spot, 20Hz, 30% power; e: 55 μm spot, 20Hz, 30% power; f: 80 μm spot, 20Hz, 30% power (the ablation parameters used for sample analysis); g: 80 μm spot, 20Hz, 40% power; h: 100 μm spot, 20Hz, 30% power. Ablation proceeded top to bottom or left to right.

with each scan taking 1.8 seconds, resulting in a total analysis time of 144 seconds. The first 6 scans (10.8 seconds) were run with the laser off; after a rise time during which the ablation and transport of ablated material to the torch stabilized, there was usually $\geq$120 seconds of signal recorded. In some cases the number of scans was increased to allow for longer traverses to examine elemental variation across grains. The signal for all elements except mercury decayed to background levels quickly (<10 seconds) after ablation was terminated. Mercury appears to be extremely "sticky" remaining in the system for extended periods of time (days). Numerous samples were then examined using this method.

4.4.5 Instrument Contamination

It should be noted that the analysis of placer gold by LA-ICP-MS has significant potential to cause instrumental contamination. Of particular concern is mercury, due to its relatively high volatility. In our experience, a significant mercury signal was observed when the laser was not firing, and the intensity of this peak was related to the number of samples examined, and their mercury contents. We found that contamination extended as far as the sampling cones at the front end of the mass spectrometer, but that this contamination disappeared relatively quickly during plasma operation (likely due to the high temperatures experienced proximally to the plasma). Some gold coloration of the cones was also observed, however it is unknown if this causes an increased gold background. Contamination in the laser setup was much more extensive, and made routine LA-ICP-MS uranium-lead dating of zircon impossible due to high background mercury levels (which mask measurement of some lead signals), even when using an alternate ablation cell. It was necessary to use an alternate ablation cell, and to replace all of the gas valves, connectors and tubing downstream of the ablation cell, as well as the tubing adaptor to the torch. Visual inspection of the interior of the gas valve most proximally downstream of the ablation cell revealed debris visible to the naked eye.

In a few cases, there was visible debris left spread over the surface of the sample mount after ablation (figure 4.3). This shows that there are reasonably large particles of material being ejected during ablation that may be entrained in the sample gas and carried into the instrument. This should be kept in mind for multi-user instruments, as introduction of this method may require careful monitoring to prevent problems for other users.

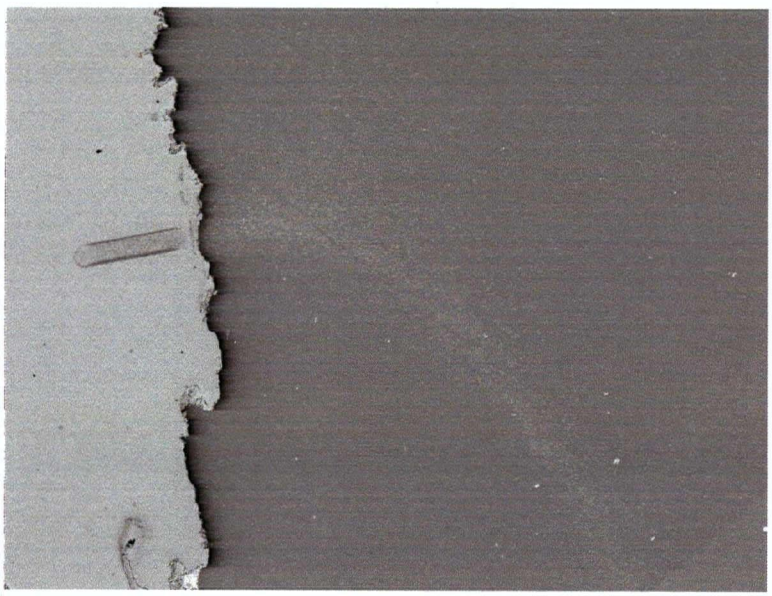

Figure 4.3: BSE SEM image of debris deposited on the sample mount during ablation. Deflection of the debris field is due to the flow of gas through the ablation cell. Width of figure is roughly 2 mm.

4.4.6 Calculations

Raw time resolved intensity data are imported into Microsoft Excel and a chart generated that shows the intensity for every isotope over the entire time of the analysis. The time window corresponding to the time when the laser was not firing is selected (the blank window), as is a range corresponding to the signal for the sample (the sample window). This allows for signals from inclusions and other abnormalities to be excluded. These features are generally easy to identify because they are 40 seconds or less in duration (the spot is 80 μm in diameter, moving at 2μm per second). The counts for each isotope during the blank window are averaged, then that number is subtracted from the intensity value recorded for each scan for that element. The internal standard correction is then made on the intensity value for each scan. The internal standard correction is:

$$X^{+}_{ISC} = \frac{\frac{[Ag]\times 0.51839}{{}^{107}Ag^{40}Ar^{+}_{BGC}\times\frac{AgAr^{+}}{Ag^{+}}} + \frac{[Ag]\times 0.48161}{{}^{109}Ag^{40}Ar^{+}_{BGC}\times\frac{AgAr^{+}}{Ag^{+}}}}{2} \times X^{+}_{BGC} \times 10000$$

Equation 4.1: Internal Standard Correction Calculation

Where X^{+}_{ISC} is the internal standard corrected value for a given isotope in acu's, $[Ag]$ is the concentration of silver as measured on the microprobe in weight %, ${}^{107}Ag^{40}Ar^{+}_{BGC}$ is the background corrected value for ${}^{107}Ag^{40}Ar^{+}$, $\frac{AgAr^{+}}{Ag^{+}}$ is the measured value for that ratio for the sample run, ${}^{109}Ag^{40}Ar^{+}_{BGC}$ is the background corrected value for ${}^{109}Ag^{40}Ar^{+}$, and X^{+}_{BGC} is the background corrected value for a given isotope in cps.

Finally, the intensity values are averaged for the sample window for each isotope, and the final value multiplied by 10000. The 10000 is simply a scale factor to obtain values that fall roughly near one for most isotopes. Although these calculations yield a value in weight %, the results have been listed as arbitrary concentration units (acus), since there are a number of factors ignored in the analysis that make it unlikely that these number are actually indicative of true concentrations, and we do not wish to present our results in a way that could be misunderstood.

4.4.7 Practical Considerations

All of the data presented as plots in the remainder of this chapter is available in appendix A.

The use of the silver argide as an internal standard was used here, but the efficacy of this procedure is difficult to ascertain because of the lack of standards available for analysis. The observation that the argide ratio appears to change over a day of instrument use warrants a more detailed examination of this variation. We speculate that argide production changes over the day due to slight changes in the instrument running conditions over the day. More detailed examination may reveal that other factors such as purging of the sample cell, or contamination of the instrument may play a role in the change of rate of argide production. The mechanisms of argide formation in the plasma are poorly understood; the argide ratio may even depend to some extent on the trace elements present in an individual sample. The argide ratio was examined for grains with varying silver contents (figure 4.4), however there may be other elements that have specific catalytic ability to form argide, or preferentially retard those processes.

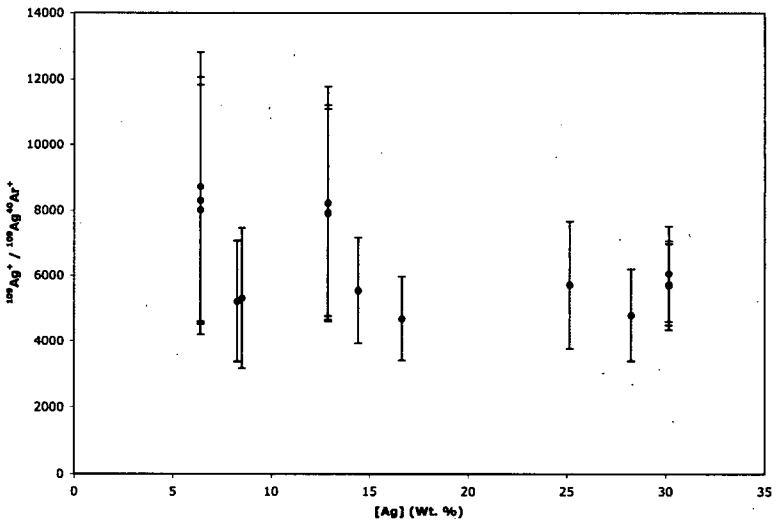

Figure 4.4: Argide ratio for samples with a range of different silver contents.

Future studies should examine argide formation more rigorously; examining the ratio for a range of grain compositions, after each sample change (just after the sample is inserted, and just before it is removed), and generally more frequently during a sample run. Future studies could also examine using some other isotope as an internal standard to account for instrument variability during determination of the argide ratio; gold argides are an obvious possible choice. Measuring the argide ratio for both isotopes of silver

would also likely be a wise choice; although the mass difference between the isotopes is small, and the effects likely small, the additional effort is minimal.

As previously mentioned, the results from the laser analysis are presented in acus rather than as wt. %. There are numerous considerations which make reporting the results in wt. % inappropriate:

- The argide ratio measured for silver is probably not identical for all other measured elements. Argide formation is poorly understood at best, but it would be unreasonable to assume that the wide range of elements being analyzed behave identically.
- Response for a given isotope is known to be somewhat dependant on its mass. This assumption is in fact known to be false; higher mass isotopes have a higher response in the MS. It would have been possible to apply an arbitrary mass response curve based on information garnered from solution ICP-MS analysis; however, the choice of correction would be somewhat arbitrary, and would just introduce another conversion factor into the calculation that would not produce appreciably more realistic results.
- The ionization efficiency differs from element to element. The first ionization energies of the elements being examined are different, so the ionization efficiency is also almost guaranteed to be different. As above, one could introduce an additional correction factor based on the ionization energies, however the correction would be somewhat arbitrary, and not worth the extra effort.

An initial analysis of the first round of data showed an almost perfect relationship between mass 202 (monitored to measure ^{202}Hg) and mass 238 (monitored to measure ^{238}U). Although it is possible that uranium is present in gold, the quality of the relationship indicates the mass 238 signal is likely due to ^{198}Hg^{40}Ar. This interference could be resolved by running the instrument in high resolution mode, however the decrease in sensitivity and increase in analysis time is not practical. ^{235}U could also be observed, however there is also an argide interference on this peak, and the ^{235}U isotopes is present in significantly lower abundance. It might be possible to measure a different mercury isotope, then look for the argide interference; however, this approach would likely be prone to error; the quantification of U in samples of placer gold where mercury is present is practically impossible using the method as presented.

The cratering produced by the selected final ablation method results in some splattering, but it is not severe. It is likely impossible to obtain the

same straight edged pits as with silicate minerals, due to the comparatively low melting point of gold alloys. The textures seen on the SEM images (Figure 4.2) indicate that there is some at least partially molten material formed during ablation. The ablation caused by this method is significantly better than that causes by the methods used in previous studies (Watling et al., 1994), which resulted in extensive melting of material directly in and around the laser path, and also resulted in sufficient splattering of the molten material that the interior of the ablation cells became coated in gold.

4.5 Results and Discussion

4.5.1 Initial Examinations

A number of placer gold samples from drainages encompassing most of the Klondike District, and one additional proximal location (Black Hills Creek, located southeast of the Klondike District), were analyzed using the multi-element method described here. For this initial regional scale examination, the samples were grouped roughly by area, as shown in Figure 4.5.

Examining the data revealed several plots capable of discriminating between samples obtained from the different areas defined in Figure 4.5. In several instances there is likely to be some overlap between the compositional fingerprints observed for the areas defined in Figure 4.5. For example, the samples collected in the Indian River drainage may record signatures similar to those observed for Sulphur and Gold Run creeks; all of these areas are located upstream of some of the Indian River samples examined. Figure 4.6 still reveals several different groupings. For example, the samples from group 5 ubiquitously show either elevated tin or platinum contents. Group 2 samples have generally elevated tin compared to most other samples from the region. The only other groups which display routinely elevated tin are groups 5, 6 and 7. Interestingly, the samples from groups 8 and 10, located geographically between group 2 and groups 5,6 and 7, have some of the lowest tin and platinum contents.

Figure 4.7 allows for some groups which overlapped in Figure 4.6 to be separated; for example, group 3 is poorly separated in Figure 4.6, however it forms a fairly well defined field at high As and Ag in Figure 4.7. Groups 9 and 10 also start to become better defined as having generally lower arsenic contents at a given silver concentration. Figure 4.7 also starts to show general trends for samples from the Yukon; silver and arsenic are reasonably well correlated.

Figure 4.8 again helps separate some of the groups: group 10 is located

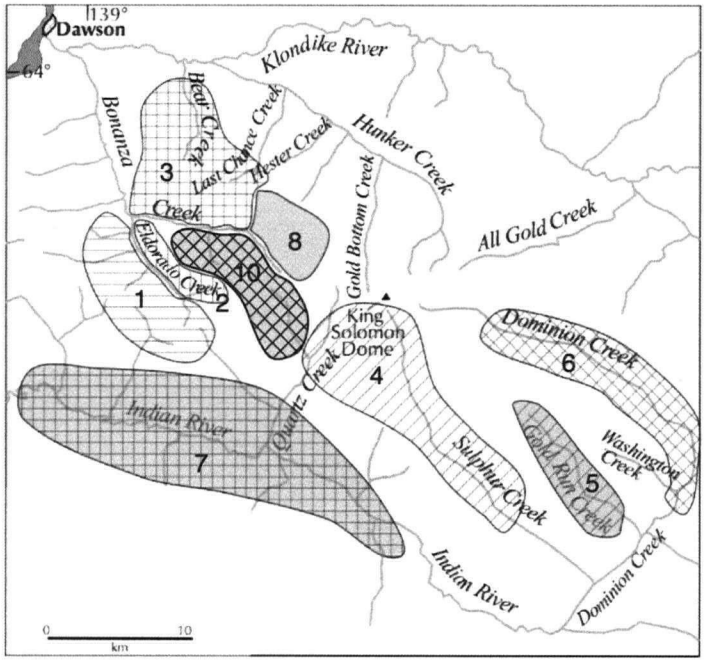

Figure 4.5: Group 1: Eldorado west, horizontal lines; group 2: Eldorado east, vertical lines; group 3: Bonanza north, crosshatch; group 4: Quartz and Sulphur Creeks, diagonal lines; group 5: Gold Run Creek, shaded diagonal lines; group 6: Dominion Creek, diagonal crosshatch; group 7: Indian River, shaded crosshatch; group 8: Carmack Forks, shaded; group 9: Black Hills Creek, not shown on map; group 10: Bonanza south, shaded diagonal crosshatch. Figure after Mortensen, J.K. et al., 2006.

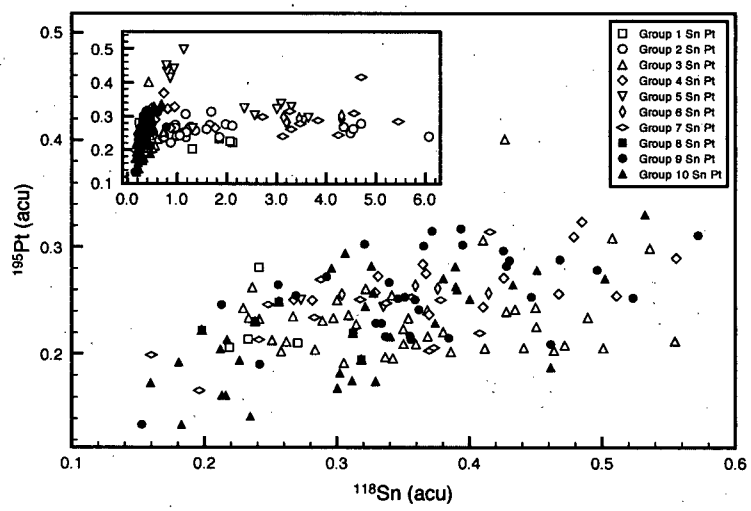

Figure 4.6: ^{195}Pt signal as acu versus ^{118}Sn signal as acu for placer gold samples obtained from different group areas (as defined in Figure 4.5) of the Klondike District, west central Yukon.

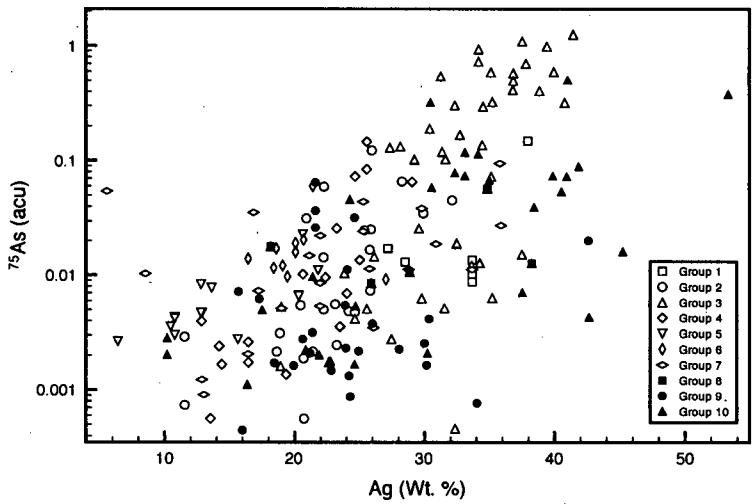

Figure 4.7: ^{75}As signal as acu versus Ag as Wt. % from EMPA for placer gold samples obtained from different group areas (as defined in Figure 4.5) of the Klondike District, west central Yukon.

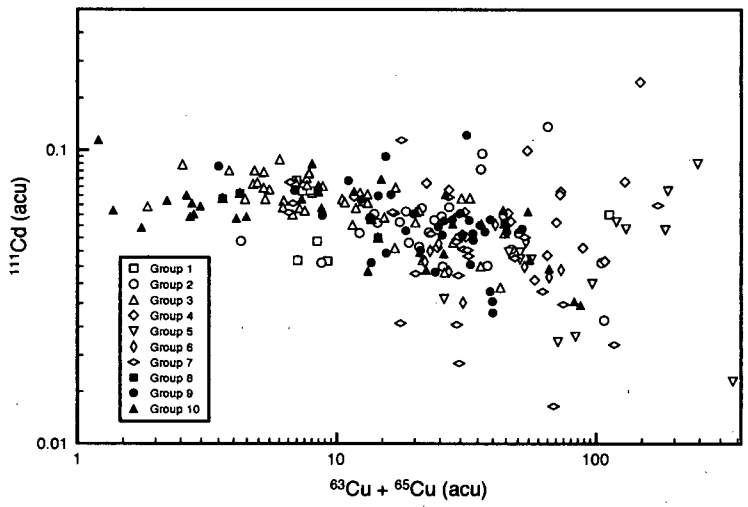

Figure 4.8: ^{111}Cd signal as acu versus combined ^{63}Cu and ^{65}Cu signal as acu for placer gold samples obtained from different group areas (as defined in Figure 4.5) of the Klondike District, west central Yukon.

near the end of the overall trend for the group, with group 3 located in a reasonably tight group at slightly higher copper content. Groups 9 and 2 roughly overlap at higher copper and slightly lower cadmium. There is a slight overall trend in the data, with grains recording higher copper concentrations generally having decreased cadmium. Groups 4 and 5 deviate the most from this trend, and are both located proximally geographically.

There are some definite trends observable in this data, but there appears to be sufficient complexity over small geographic ranges that a more detailed examination is necessary. Several of the grouping were broken down even further and examined.

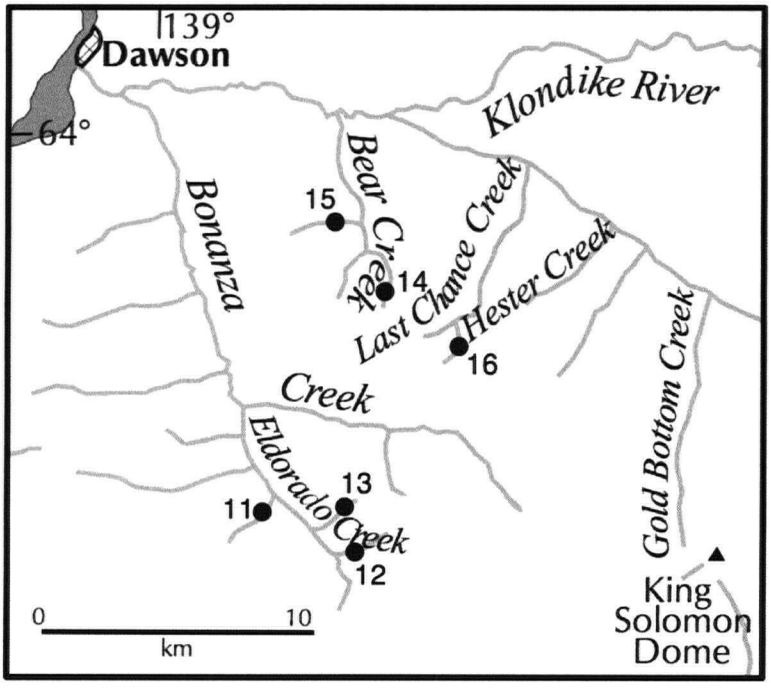

Figure 4.9: LA-ICP-MS analysis subgroup definitions. Group numbers are indicated directly on the map. Group 11: Nugget Gulch; group 12: upper Eldorado Creek; group 13: Gay Gulch, group 14: upper Lindow Creek; group 15: Discovery Gulch; group 16: upper Last Chance Creek. Group 17 is from Black Hills Creek, not shown on this map. Figure after Mortensen et al., 2006.

Figure 4.10 allows for reasonable distinction between groups even over this much smaller geographic range: group 11 is fairly isolated at high mer-

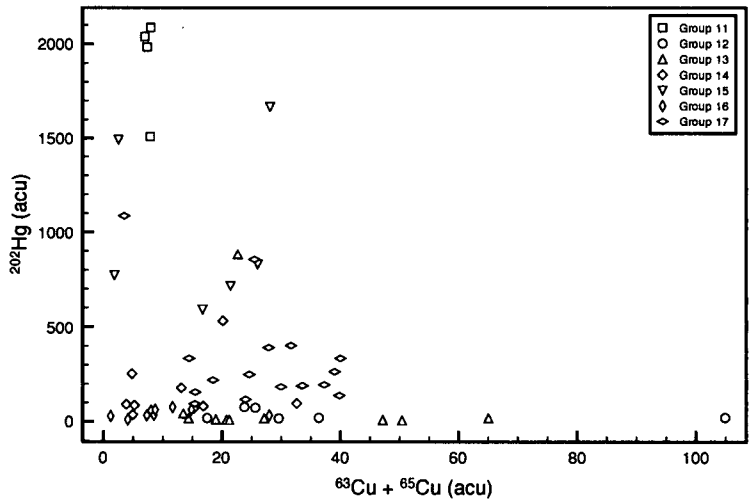

Figure 4.10: ^{202}Hg signal as acu versus combined ^{63}Cu and ^{65}Cu signal as acu for placer gold samples obtained from different group areas (as defined in Figure 4.9 of the Klondike District, west central Yukon.

cury, group 17 is fairly well distinguished at moderate mercury and slightly elevated copper. Groups 12, 13 and 16 have essentially no mercury, with the copper contents differing slightly; 16 having the least and 12 having the most.

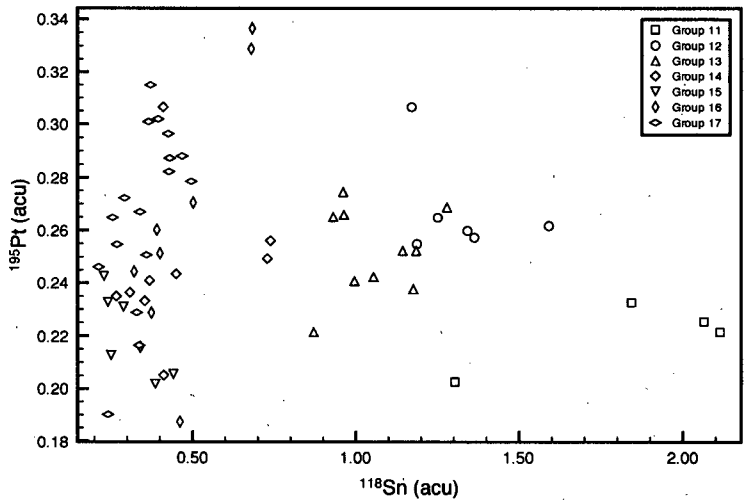

Figure 4.11: ^{195}Pt signal as acu versus ^{118}Sn signal as acu for placer gold samples obtained from different group areas (as defined in Figure 4.9) of the Klondike District, west central Yukon.

Figure 4.11 also shows a number of reasonably well distinguished groups. Group 11 is again well separated, displaying low platinum and high tin contents. Groups 12 and 13 have similar platinum contents, however group 13 has definitely lower tin. This plot clearly distinguished both of those groups from group 16 which has very little tin, which contrasts the grouping in Figure 4.10. The remainder of the groups all have little tin, and some separation can be made based on the platinum content, however the separation is not as clear.

4.5.2 Detailed Discussion

Unfortunately, although it is easy to measure where an individual placer sample was collected, it is extremely difficult to locate geographically where that gold originally came from. It is also difficult to determine how many lode sources are contributing to a given placer deposit or sample.

Even considering these difficulties, there are some interesting initial results from this reconnaissance study. For example, there has previously been a proposed compositional break moving east to west across Eldorado Creek. Gold compositions (measured by EMPA) similar to those seen in group 11 are seen southwest of the location of group 12; if the compositional fingerprint measured for group 11 is similar at that location, then Figure 4.10 indicates a trend in the north-south direction, possibly indicating a single deposit varying in concentration over this distance, rather than several discrete deposits of vastly different type. The presence of boiling textures in veins located near Eldorado Creek (Mortensen, J.K., pers. comm..) may explain the apparent 'step' in major element concentrations, with the LA-ICP-MS data indicating the deposition of gold was continuous over this distance.

Although the majority of grains examined using LA-ICP-MS did not exhibit internal compositional variability, several grains did reveal potentially interesting compositional features. These were most likely usually caused by the ablation of mineral microinclusions; these were identified by the time frame over which the signal was modified. With the laser being operated using an 80 μm spot moving at 2 μm per second, an inclusion present at the surface of the grain should modify the signal for 40 seconds. Inclusions which are present just below the surface, or which are small enough to be completely ablated in less than 40 seconds may affect the signal for less time (but not more).

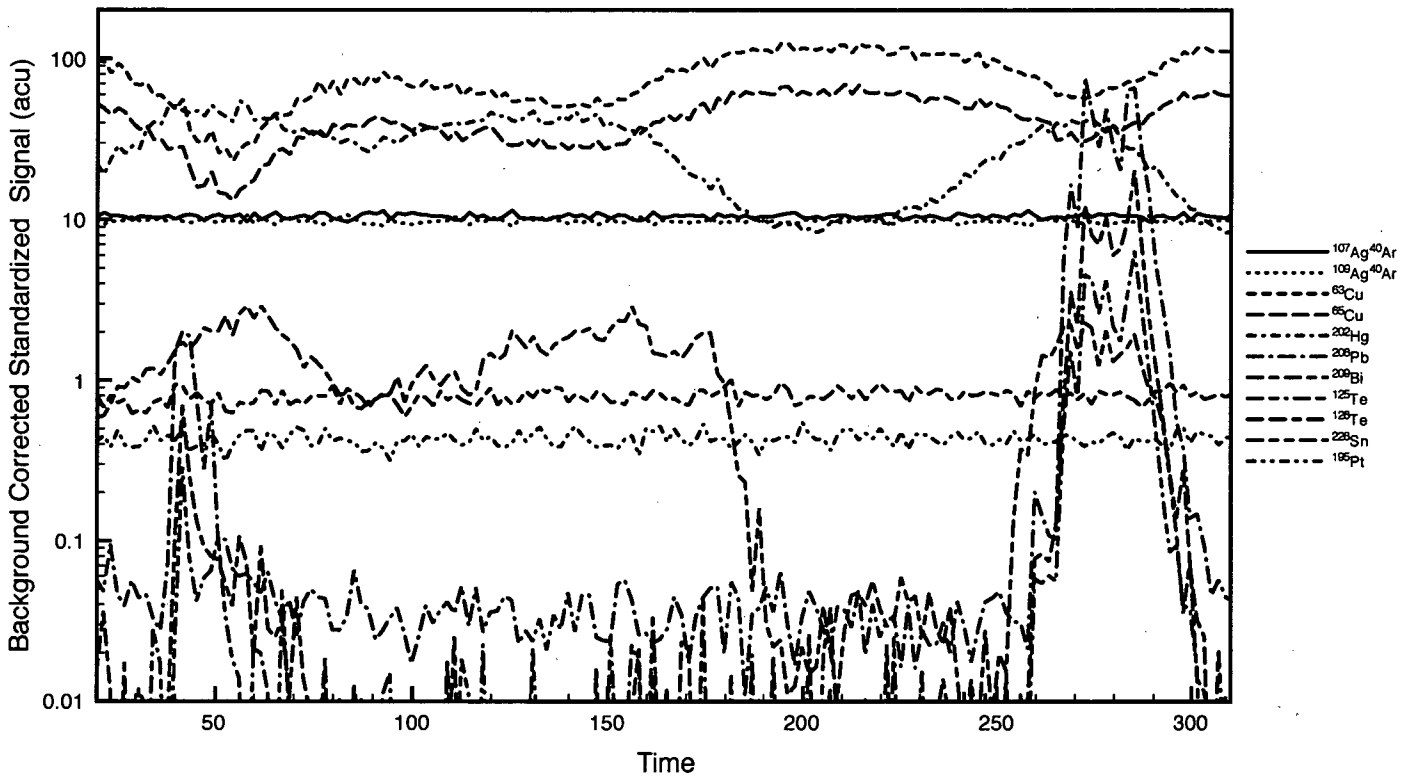

Figure 4.12: Laser signals over time for a placer gold sample from the Klondike. Initial background window, signal rise time, and all elements for which no non-zero signal were observed have been removed.

Figure 4.12 shows an abnormal LA-ICP-MS run displaying several compositional features. The response between signals for elements where multiple isotopes were measured matched quite well, which indicates for these elements that it is very likely that the signal is actually due to the element of interest. There is also no drastic evidence of elemental fractionation. One interesting feature present here that was found in several samples was the inverse relationship between copper and mercury. This may due to multistage deposition of metals during deposit formation, variable mobility of the metals and chemical leaching, or some other as yet unidentified process. The relationship observed between mercury and bismuth is also interesting; this may be due to similar behavior of these metals during deposit formation (partition coefficients into gold alloys, transport mechanisms in ore fluids, identical metal source), or to post-deposition processes.

The feature starting at ~250 seconds is likely an inclusion, this one containing significant Pb and Te, and possibly Bi and Hg. It is interesting to note the variation in the signal for other elements near the inclusion; this may be due to the presence of these elements in the inclusion and their diffusion into the alloy, or may indicate changes in fluid composition during deposition of the gold alloy leading up to or after formation of the inclusion. If the latter is the case, then the gold could be used as direct evidence of the changes in fluid chemistry during deposit formation. The similar compositional spike at ~40 seconds may also be due to an inclusion that was quite small, or deeply buried. Subsequent or prior examination of this grain by SEM might be used to identify the presence, location and composition (using EDS) of microinclusions; though any subsurface inclusions would be overlooked.

Figures 4.13, 4.14 and 4.15 show several time resolved LA-ICP-MS signals and the location of those traverses on a backscattered electron image of the grain. The features seen in this case are too large to be inclusions, and the gradual change in composition is also not consistent with the sharp transition that would be expected for the ablation of an inclusion. This may be another instance where the composition of the fluid from which the gold formed was changing over time, and the gold is recording those changed. The increase in Bi, Te and Pb (possibly associated with cooler and/or late fluids such as those present in epithermal deposits) supports the argument that the changing composition reflects a change in fluid chemistry. As the grain forms over time, it is likely that the hydrothermal system forming them is cooling, and reasonable that these later stages may be enriched in metals that are more easily carried in these later, cooler fluids.

The use of LA-ICP-MS has allowed the quantification of numerous ele-

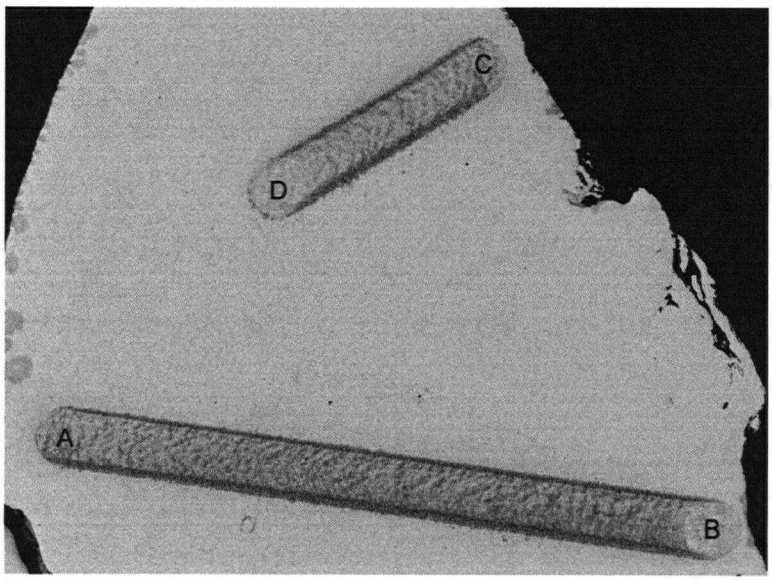

Figure 4.13: BSE SEM image of several ablation tracks from the analysis of a placer gold grain from Black Hills Creek, west-central Yukon. Image is roughly 1.1 mm across.

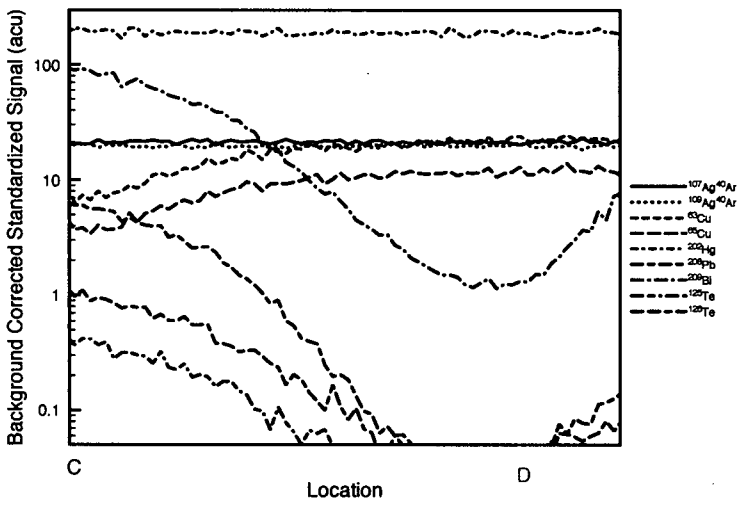

Figure 4.14: Laser signals over time for a placer gold sample from the Klondike. Initial background window, signal rise time, and all elements for which no non-zero signal were observed have been removed. Locations correspond to positions on Figure 4.13

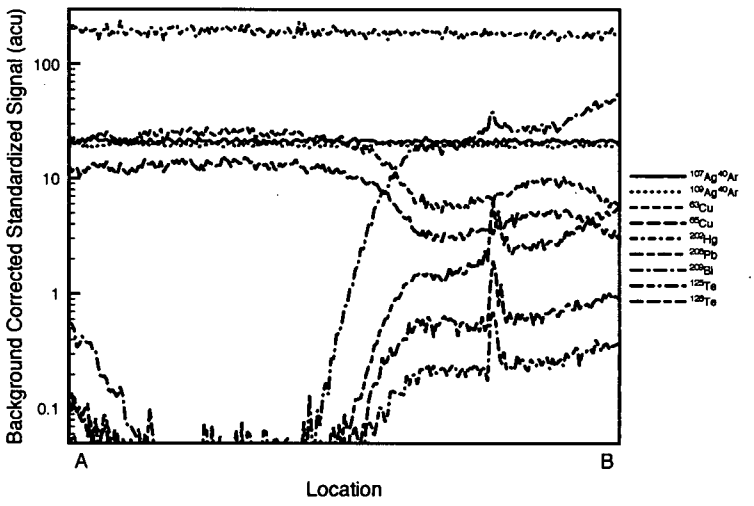

Figure 4.15: Laser signals over time for a placer gold sample from the Klondike. Initial background window, signal rise time, and all elements for which no non-zero signal were observed have been removed. Locations correspond to positions on Figure 4.13

ments not previously measured in natural gold samples. Initial examination of these results has produced a much more detailed picture than previously available of the compositional variation in gold deposits across the Klondike.

4.6 Future Work

Significant work remains to be done in the application of LA-ICP-MS to the study of gold in the Klondike, and worldwide. The method as presented appears to work reasonably well, but requires some additional development before it can be applied more broadly. Most of these changes have already been discussed. Additionally, the measurement of uranium appears to be practically impossible, so the measurement of mass 238 can be deleted from the method.

The formation of argides in general needs to be addressed in greater detail, as previously mentioned: how does the argide ratio change over an hour or a sampling session; how does it vary session to session or between instruments; is it dependant on trace element content of the samples? A more thorough investigation of the argide ratio for a broad range of samples, and more frequent measurement of this ratio is definitely warranted. It may be worth examining measuring gold argide during normal sample runs; since gold and silver content are known for each grain analyzed by the laser, comparing the signals from the silver and gold argides and the known concentration could give indications if elemental fractionation is occurring.

Additional elements of interest should also be added to the method, especially for samples for the Klondike. Since platinum appears to be ubiquitous in Klondike gold, we propose to also measure palladium and rhodium in the future; platinum : palladium ratios are commonly of interest in studying platinum group element deposits. Measuring rhodium will give additional information on the relative distributions of any platinum group elements present. Furthermore, cadmium was detected in a number of samples, so we propose to include the measurement of antimony and indium, since these elements are seen in association with cadmium in several deposit types.

It may also be worthwhile to examine multiple isotopes for elements of interest; the isotope systematics of elements (such as lead, platinum, tin) in placer gold has not previously been examined, and may prove extremely interesting in terms of deposit type fingerprinting, ore deposition models or metallogeny.

Future work focusing on the application of this method to the Klondike should attempt to define compositional fingerprints for the lode sources that

have been identified from the Klondike. These samples, coming from known locations and known to be from a single lode source, will allow a much more specific examination of any possible composition trends in the lode deposits in the Klondike. The fact that some trends and definite difference using the samples presented here is encouraging that the future study of the lodes will prove interesting. Isolating individual lode deposit fingerprints will also help understand the results from the placer samples. It will hopefully be possible to link results from individual placer gold grains to specific lode deposits, which may help define their possible extents. Additionally, if there are placer gold grains found with compositional fingerprints that do not match known lode deposits, it is a strong indication that there are as yet undiscovered lode sources present. This will also help to guide future exploration in the region.

There has also been a good deal of work done examining the presence, number and type of mineral microinclusions present in placer gold. Examining these results in light of the trace and minor element composition of the gold grains in which they were located should prove interesting and help define the link between mineral microinclusions and gold composition. Together, these methods may provide significant new insight into the genesis of gold deposits in the Klondike District.

LA-ICP-MS will also be useful in examining other specific physical phenomenon seen in placer gold. The origin of the gold rich rims seen in placer gold deposits worldwide is still debated, and LA-ICP-MS represent a new tool with which to examine this problem. Currently, the composition definition of these rims has only been in terms of gold and silver; extending this range using LA-ICP-MS may help support or disprove the numerous hypotheses available to explain rim formation. Ablating at a single spot starting on the outside of an unpolished grain and monitoring the LA-ICP-MS signal over time should reveal the minor and trace element concentration changes over the rim transition. This may be an application in which monitoring for elemental fractionation using the gold argide may prove useful, since fractionation is much more likely to occur in a deep ablation pit. Alternatively, numerous raster scans over the same area of a grain would provide a number of scans, each measuring a different section of the grain moving from the rim towards the core.

Gold crystallinity is another aspect of placer gold research to which LA-ICP-MS has application. Recent studies have indicated that the major element composition of placer gold does not directly relate to internal crystallographic structure (Chapter 5), but it would definitely be worth examining the trace element composition for grains exhibiting different crystallographic

features, and to search for trace element composition variation in a grain which displays multiple internal crystallographic domains.

A broader application of this method is to the study of gold deposits worldwide. One could develop a database of compositional fingerprints for different gold deposits and gold deposit types. This database would be useful forensically, as has been done previously, but would also have academic applications in understanding the partitioning of various elements into native gold alloys under different conditions. This study presented the possibility that gold grains can display compositional variation that may be indicative of changes in ore fluid chemistry; if this is true, then native gold from a particular deposit might be used to examine the changes in ore fluid chemistry during formation of that deposit. The composition of placer gold may prove to be an indicator of the source of the metal in a deposit, providing an additional method to probe this aspect of a deposit and inform any model describing its formation. A database of gold compositions from different deposit types might also find use as an exploration tool; a placer gold sample could be used to identify the deposit type from which the placer deposit was derived, which could play a role in exploration decisions.

This method is still in its infancy, however there are already early indications that it should prove to be extremely useful in the study of gold deposits from the Klondike, and possibly in the study of gold containing deposits worldwide.

4.7 References

Boshoff, F., Barzev, A.I., Theron, S.J., de Wit, M.C.J. AARL Project No. R/94/208 gold characterization study. 2005. Anglo American Research Laboratories (Pty) Limited, Johannesburg, the Republic of South Africa.

Grigorova, B., Anderson, S., de Bruyn, J., Smith, K., Stúlpner, K., Barzev, A. The AARL gold fingerprinting technology. Gold Bulletin, 1998, Vol. 31, No. 1, pp. 26-29.

Kogan, V.V., Hinds, M.W., Ramendik, G.I. The direct determination of trace metals in gold and silver materials by laser ablation inductively coupled plasma mass spectrometry without matrix matched standards. Spectrochimica Acta, Vol. 49B, No. 4, pp. 333-343.

McCandless, T.E., Baker, M.E., Ruiz, J. Trace element analysis of natural gold by laser ablation ICP-MS: a combined external/internal standardisation approach. Geostandards Newsletter, 1997, Vol. 21, No. 3, pp. 271-278.

Mortensen, J.K., Chapman, R., LeBarge, W., Crawford, E. Compositional studies of placer and lode gold from western Yukon: Implication for lose source. In: Yukon Exploration and Geology 2005, D.S. Emond, G.D. Bradshaw, L.L. Lewis and L.H. Weston (eds.), Yukon Geological Survey, 2006, pp. 247-255.

Outridge, P.M., Doherty, W., Gregoire, D.C. Determination of trace elemental signatures by laser ablation inductively coupled plasma mass spectrometry as a potential aid for gold exploation. Journal of Geochemical Exploration, 1998, Vol. 60, pp. 229-240.

Pouchou, J. L., Pinchoir, F. "PAP" (phi-rho-Z) procedure for improved quantitative microanalysis. In: Microbeam Analysis, J.T. Armstrong (ed.), San Francisco Press, San Francisco, California, USA, 1985, pp. 104-106.

Watling, R.J., Herbert, H.K., Delev, D., Abell, I.D. Gold fingerprinting by laser ablation inductively coupled plasma mass spectrometry. Spectrochimica Acta, 1994, Vol. 49B, No. 2, pp. 205-219.

Chapter 5

Examining the Internal Crystallographic Structures of Placer Gold[1]

5.1 Introduction

Crystalline gold has been commonly observed in placer deposits in the Klondike, and worldwide (e.g., Taber, 1942; Francis, 2004; Mauthner, 2004). Aside from descriptions of external morphology (McCready, 2003), studies investigating this crystalline nature have been lacking, and attempts to use crystallinity to inform other features or processes such as gold rich rims and their formation have been essentially absent. The absence of these studies may relate to the difficulty in obtaining crystallographic data from placer gold. Gold and gold alloys are all relatively soft, and crystallographic information will be distorted or lost during preparation for many procedures such as powdering for X-ray powder diffraction. The application of several previously underutilized methods for examining crystalline structures was explored as applied to placer gold.

If a suitable method for examining the internal crystal structure of placer gold could be developed, that information could provide insight into several qualities related to place and lode gold deposits. First, it is unknown if there are differences in the internal crystallography of gold from different lode sources. It is already known that some deposits tend to produce externally crystalline gold, while others do not. This crystalline character is however quickly lost during alluvial transport. If internal crystallography is retained during transport and can be related to source type, then examining the internal crystallography of a sample suite may inform the number and or type of lode source deposits. Examining a number of samples downstream from a lode may also inform any changes in crystallography during transport. If internal crystal structures are destroyed during trans-

[1]This chapter has not yet been submitted for publication

port, then it may be possible to relate the percent crystallinity or amount of deformation present to transport distance. Gold crystallinity may also help explore core/rim relationships. If crystallite boundaries extend across the compositional boundaries between the core and rim it could indicate that rims formed mainly by chemical leaching. If the gold rich rims have a unique crystallographic signature in addition to their distinct chemical identity, then it may indicate that rims form by the growth of new gold. In this Chapter we provide a general overview and some reconnaissance evaluation of some of the methods currently available, in the hope that other workers studying placer gold may find additional uses for these methods.

5.1.1 Previous Work

Some basic physical science research has been done examining gold and gold alloys, and their crystal structures (Berndt et al., 1970; Marcus et al., 2004). There was also been some work examining crystal structure defects, and methods for examining those defects including acid etching (Hashimotot et al., 1976). X-ray powder diffraction was also used in one study of gold-indium and gold-tin alloys (Stratton et al., 1966).

There has been a good deal of work examining the role of bacteria in the formation of crystalline gold, and in the formation of gold rich rims on placer gold. Some studies have examined the specific sites of metal deposition on bacteria (Beveridge et al., 1980), and the individual peptides (Kulp et al., 2004) involved in catalyzing the precipitation of the gold crystallites. Several studies have investigated the ability of bacteria to precipitate crystalline gold in vitro for the purposes of producing novel materials (Klaus et al., 1999; Klaus-Joerger et al., 2001; Nair et al., 2002; Senapati, 2005), or as proxies to natural placer gold formation (Southam et al., 1994). Several studies have also examined the remnant signatures present in placer gold that indicate that biomineralization has occurred, such as elemental signatures (Southam et al., 1996; Southam, 1998; Reith et al., 2005), and surface features (Watterson, 1991; Knight, 1993; Watterson, 1994).

Several of these papers employed transmission electron microscopy (TEM) to investigate the crystalline nature of gold grains. Most of these studies simply examined external crystal morphology on the micro scale, though one also examined internal crystal characteristics. Unfortunately, most these studies examined only in vitro generated gold grains / aggregates; only one example of internal structure for a natural placer gold grain is given (Southam, 1998).

One study has used chemical etching (aqua regia) to examine internal

crystal structure, and used the results as evidence of the growth of placer grains in the surficial environment and of individual placer grains resulting from the aggregation of multiple crystals (Craw, 1992). Their study confirmed that features seen in etched grains were not due to compositional differences, but did not otherwise prove that the features were crystallographic in nature.

5.1.2 Unanswered Questions and Goals

The one previously recorded attempt at examining crystallographic texture of placer grains is encouraging; however, it remains to be proven that the observations made post acid etching are representative of crystallographic texture. Confusing results from the acid treatment of placer gold have occurred in the past (Watterson, 1991; Knight, 1993; Watterson, 1994).

There has also been considerable interest in examining the role of bacteria in the generation of crystalline gold. Much of this work has focused on the mechanisms of the formation of this gold. Classification of the gold has been limited to classifying the newly formed gold as pseudocrystalline (morphologically crystalline, but incapable of producing electron diffraction patterns) or crystalline (morphologically crystalline, and capable of producing an electron diffraction pattern). Comparisons of the crystallographic texture of this newly formed gold to that of the grains to which it added have not been performed.

This study seeks to explore the application of several previously unutilized methods for the analysis of crystallographic texture to placer gold, and to reexamine the use of some of the method previously employed. The methods will not be used to examine a particular problem in depth, but are being presented as possible methods for examining a number of aspects of placer gold currently under investigation.

5.2 Methods

Placer gold samples were dried in the laboratory by being rinsed with ethanol several times and allowed to air dry at ambient temperature overnight. Gold was then manually separated from other heavy minerals under a binocular microscope. Gold grains were then roughly sorted by size and mounted onto adhesive sheet with their smallest axes parallel to the sheet. The grains were then cast into 1" diameter epoxy pucks using Buehler epoxide resin (5:1 resin:hardener), allowed to cure overnight at ambient temperature and finally baked at 60°C for >5 hours. After cooling, the pucks were ground

using Buehler carbimet SiC paper (grits 600, 400, 320, 240) on a Buehler Handimet 2 roll grinder so as to expose a section roughly bisecting the grains. Polishing was continued using a Buehler Minimet 100 automated polisher with texmet 1000, and 6, 3 and 1 μm diamond paste and Buehler Metadi extender cutting fluid. Polishing times and pressures were 6 minutes at 4 lbs; 8 minutes at 2 lbs and 10 minutes at 1 lb for the 6, 3 and 1 μm pastes respectively, with the soft stop option on in all cases. The pucks were then polished for five minutes at 0.75 kg pressure on a Buehler petro-thin polisher using Buehler micropolish 0.3 μm alumina powder and water as coolant and lubricant. Final polish was obtained using a Chemomet pad and Buehler Masterprep 0.05 μm alumina suspension at 0.5 kgs pressure with water as lubricant and coolant. Mounts were washed with soap and rinsed with hot tap water between each polishing step.

Samples were then vacuum carbon coated and examined on a Philips XL30 scanning electron microscope (SEM) equipped with a Princeton Gamma-Tech energy dispersion X-ray spectrometer (EDS). Microprobe analysis were then performed on these polished, coated samples measuring Au, Ag, Hg and Cu using a Cameca SX-50 electron microprobe operating in wavelength dispersion mode under the following conditions: excitation voltage, 20 kV; beam current, 20 nA; peak count time, 40s; background count time, 20s; spot diameter 5μm. Au, Ag and Cu element samples were used to standardize the location of their characteristic X-ray lines, and HgTe was used for Hg. Ag and Au calibrations were monitored over the course of each run by multiple measurements of an Au80:Ag20 standard material. PET crystals were used for Au, Au and Hg, an LIF crystal was used to measure Cu. The following lines were observed: Au, Mα ; Ag Lβ ; Cu, Kα ; Hg, Mβ. Data was reduced using the PAP (phi-rho-Z) method of Pouchou and Pinchoir(1985); peaks were deemed acceptable if the total measured wt% of the four measured elements was between 98 and 102%. Detection limits of 0.20, 0.10, 0.05 and 0.20 wt% were found for Au, Ag, Cu and Hg respectively.

Electron backscatter diffraction (EBSD) experiments were performed on several samples as well.

The carbon coat on the samples was then removed by repeating the final polishing step. The final two polishing steps were repeated between subsequent etching steps. The first etchant used was a mixture of 1.38 g KI and 0.39 g I_2 in 30 ml distilled water. This generates the I_3^- anion in solution which is a potent oxidant. This etchant generated appreciable observable surface effects almost immediately at ambient temperature, but was usually left to act for 20 minutes to obtain good detail and relief. The second etchant used was aqua regia, which generated visible changes after

10 minutes at ambient temperature, but was usually left for up to an hour to ensure good surface feature development. These samples were rinsed with distilled water and ethanol, then allowed to air dry before being vacuum carbon coated and examined again on the SEM in secondary electron (SE) mode. Although numerous other etchants are available (Voort, 1984); these were chosen since their components are commonly available, they store well, and are relatively non-toxic.

One grain that had been etched using the iodine based etchant was soaked in a concentrated (sub-saturated) aqueous potassium iodide solution for two hours, then rinsed with water and ethanol, dried and carbon coated before re-examination on the SEM.

The samples were prepared for X-ray diffraction analysis by repeating the final two polishing steps. No carbon coating is required prior to X-ray analysis. The epoxy pucks did need to be ground down significantly (to less than 10 mm in diameter and less than two mm thick) in order to fit into the X-ray diffraction instrument. A Bruker D8 Discoverer X-ray diffractometer equipped with a Hi-star area detector for GADDS (General Area Detector Diffraction) was used for X-ray diffraction analysis. A 0.5 mm^2 X-ray beam (Cu Kα and Kβ) was used, with the area detector located 6 cm from the sample. The sample, X-ray source and detector were orientated to record the 2θ range of from 30 to 90 degrees, allowing collection of reflections from the [1,1,1] ($2\theta = 38.3^o$), [2,0,0] ($2\theta = 44.4^o$), [2,2,0] ($2\theta = 64.7^o$), [3,1,1] ($2\theta = 77.6^o$), and [2,2,2] ($2\theta = 81.9^o$) faces. This method rotates the sample 360^o around an axis perpendicular to the sample surface, centered on the centre of the impinging X-ray beam; data collection for this rotation was divided into 72 five degree sections. Pole figures were calculated from this data using Bruker GADDS software.

5.3 Results

It has previously been noted that the composition of placer gold affects how quickly it is removed by chemical etching. To ensure that the features seen in this study were not caused exclusively by compositional variation across the grains, numerous microprobe analyses were made across several of the grains being studied. Also, several EDS X-ray maps were recorded. As seen in Figures 5.1, 5.2, 5.3, 5.4 and 5.5, neither of these methods revealed any significant compositional variation for this particular grain.

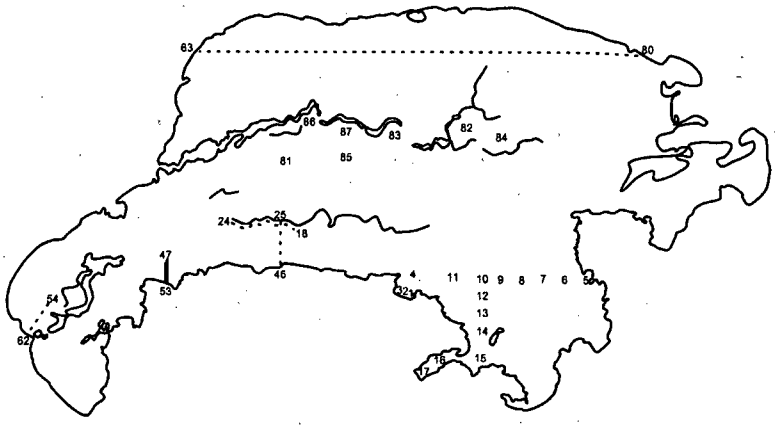

Figure 5.1: Locations of probe analysis across a grain. Grain size is approximately 1 x 0.4 cm.

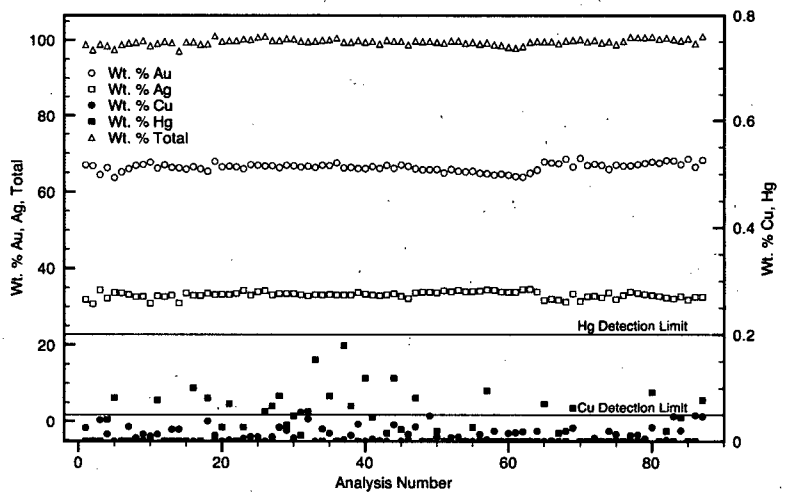

Figure 5.2: Probe results for analysis locations indicated in Figure 5.1.

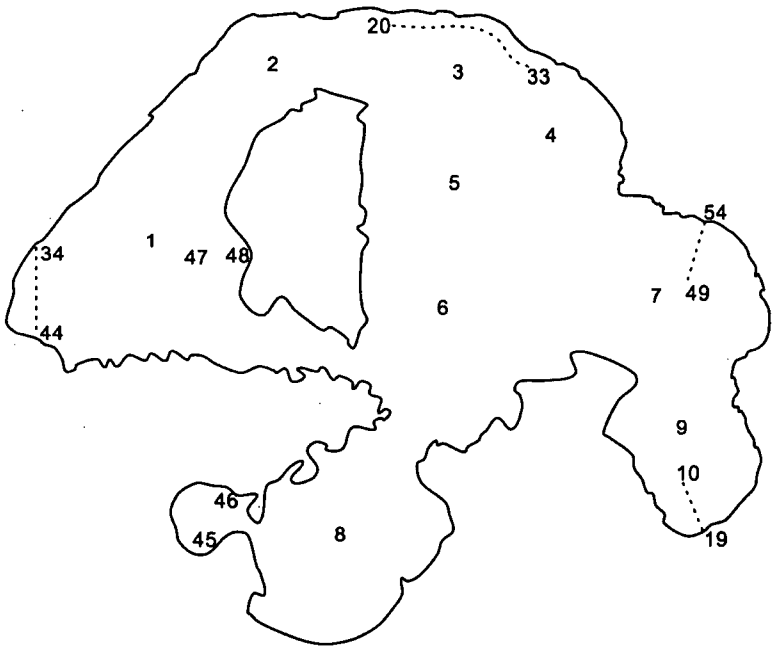

Figure 5.3: Locations of probe analysis across a grain. Grain size is approximately 2.5 x 2.5 mm.

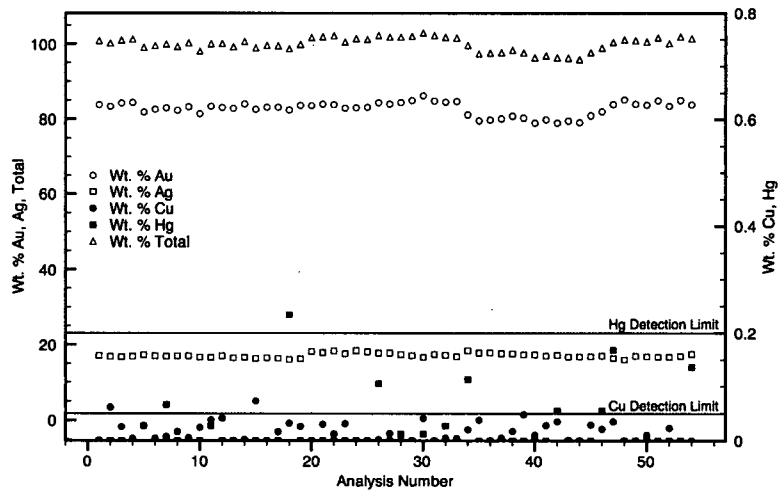

Figure 5.4: Probe results for analysis locations indicated in Figure 5.3.

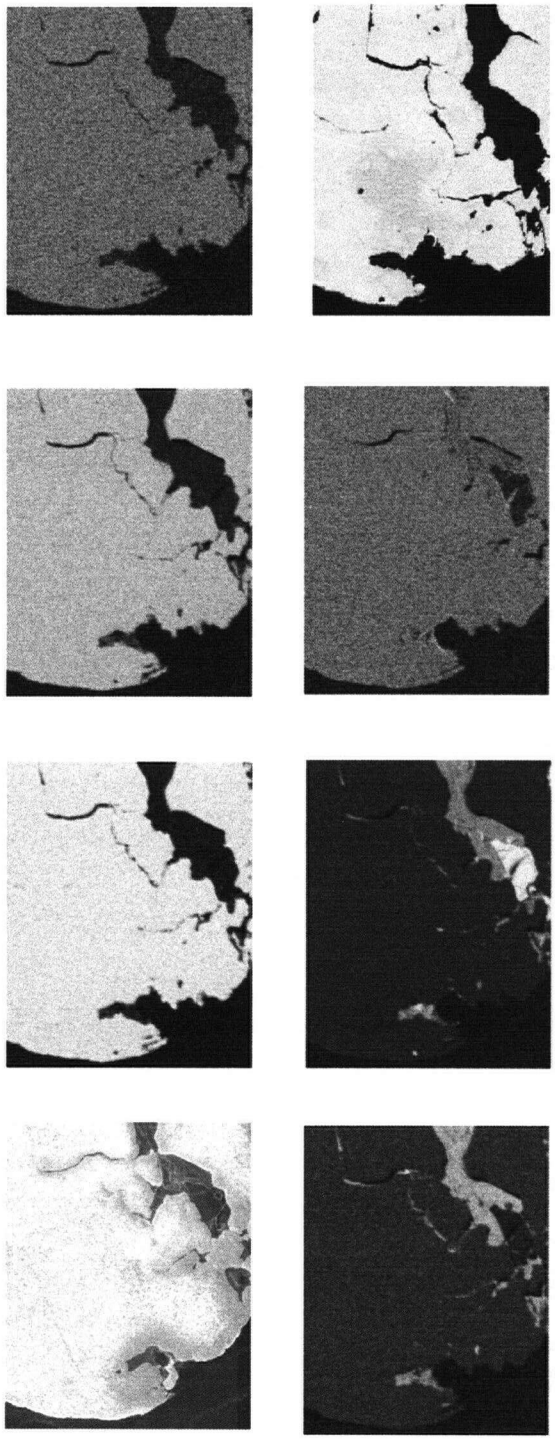

Figure 5.5: XRD maps of one portion of the grain in Figures 5.1 and 5.2. From top left, clockwise: SE SEM image of grain etched with KI/I_2, Au EDS map, Ag EDS map, Cu EDS map, SE SEM image of grain etched with aqua regia, Fe EDS map, Si EDS map, Al EDS map.

The chemical etching resulted in the development of significant surface topography. The resulting surface shows zoning visible to the naked eye, as well as extremely small scale zoning visible only at high magnification on a SEM. After etching, some portions of the grains took on the look of roughly polished gold (matte yellow) to the naked eye, while other section appeared grey to black (figure 5.6). These different visual appearances are likely due to the differences in reflectivity produced by the microscale surface topography (figure 5.7). It was our initial conclusion that the resulting topography was a direct manifestation of the underlying crystallographic texture; crystallites exposing different crystal faces at the surface would exhibit different rates of dissolution, developing surface topography.

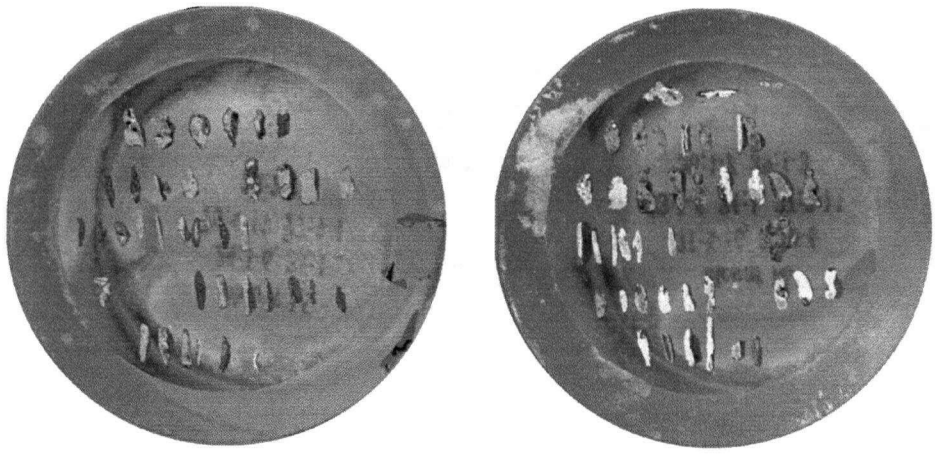

Figure 5.6: Mounts containing a number of aqua regia etched grains. Each mount is 2.5 cm in diameter.

Similar topographical features were observed using either etchant. Figure 5.8 shows a comparison of the results from etching a grain with KI/I_2 and aqua regia. Image pairs left and right were taken at roughly the same position on the grain; the shape of grains is not identical between etching methods because some material is lost during polishing between etchings. White boxes indicate regions where there is strong evidence for similar features observed between etching methods. Figures 5.9 and 5.10 show several more comparisons between different etching methods, and methods of viewing the resulting features.

EDS examination of the etched surfaces revealed the presence of silver,

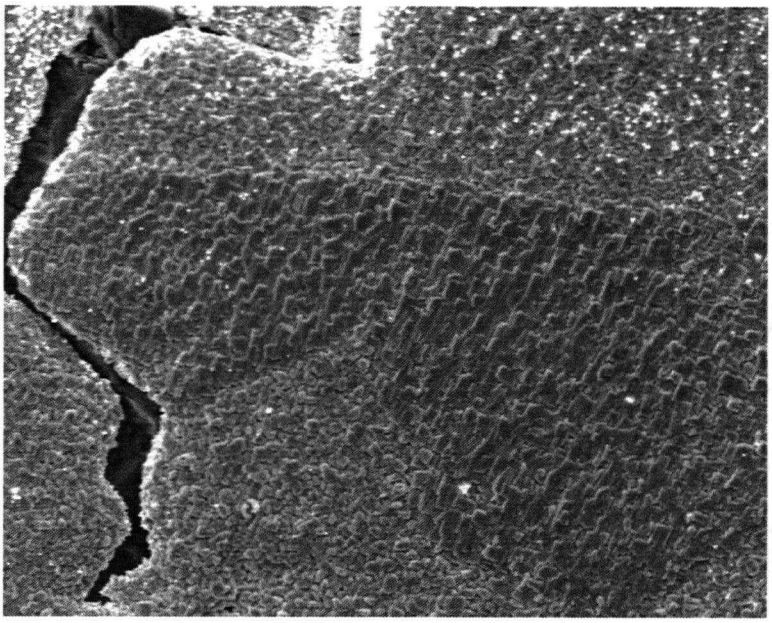

Figure 5.7: Detailed SEM image of the surface topography of an etched grain. Width of image is 0.1 mm.

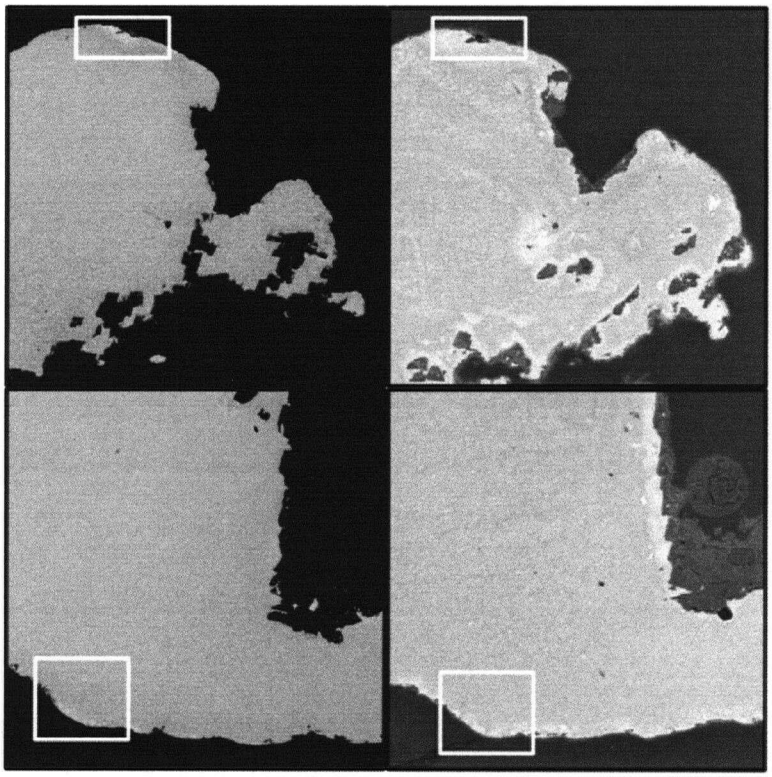

Figure 5.8: Comparison of etching by KI/I_2 and aqua regia of grain in Figures 5.3 and 5.4. Right side images are of a surface etched with KI/I_2, left side images were etched with aqua regia. Width of each image is roughly 0.3 mm. White boxes are areas of interest discussed in the text.

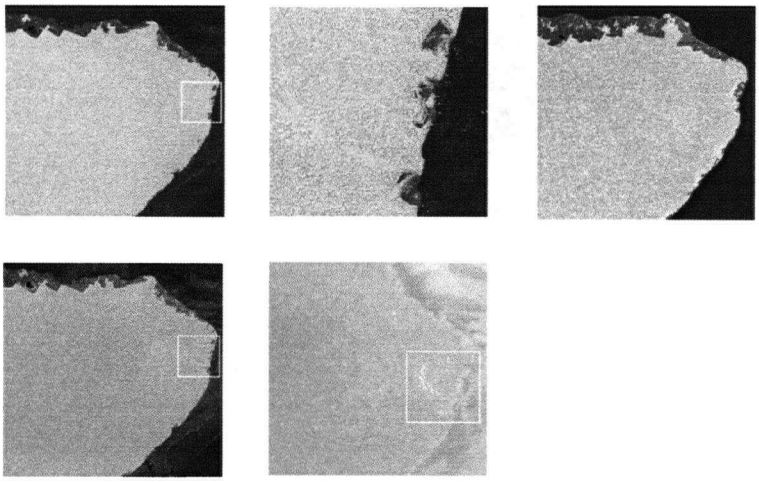

Figure 5.9: Comparison of etching by KI/I_2 and aqua regia of grain in Figures 5.3 and 5.4. From top left, clockwise: BSE SEM image of KI/I_2 etch, BSE SEM image of KI/I_2 etch (expansion of area in white box on other images), SE SEM image of aqua regia etch, reflected light image of KI/I_2 etch, SE SEM image of KI/I_2 etch.

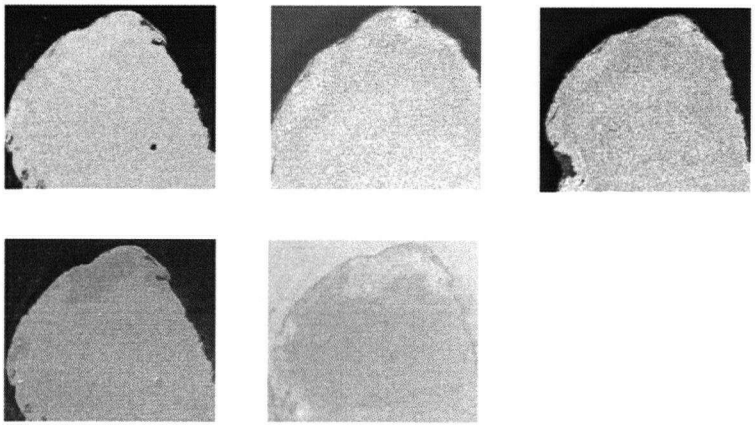

Figure 5.10: Comparison of etching by KI/I_2 and aqua regia of grain in Figures 5.3 and 5.4. From top left, clockwise: BSE SEM image of KI/I_2 etch, BSE SEM image of KI/I_2 etch, SE SEM image of aqua regia etch, reflected light image of KI/I_2 etch, SE SEM image of KI/I_2 etch.

gold and halogen (iodine for sample etched with KI/I_2, chlorine for samples etched with aqua regia). The most likely explanation for this result is the precipitation of insoluble silver halide salts onto the grain surfaces during the etching process (gold halides are generally much more soluble than the silver equivalents). As the etchants dissolve the gold and silver in the sample, the concentration of silver halide near the surface quickly increases above its solubility, and it begins to precipitate. This left open the possibility that the surface topography was due to the formation of crystalline silver halides, and was not at all representative of the crystallographic texture of the gold.

In an attempt to examine the underlying etched surface free of any silver halides, one sample was bathed in concentrated aqueous potassium iodide, which can dissolve silver iodide. This sample took on the appearance of roughly polished copper. Examination of this sample after carbon coating revealed that halogens were absent (only silver and gold were seen), but also that there was still some surface topography present (figure 5.11). Assuming that composition and crystallographic texture are the only factors that affect the rate of dissolution, the variations in surface topography seen in this sample are indicative of crystallographic texture. Qualitatively, the regions identified in the etched, and etched then washed sections are the same, indicating that the features seen after etching are representative of the underlying crystallographic texture. This is advantageous; the topographic features are generally more prominent in the unwashed samples, and the washing step is one of the more time consuming in the sample preparation.

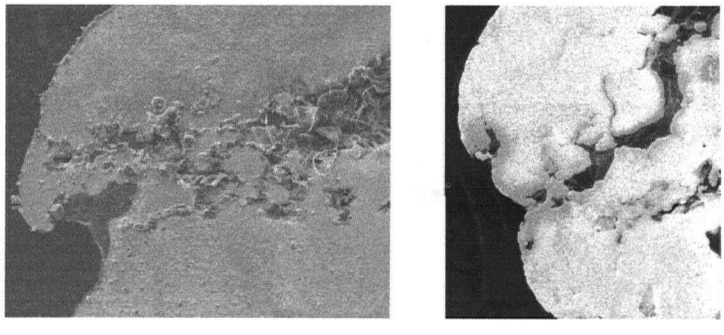

Figure 5.11: Comparison of the surface topography between an etched (right) and an etched, washed (left)section of a grain.

There has been controversy in the past as to the cause of the features

seen after acid etching; X-ray diffraction was used to confirm the nature of the underlying crystallographic texture of several samples. By comparing the results of the X-ray analysis to the etching results, it should be possible to confirm that the etching features are indicative of underlying crystallographic texture. A comparison of the results obtained from chemical etching and XRD is shown in Figure 5.12.

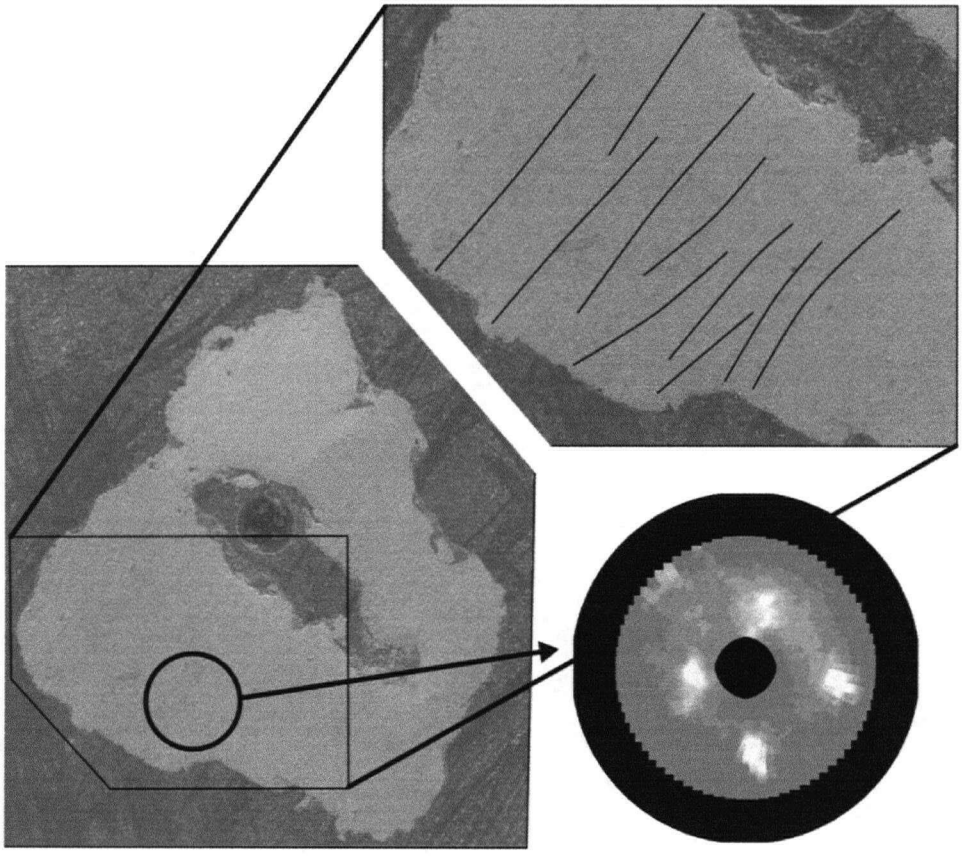

Figure 5.12: SEM image of surface topography from chemical etching, and the [2,2,0] pole figure recorded on that area. Image in top right is an enlargement of the boxed are on the bottom left image. Black lines denote linear features seen post-etching.

Electron backscatter diffraction is a method used mainly in metallography and materials chemistry to examine the crystallographic texture of a material. It relies on similar principals as X-ray diffraction, but instead uses

a beam of electrons. If successful, this method would have made it possible to map the extent and orientation of the crystalline domains within a grain. It might also have provided a way to measure the percent crystallinity of a grain by examining the relative areas of amorphous and crystalline material. Unfortunately, EBSD was unsuccessful in identifying any crystalline structure in a number of placer gold samples, some which had external crystalline structure. There are some limitations to the method; the electrons do not penetrate deeply into the sample, so the surface to be examined must be very carefully prepared to expose a layer of undeformed material with properties true to the sample. Secondly, the crystal structure must be generally undeformed; deformed crystalline lattices will be identified as amorphous material by EBSD.

5.4 Discussion

The likely reason for the failure of EBSD in this case is crystal structure deformation present in the samples due to physical processes during alluvial transport or possibly during polishing. All of the samples tested had experienced at least some alluvial transport, and the soft nature of gold and gold alloys has likely resulted in this transport causing deformation of any crystal structures present sufficient to thwart EBSD analysis. It may even have been the case that the samples had been deformed by geological forces before being liberated into the alluvial environment. Other metallic samples examined by EBSD are commonly annealed prior to analysis in order to relieve these deformations and allow EBSD examination, however annealing the placer gold samples would likely destroy the very detail the we are seeking to examine.

Transmission electron microscopy (TEM) has been used previously, and its use is comparatively well documented. Sample preparation for TEM is more difficult than for any of the other methods discussed here, and can only examine very small regions at a time. Previous studies have also generally only been able to identify well formed crystals. It is therefore unclear whether this method can obtain results from deformed samples, or if it (like EBSD) only works for undeformed or annealed samples.

Neutron diffraction could also theoretically be used to examine the crystal structure of gold, however this method can be difficult to perform because a nuclear reactor or other radioactive neutron beam source is needed. Furthermore, the method is typically used to examine single crystals; it is an advantage over single crystal X-ray diffraction because it is much more

sensitive to light elements, and can differentiate between isotopes. These advantages are not likely to be useful in the study of placer gold samples (gold is monoisotopic, an essentially all of the elements are heavy in placer gold), so the additional difficulty in pursuing this method is not warranted.

Several comparisons between the results of chemical etching and X-ray analysis were made. The first comparison was for an externally crystalline grain collected from a small tributary named #7 Pup in the Klondike District of west-central Yukon.

Figure 5.13 indicates that chemical etching is reflective of crystallographic texture. For spot 1, almost all of the area being analyzed appears to be a single zone by chemical etching, and there is essentially only one orientation seen using X-ray diffraction (the three points all arise from a single orientation). Spot 2 has a mixture of zones as evidenced by chemical etching, with the majority of the spot being located on the 'dark' zone the same zone on which spot 1 is located. The most intense reflections on the pole figure correspond to those observed for spot 1, indicating that the 'dark' phase as evidenced by etching is responsible for this pattern. The less intense set of reflections present in the pole figure for spot 2 is likely caused by reflections from the 'light' zones produced by etching. Close examination of the pole figure for spot 1 reveals some intensity at these positions, consistent with that spot being analyzed including some 'light' areas.

These results, where only a few zones are seen from etching, and few orientations indicated by X-ray diffraction, contrast those seen in Figure 5.14, which shows a sample that revealed numerous zones after chemical etching, and presented an extremely complex pole figure. This again confirms that the etching is revealing crystallographic texture; the numerous zones indicated by etching correspond to the numerous crystallite orientations observed on the pole figure.

The results in Figures 5.12, 5.13 and 5.14 also show how etching and X-ray diffraction reveal crystallographic texture. The grain in Figure 5.13 reveals two well defined zones after etching, with fairly well defined borders between them. There are some linear features visible, which may indicate crystallite deformation, and are evidenced in the pole figure by a smearing of the points. Figure 5.12 shows this phenomenon to a greater extent; there are multiple linear features evident (highlighted on the enlarged portion of the SEM image), all lying at generally the same orientation, but with some scatter. This indicates that the etching is accurately revealing a spread in crystallite orientations, evidenced by the spread of the points in the pole figure (especially when compared to Figure 5.13). Figure 5.14 is the most extreme example. There are some zones as evidenced by etching with well

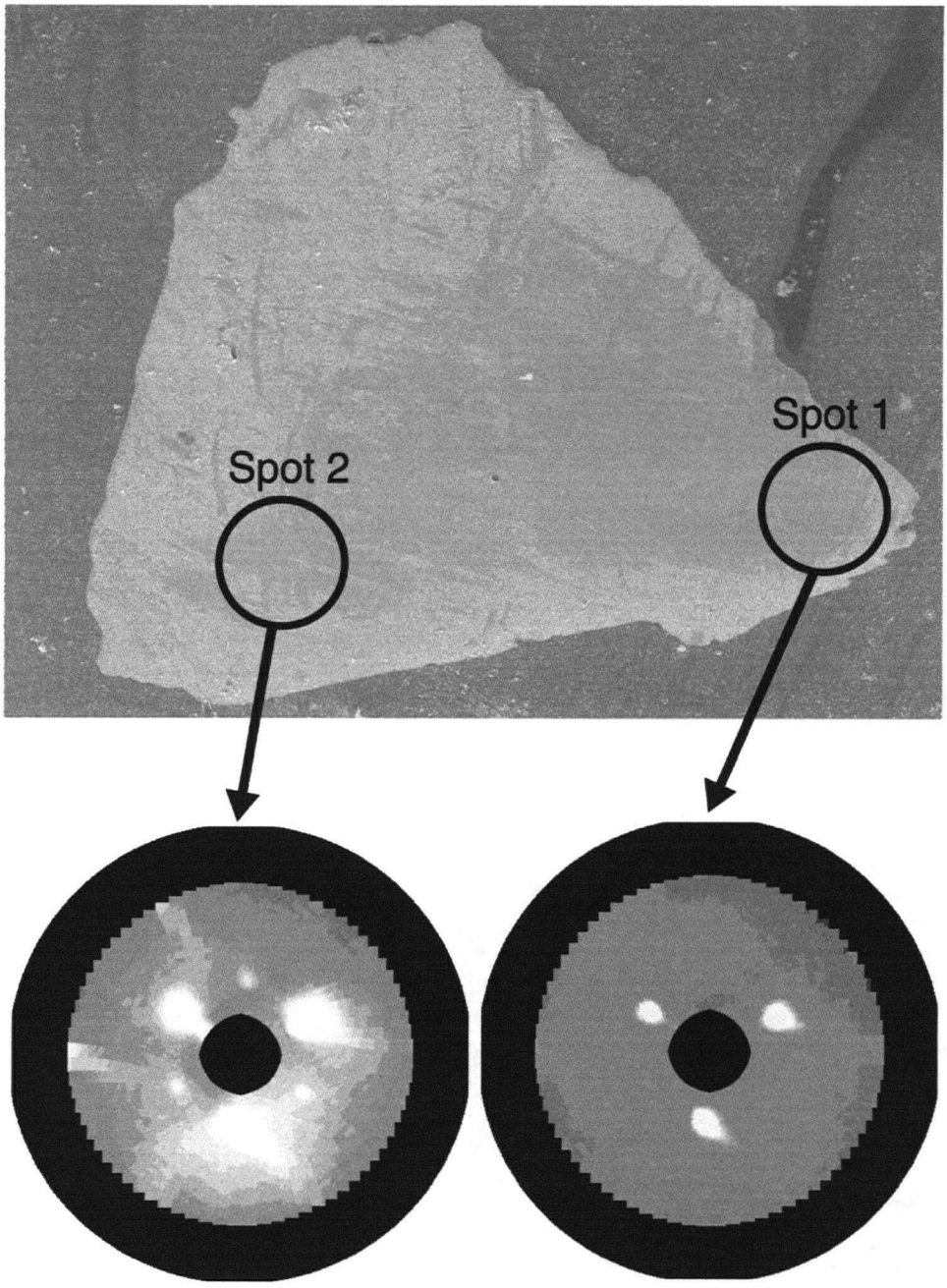

Figure 5.13: Comparison of chemical etching surface features and [2,2,0] pole figures calculated for several areas of a single grain.

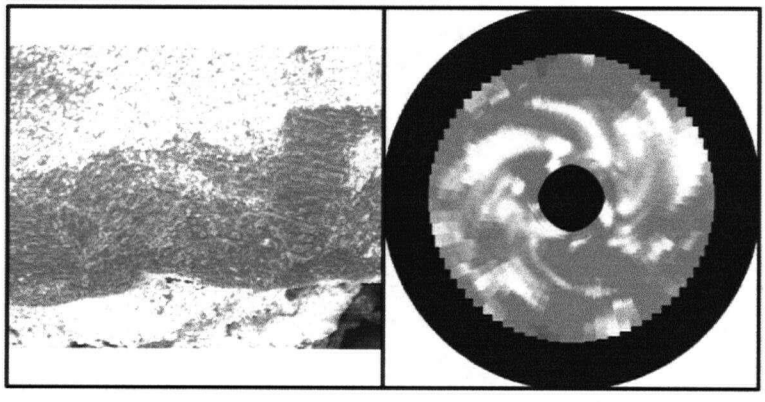

Figure 5.14: Comparison of chemical etching surface features and [2,2,0] pole figures for a visibly complex sample.

defined borders, and these likely produce the well defined points on the pole figure. Other regions of the sample (such as at the centre of the image) indicate that several orientations are present, but there are gradational contacts between them; these likely produce the smeared points seem in the pole figure.

5.5 Conclusions

This work has shown that there is a definite relationship between internal crystallographic texture and features seen after acid etching in placer gold. Each of these methods has advantages and disadvantages. Comparing chemical etching to X-ray analysis, etching is much faster, and provides better spatial resolution, however the information is qualitative and the method is sample destructive. Data from the X-ray analysis can be examined qualitatively as well, but can also be examined quantitatively. The qualitative information is still superior to that from etching; for example: counting the number of orientations seen is much less subjective. The data could also be used to calculate the relative amounts of crystallites at each orientation by integrating the intensity of the reflections seen for each orientation. Additional studies could also be performed examining the crystallographic texture with respect to the overall shape of the grains. For example, it is generally observed that grains flatten with transport, and it is generally postulated that this is due to hammering of grains between harder rock clasts and bedrock during alluvial transport. It is also possible that grains flatten by smearing or rolling. The crystallographic texture formed by each of these processes should be different.

A better understanding of the processes that cause placer grain shape change may help improve models that used placer grain shape change to estimate transport distance. For example, the grain in Figure 5.13 was obtained very near (within 100 m of) a lode source from which is was most likely liberated, whereas the grain in Figure 5.12 has experienced much more (several km) transport. A qualitative comparison of these two grains indicates that the internal crystallographic structure appears to become progressively deformed during alluvial transport; a more detailed study of this phenomenon is definitely warranted.

Crystallographic information may also be useful in examining the processes of gold rich rim formation. Experimental studies with chemical leaching could be performed to determine if crystallographic texture is retained during this process. Likewise, it would be interesting to see if biomineralized

gold has crystallinity, and if that crystallinity is templated on the surface on which is it is deposited. It will also be important to examine the effects of physical deformation; gold rich rims are generally observed in grains that have been exposed to the environment for a significant amount of time, and so have usually experienced significant alluvial transport. The physical processes of alluvial transport will likely have an effect of crystallinity, especially near the surface, and it will be important to deconvolute these physical effects from any crystallographic texture imposed by rim forming processes. There is already some evidence that the physical processes of alluvial transport leaves a crystallographic fingerprint. Figure 5.11 shows the results of etching on a placer gold grain, with edge features visible in both images (top right); this is the grain examined by microprobe (Figures 5.1 and 5.2) and EDS (Figure 5.5), revealing no gold rich rim. The lack of compositional variation around these edge features means that physical processes are likely the cause of these features.

Another interesting study would be to examine in more detail the relationship between the crystallographic texture of the gold and the orientation of the halide that forms during etching. This may be possible by measuring X-ray diffraction patterns on samples that have been weakly etched; the pattern observed would be a combination of reflections from the underlying gold and the halide layer, allowing the relationship between their orientations to be determined.

These methods should provide several new ways to characterize gold deposits; certain deposit types may contain gold grains that are monocrystalline, and others may contain numerous crystalline domains. This might also be indicative of the environment in which the gold formed; gold growing in cavities might be expected to be monocrystalline, whereas gold forming as a replacement mineral or forming late and into extremely small spaces might be expected to have multiple crystalline domains. Trace or major element concentration may also dictate the probability, extent or nature of the crystallinity of the gold.

5.6 References

Berndt, A. F., Cummins, J. D. The Crystal Structure of the Au_2Hg Phase. Acta Crystallographica, 1970, Vol. B26, pp. 864-867.

Beveridge, T.J., Murray, R.G.E. Sites of Metal Deposition in the Cell Wall of Bacillus subtilis. Journal of Bacteriology, 1980, Vol. 141, No. 2, February, pp. 876-887.

Craw, D. Growth of Alluvial Gold Particles by Chemical Accretion and Reprecipitation, Waimumu, New Zealand. New Zealand Journal of Geology and Geophysics, 1992, Vol. 35, pp. 157-164.

Crawford, E.C., Mortensen, J.K. (2007): An ImageJ plugin for the rapid morphological characterization of separated particles and an initial application to placer gold analysis. Computers and Geosciences, submitted.

Francis, C.A. Gold Crystals: A Primer. Rocks and Minerals, 2004, Vol. 79, January/February, pp.24-29.

Hashimoto, S., Miura, S., Kubo, T. Dislocation Etch Pits in Gold. Journal of Materials Science, 1976, Vol. 11, pp. 1501-1508.

Klaus, T., Joerger, R., Olsson, E., Granqvist, C. Silver-Based Crystalline Nanoparticles, Microbially Fabricated. Proceeding of the National Academy of Sciences, 1999, Vol. 96, No. 24, pp. 13611-13614.

Klaus-Joerger, T., Joerger, R., Olsson, E., Granqvist, C. Bacteria as Workers in the Living Factory: Metal-Accummulating Bacteria and their Potential for Materials Science. TRENDS in Biotechnology, 2001, Vol. 19, No. 1, January, pp. 15-20.

Knight, J. Preliminary Evidence for the Involvement of Budding Bacteria in the Origin of Alaskan Placer Gold : Comment and Reply. Geology, 1993, Vol. 21, No. 3, pp. 279-280.

Kulp III, J. L., Sarikaya, M., Evans, J.S. Molecular Characterization of a Prokaryotic Polypeptide Sequence that Catalyzes Au Crystal Formation. Journal of Materials Chemistry, 2004, Vol. 14, pp. 2325-2332.

Marcus, P. M., Jona, F. Metastable Phases of Silver and Gold in Hexagonal Structure. Journal of Physics: Condensed Matter, 2004, Vol. 16, March, pp. 5199-5204.

Mauthner, M. Morphology of Gold Crystals from the Yukon Territory, Canada. Rocks and Minerals, 2004, Vol. 79, March/April, pp.100-109.

McCready, A. J., Parnell, J., Castro, L. Crystalline Placer Gold from the Rio Neuquén, Argentina: Implications for the Gold Budget in Placer Gold Formation. Economic Geology, 2003, Vol. 98, pp. 623-633.

Nair, B., Pradeep, T. Coalescence of Nanoclusters and Formation of Submicron Crystallites Assisted by Lactobacillus Strains. Crystal Growth and Design, 2002, Vol. 2, No. 4, pp. 293-298.

Pouchou, J. L., Pinchoir, F. (1985): "PAP" (phi-rho-Z) procedure for improved quantitative microanalysis. In: Microbeam Analysis, J.T. Armstrong (ed.), San Francisco Press, San Francisco, California, USA, pp. 104-106.

Reith, F., Rogers, S. L., McPhail, D. C., Webb, D. Biomineralization of Gold: Biofilms on Bacterioform Gold. Science, 2006, Vol. 313, 14 July, pp. 233-236.

Senapati, S., Ahmad, A., Khan, M. I., Sastry, M., Kumar, R. Extracellular Biosynthesis of Bimetallic Au-Ag Alloy Nanoparticles. Small, 2005, Vol. 1, No. 5, pp. 517-520.

Southam, G. Quantification of Sulfur and Phosphorous Within Secondary Gold Rims on Yukon Placer Gold. Geology, 1998, Vol. 26, No. 4, April, pp. 339-342.

Southam, G., Beveridge, T. J. The Occurrence of Sulfur and Phosphorous Within Bacterially Derived Crystalline and Pseudocrystalline Octahedral Gold Formed in vitro. Geochimica et Cosmochimica Acta, 1996, Vol. 60, No. 22, pp. 4369-4376.

Southam, G., Beveridge, T. J. The in vitro Formation of Placer Gold by Bacteria. Geochimica et Cosmochimica Acta, 1994, Vol. 58, No. 20, pp 4527-4530.

Stratton, R. P., Kitchingman, W. J. Stacking Fault Densities in Hexagonal Gold Alloys. British Journal of Applied Physics, 1966, Vol. 17, pp. 1039-1042.

Taber, S. Gold Crystals from the Southern Appalachians. American Mineralogist, 1942, Vol. 27, pp. 219-229.

Voorts, V. Metallography, Principles and Practice. Murphy, A. and Hazlett, S. (eds.), McGraw-Hill Book Company, New York, NY, USA, 1984. pp. 629, 685-686

Watterson, J. R. Artifacts Resembling Budding Bacteria Produced in Placer-Gold Amalgams by Nitric Acid Leaching. Geology, 1994, Vol. 22, December, pp. 1144-1146.

Watterson, J. R. Preliminary Evidence for the Involvement of Budding Bacteria in the Origin of Alaskan Placer Gold. Geology, 1991, Vol. 20, April, pp 315-318.

Chapter 6

Concluding Remarks

6.1 Relations between individual studies

This work has been presented as several chapters that are intended to be submitted for publication as individual manuscripts. Due to this layout, there is significant overlap between studies, and much of this overlap has been discussed already in each chapter. In particular:

- The morphological analysis plugin and method described in Chapter 2 was used extensively to generate the morphological data which is examined thoroughly in Chapter 3.
- A significant number of electron microprobe analyses performed, and the results from these analyses were used extensively in Chapter 3, but were also utilized in Chapters 4 and 5.
- The results of the study presented in Chapter 3 guided the experimental work described in Chapter 4. The time and cost required for LA-ICP-MS analyses meant that is was impractical to examine every grain, hence the subset of grains measured from each sample was selected based on the populations identified using the methods described in Chapter 3.
- The crystallinity work described in Chapter 5 was also informed extensively by compositional information, from the SEM, EMPA and LA-ICP-MS analysis.
- In the future this work is likely to become even more intertwined. Examination of crystalline features may be used to examine transport distance relationships, LA-ICP-MS may be used to distinguish between population in a placer sample, permitting refinement of the shape : transport distance model.

6.2 Summary of Project Results

Results of this project represent numerous significant advances over past work; however there are still some limitation to the research. Multiple new pathways for future research in this field are described below.

- The plugin appears to work well, and has already garnered some early interest from other researchers in the field. Hopefully this interest will grow, and many other users can find utility in the plugin. It has been mentioned that use of the plugin could be applied to other problems, however none of these uses have been tested. The macro also still does not completely eliminate subjectivity from the process; the manual arrangement of grains is the most likely step in the process to introduce error.

- The shape : transport distance study is a vast improvement over past similar attempts. It is based on a significantly larger data set, and takes a much more statistically rigorous approach. Introduction of gradient corrected distances represents a significant improvement over previous studies which only examined horizontal transport distances. As developed, it appears that the model should be able to make reasonably accurate predictions of source locations, and some predictions have been made, however the accuracy of these predictions has not been verified thus far.

- The laser ablation method as described provides important new insight into the compositional range of placer gold in the Klondike District, and represents the first application of LA-ICP-MS to the study of a large range of natural gold samples. This method will likely find significant utility in the future for examining many of the features of placer gold, and may also find an important role in the study of mineral deposits of all types which contain native gold or gold alloys.

- This work has shown that chemical etching and X-ray diffraction can both be used to probe gold crystallinity. Unfortunately, the amount of work completed on this topic was somewhat limited, making conclusions about many aspects of crystallinity difficult. The development and confirmation of several new methods for examining these features in a qualitative and potentially quantitative manner is still a significant advance over all previous methods.

6.3 Future Work

This thesis forms part of an on-going project, and results of the work suggest a number of new avenues for the research:

- It may be possible to develop a method to automatically position grains for morphological analysis, simultaneously image grains in both cross sections, or otherwise automate image analysis, again increasing the speed at which data can be accumulated, and reducing the subjective influence on the analyses. Ideally this method could be extended to record true three dimensional grain shape, allowing fully objective measurements of morphological parameters with no approximation or assumption necessary.

- The predictions of the shape : transport distance model could be rigorously tested in the Klondike. Now that improved guidelines for sampling have been developed, a much more detailed case study examining a single drainage could also be performed. Perhaps of more interest would be carrying out similar studies in different locations worldwide to test the general applicability of the method, and to determine if the model developed here is universally applicable.

- A similar approach could be used to test specific grain shape : transport distance relationships, focusing on extremely short and much longer transport distances, or examining locations with more complex depositional histories or environments, or involving significantly different gold compositions. If successful, the short distance model could be used to pinpoint sources once a general location had been predicted, and the long transport distance model would extend the useful range of the model. Examining the other details could produce a range of models applicable to individual geographic settings, producing a "toolbox" for the identification of lode gold deposits from placers worldwide.

- The addition of additional shape parameters to the shape : transport distance model should be investigated. Development of the predictive model using two variables (wt.% Au and HSE) was already quite computationally demanding and addition of more variables would likely require specialized programming and/or the use of a more powerful mathematical analysis package.

- The methods described in Chapter 5 should be applied more extensively to the study of placer gold. There were a vast range of interesting crystallographic features seen, suggesting that a wealth of information may be available from the method. Several ideas for extensions of this study were already discussed in Chapter 5, including a detailed examinations of crystal deformation during transport, the relationship between composition or deposit type and crystallographic texture, and the exact processes that occur during chemical etching.

- The use of laser ablation will likely play an important role in many of these projects, since understanding composition is often a first and vital step to understanding other processes.

- The laser ablation study should also be extended to include samples from any location where native gold is present. Developing a database of minor and trace element compositions in gold could play an important role in exploration, and in understanding the genesis of and source of metals in ore deposits. There are also the forensic applications for which LA-ICP-MS analysis of gold has already been used. Additional studies could include using this method to examine isotopic systematics. Our work has shown that, at least for the Yukon, platinum group elements are present in significant concentrations; suggesting that Re/Os dating methods could potentially be applied to samples of native gold, providing another tool for directly dating deposit formation. It would be interesting to test how broad an applicability the method can find; future work could include the LA-ICP-MS analysis of native silver and/or native platinum group element samples.

- This project is still ongoing, and other researchers have performed extensive work examining mineral microinclusions. Future efforts should include an attempt to rationalize results between these studies and the work described here. Especially interesting would be comparisons of trace and minor element compositions and types of microinclusions present.

Appendix A

Electronic Data

The DVD included contains the data which was summarized and synthesized into the chapters of this thesis. This appendix contains descriptions of the files on the DVD.

A.1 Composition Data.xls

This worksheet (Saved in the native format for Microsoft Excel 2004 for Mac, version 11.3) contains all of the probe data collected on the entire sample suite. The organization of the data is as follows:

Column A : Sample ID

Column B : Grain Group. This number is used to distinguish between the photographs recorded at two different orientations, and is not needed on this worksheet, so the generic -0x- is used.

Column C : Grain ID. This is the sequential number given to consecutive grains on a given grain mount.

Column D : Grain Number. These are the sequential numbers given to all of the grains in a sample (contiguous across grain mounts).

Column E : Weight % Copper.

Column F : Weight % Silver.

Column G : Weight % Gold.

Column H : Weight % Mercury.

Column I : Fineness..

Column J : Total Weight %.

Columns K to R : Cells to list a combined grain identification code and identify grains with over and under total analyses. The combined grain identification code is used by other worksheets to cross reference to composition data for and particular grain.

Each row represents the data for a particular grain. Rows 3 to 10 contain analyses that were rejected because of high or low totals, rows 14 to 4779 contain analyses deemed acceptable.

A.2 KDE Fitting Files

These worksheets (Saved in the native format for Microsoft Excel 2004 for Mac, version 11.3) contain the calculated KDEs and modeled fits to that data, including the parameters of the populations used to generate that model. There is an individual worksheet provided for each sample.

A.2.1 Calculations tab

This tab contains all of the data. Cells C10:F19 contain the parameters of the fitted model populations, with each row representing a different population. Cells C10:C19 contain the weight % Au values, and cells E10:E19 the standard deviations on those values. Cells E10:E19 contain the HSE values, and cells F10:F19 the standard deviations on those values Cells K10:K19 indicate the number of grains that any given population represents in a sample. Cell K8 is the number of grains measured for that sample. Cell K7 is the total % error difference between the sum of the fitted model populations and the KDE calculated from the measured data.

Cells L27:DH128 contains the calculated normalized KDE values, with cells L27:DH27 containing the projection of the probability density surface onto the HSE axis, and K28:K128 the projection onto the weight % Au axis. The values of the probability density surface are contained in cells L28:DH128. Cells L26:DH26 contain the HSE coordinates and J28:J128 the weight % Au coordinates.

Cells L137:DH238 contains the raw summed KDE generated from the model population values, with cells L137:DH137 containing the projection of the probability density surface onto the HSE axis, and K138:K238 the projection onto the weight % Au axis. The values of the probability density surface are contained in cells L138:DH238. Cells L136:DH136 contain the HSE coordinates and J138:J238 the weight % Au coordinates.

Cells L243:DH344 contains the normalized summed KDE generated from the model population values, with cells L243:DH243 containing the projection of the probability density surface onto the HSE axis, and K244:K344 the projection onto the weight % Au axis. The values of the probability density surface are contained in cells L248:DH344. Cells L242:DH242 contain the HSE coordinates and J244:J344 the weight % Au coordinates.

Cells L351:DH451 contains the difference between the normalized fitted model and the calculated KDE values, with cells L350:DH350 containing the projection of the probability density surface onto the HSE axis, and K351:K451 the projection onto the weight % Au axis. The values of

the probability density surface are contained in cells L351:DH451. Cells L349:DH349 contain the HSE coordinates and J351:J451 the weight % Au coordinates.

A.2.2 KDE Output tab

This tab contains a plot of the calculated KDE values, the height and color of the surface at any given point represents the probability of recording a grain with the values at those coordinates (dark values are low probability, white is high probability). The upper wall shows the projection of the probability surface onto the weight % Au axis, and the left wall shows the projection onto the HSE axis.

A.2.3 Fitted Data tab

This tab contains a plot of the KDE calculated from the fitted model populations. The description of the figure is the same as per the KDA Output tab.

A.2.4 Difference plot tab

This plot shows the difference at each point over the HSE : weight % Au area between the KDE calculated from the experimental data and the KDE calculated from the fitted model populations.

A.3 Morphological Data

These worksheets (Saved in the native format for Microsoft Excel 2004 for Mac, version 11.3) contain all of the morphological parameters measured by the plugin, as well as the morphological parameters calculated from those values. There is an individual worksheet provided for each sample.

A.3.1 tabs -01 and -02

These tabs contain the data as imported from the text files that the plugin outputs. Tab -01 contains the data from the photographs taken in the first orientation, and tab -02 the data from orientation 2. Each row represents the values from an individual grain. The data in the columns is:

Column A : Photo Number (grains are photographed in groups, each group has a consecutive photo number)

Column B : Particle Number (these are the sequential numbers given to each grain within a group)
Column C : Area
Column D : Perimeter
Column E : Feret
Column F : Breadth
Column G : Convex Perimeter
Column H : Convex Area
Column I : Radius of the smallest circumscribing circle
Column J :Radius of the largest inscribed circle
Column K : A placeholder value used for counting
Column L : The x coordinate of the centre of the grain on the photograph
Column M : The y coordinate of the centre of the grain on the photograph
Columns N - FU : Fourier Parameters as listed in the column headings

Photo and particle number, x and y position, the placeholder and all the fourier parameters values are unitless, area values (area, convex area) are given in mm^2, the remainder of the values are in mm.

Row 1 contains a title for the tab, row 2 contains the column headings and rows 3 and below contain grain data.

A.3.2 3D parameters tab

Row 1 contains a title for the tab, rows 2 and 3 contain column headers. The data is contained in rows 4 and up with each row containing the data for an individual grain. The data on this page is in order by grain number starting with number 1 at row 4; these are the grain numbers listed in the "Composition Data" worksheet. The columns contain the following data:

Column A : Minor axis length
Column B : Intermediate axis length
Column C : Major axis length
Column E : Hofmann Shape Entropy
Column F : Corey Shape Parameter
Column G : Cailleux Shape Parameter
Column I : Area Roughness Parameter
Column J : Perimeter Roughness Parameter

A.3.3 My parameter tab

This tab contains the data from tabs -01 and -02 regrouped to allow for calculation of the shape parameters listed on the "3D parameters" tab.

A.4 Perimeter and Number images

These are the processed photos indicating the identified outlines and assigned particle numbers. The files are organized by sample ID and orientation. For example, the photo of group 25 in orientation 2 from sample 7 is located in the folder "EC-07-0x-xxx" (sample 7), then the folder "EC-07-02-xxx" (orientation 2), file "EC-07-02-025PPerim.jpg" (group 25).

A.5 Processed Photos

These are the photos prepared for processing through the plugin (cropped and obvious grit deleted). The organization of these files is the same as per the "Perimeter and Number images" except the files end ###P.jpg instead of ###PPerim.jpg.

A.6 Text Outputs

These are the text files containing the morphological data as output by the shape analysis plugin. The organization of these files is the same as per the "Perimeter and Number images" except the files end ###P.txt instead of ###PPerim.jpg.

A.7 Shape Analysis Plugin.zip

This archive contains all of the necessary files to install, modify and test the function of the shape analysis plugin described in Chapter 2. This is the format of the files as submitted to Computers and Geosciences.

A.8 Laser Ablation Data Files

This folder contains all of the raw data as exported from the mass spectrometer in .FIN format. These files are comma delimited lists of the counts per second measured for each isotope recorded against the time during the scan at which those count were recorded. There is also some header information including the time at which the data was recorded. The multi-element runs are in the folder titled "Multi Element", argide ratio measurement runs are in the folder "Argide".

A.9 Laser Ablation Data.xls

This is Microsoft Excel spreadsheet containing the background and internal standard corrected counts for all of the sample analyzed.

A.10 Sample Locations.xls

This is a Microsoft Excel spreadsheet containing the location of each sample, and the code it has been assigned. It also includes some qualitative example on where the samples were taken from.